Integration of biocatalysis and simulated moving bed chromatography for the high-yield production of rare sugars

DISS.ETH NO 22340

Integration of biocatalysis and simulated moving bed chromatography for the high-yield production of rare sugars

A thesis submitted to attain the degree of
DOCTOR OF SCIENCE of ETH ZURICH
(Dr.sc. ETH Zurich)

presented by
Nina Wagner
Dipl.-Ing., BOKU University, Vienna

born 17.12.1982
citizen of Austria

accepted on the recommendation of
Prof. Dr. Sven Panke (ETH Zurich, Switzerland), examiner
Prof. Dr. Marco Mazzotti (ETH Zurich, Switzerland), co-examiner

2014

Acknowledgements

We are indebted to the Swiss National Science Foundation for funding this PhD thesis as part of the SNF project 200021-121918/1 „Process intensification with integrated multi-enzyme systems“.

Abstract

Rare monosaccharides are typically difficult to interconvert from available bulk sugars by traditional chemical synthesis as the multifunctionality of sugars leads to a strong requirement for protection-group chemistry. This favors the use of substrate- and stereoselective enzymes. In principle, enzyme cascades based on available iso- and epimerases allow the facile and generic synthesis of many rare monosaccharides from a set of inexpensive bulk sugars such as D-glucose, D- galactose, L-sorbose and D-fructose. However, isomerization and epimerization reactions suffer from an unfavorable position of the thermodynamic equilibrium imposing a severe yield limitation, frequently between 20 and 70%, and thus preventing the industrial application of such enzyme casdades. However, the equilibrium problem can be overcome by integrating biocatalysis and separation into one operation. In this work we have investigated a novel integrated process strategy consisting of enzymatic conversion in an enzyme membrane reactor (EMR), substrate and product separation in a simulated moving bed (SMB) chromatography unit and nanofiltration (NF) concentration of the recycled substrate for improving the yields in rare sugar production. This enabled a theoretical yield of 100% during continuous operation.

Starting from the previously mentioned bulk sugars most of the possible rare hexose sugars can be produced combining a maximum of three available isomerase and epimerase enzymes. Therefore, this strategy in principle offers a generic route for rare sugar manufacturing. Here, we selected the rare sugar D-psicose as target compound. D-Psicose can be produced from D-fructose in a single-step enzymatic conversion at the C3 position using the enzyme D-tagatose epimerase, or in a three enzyme reaction cascade from sucrose via sucrose hydrolysis to fructose and glucose, fructose/glucose isomerization and finally the epimerization from fructose to psicose. First, an experimental implementation of the one enzyme process concept was realized to confirm the principal feasibility of the integrated process concept for high-yield production of D-psicose. The integrated process implementation allowed shifting product yield from 25% (possible in batch operation) to 97% and additionally constituted the first experimental report on the proposed integrated set-up. Moreover, a number of important practical aspects were analyzed such as process stability and robustness and an accelerated start-up procedure was suggested.

Rational design of the integrated process required a detailed characterization of all involved unit operations. A particular focus of this work was therefore on the design and optimization of the SMB separation of D-fructose and D-psicose on Ca^{2+} substituted SMB ion exchange material. To this end, chromatographic parameter estimation was

established based on the inverse method which allowed the accurate parameterization of the adsorption and kinetic behavior over a wide temperature range (20 to 70°C). A true moving bed (TMB) model was established for the description of SMB performance and further applied for the multi-objective optimization of the SMB separation employing a Pareto approach. The optimization revealed the optimal SMB operation point at high temperatures (70°C) indicating that the decreased selectivity of the stationary phase at higher temperatures could be fully compensated by the gain in mass transfer affording an overall higher productivity. Based on these results, a comprehensive design and cost-based optimization strategy was established based on an integrated process model.

An important objective of the presented model constituted the incorporation of the temperature dependence of the enzyme kinetics and stability at elevated temperatures. A model-based parameter estimation procedure was established which allowed to evaluate thermodynamic and kinetic enzyme parameters as a function of the EMR operating temperature. This finally enabled us to investigate the EMR temperature as a design variable during process optimization and to devise an enzyme-efficient method to operate the EMR at constant conversion, a prerequisite for robust operation of the integrated process and a major challenge due to the inherent instability of the biocatalysts under elevated temperatures.

Finally, we applied the process concept to the multi-enzyme scenario which involved the use and characterization of two further biocatalysts (invertase, D-xylose isomerase) and the extension of the SMB separation to a 3-component mixture. The presented successful experimental operation of a complex multi-enzyme integrated process represents the first attempt implementing a separation integrated reaction cascade and allowed the stable production of D-psicose in high purities (99%) and high yields (96%).

Zusammenfassung

Seltene Zucker können in der Regel nur schwer durch traditionelle chemische Synthese aus verfügbaren Zuckern hergestellt werden, da ihre Multifunktionalität den Einsatz von Schutzgruppenchemie nötig macht. Diese Tatsache begünstigt die Nutzung von substrat- und stereospezifischen Enzymen. Im Prinzip, erlauben Enzymkaskaden basierend auf verfügbaren Isomerasen und Epimerasen eine einfache und generische Synthese der meisten seltenen Monosaccharide aus einer Reihe von preiswerten Zuckern wie zum Beispiel D-Glucose, D-Galactose, L-Sorbose und D-Fructose. Isomerisierungs- und Epimerisierungsreaktionen weisen jedoch typischerweise eine ungünstige Position ihres thermodynamischen Gleichgewichts auf. Diese führt oftmals zu schwerwiegenden Ausbeutelimitationen zwischen 20 und 70% und steht so einer industriellen Nutzung solcher Enzymekaskaden im Wege. Das Gleichgewichtsproblem kann aber durch Integration der biokatalytischen Umwandlung mit einem Separationsschritt überwunden werden. In dieser Arbeit haben wir eine neue Prozessstrategie, bestehend aus enzymatischer Umsetzung in einem Enzym-Membranreaktor (EMR), Trennung des Substrats und Produkts mittels Simulated Moving Bed (SMB) Chromatographie und Konzentration des Recyclingstroms mittels einer Nanofiltrationsanlage (NF) erforscht um so die Ausbeuten in der Produktion von seltenen Zuckern zu erhöhen. Theoretisch erlaubt eine solche Prozessstrategie eine Ausbeute von 100% während kontinuierlichem Betrieb.

Ausgehend von den vorher erwähnten Zuckern können die meisten der möglichen seltenen Hexosezucker produziert werden, in dem maximal drei verfügbare Iso- und Epimerasen kombiniert werden. Damit bietet diese Strategie grundsätzlich eine generische Möglichkeit seltene Zucker industriell herzustellen. In dieser Arbeit wurde der seltene Zucker D-Psicose als Zielsubstanz gewählt. D-Psicose kann mittels des Enzymes D-Tagatose Epimerase in einem einzelnen enzymatischen Umwandlungsschritt an der C3 Position aus D-Fructose oder in einer dreistufigen Reaktionskaskade von Saccharose, über einen Hydrolyse- Schritt zu D-Fructose und D-Glucose, Isomerisierung von D-Glucose und D-Fructose und einem abschliessenden Epimerisierungsschritt von D-Fructose nach D-Psicose hergestellt werden.

Zunächst wurde eine experimentelle Implementierung des einstufigen Enzymprozesses realisiert um die grundsätzliche Eignung des integrierten Prozesskonzepts zu zeigen, die D-Psicose Ausbeuten zu erhöhen. Tatsächlich, erlaubte es die Implementierung des integrierten Prozess die Ausbeute an Produkt von 25% (möglich im Batch Betrieb) auf 97% zu erhöhen und stellte gleichzeitig die erste experimentelle Realisierung des vorgeschlagenen Integrationskonzept dar. Ausserdem wurden eine Reihe wichtige

praktische Aspekte analysiert so wie die Stabilität und Robustheit des Prozesses und ein beschleunigtes Anfahrprozedere für unsere Anlage ermittelt.

Eine rationale Auslegung des integrierten Prozesses macht eine detaillierte Charakterisierung der involvierten Prozesseinheiten notwendig. Ein besonderer Fokus dieser Arbeit lag deshalb auf der Auslegung und der Optimierung der Trennung von D-Fructose und D-Psicose mittels SMB unter der Verwendung von Ca^{2+}-substituierten Ionenaustauchmaterial. Basierend auf der Inversen Methode wurden dazu die chromatographischen Parameter geschätzt, die eine akkurate Parametrisierung des Adsorptions- und kinetischen Verhalten über einen weiten Temperaturbereich (20 bis 70°C) erlaubt. Für die Beschreibung der Performance der SMB wurde ein True Moving Bed (TMB) Modell etabliert, das dann auch für eine Mehrkriterien-Optimierung der SMB Trennung auf Basis eines Pareto Ansatzes verwendet wurde. Die Optimierung zeigte, dass die SMB optimaler Weise bei hohen Temperaturen betrieben wird (70°C), was darauf hindeutet, dass die geringere Selektivität der stationären Phase bei höheren Temperaturen vollständig durch den erhöhten Masstransfer (der wiederum höhere Produktivität ermöglicht) kompensiert werden kann.

Als nächstes wurde eine umfassende Design- und kostenbasierte Optimierungsstrategie basierend auf einem integrierten Prozessmodel etabliert. Eine wichtige Zielsetzung bei der Modellentwicklung stellte die Eingliederung der Temperaturabhängigkeit der Enzymkinetik und -stabilität bei erhöhter Temperatur dar. Deshalb wurde eine Methode zur modell-basierter Parameterschätzung etabliert, die es uns ermöglichte thermodynamische und kinetische Parameter des Enzymes als Funktion der EMR Betriebstemperatur abzuschätzen. Das ermöglichte uns zum einen die EMR Betriebstemperatur im Zuge der Prozessoptimierung als Designgrösse zu untersuchen und zum anderen eine enzym-effiziente Methode zu entwickeln die es uns erlaubte den EMR bei konstanter Konversion zu betreiben, eine Grundvoraussetzung für den stabilen Betrieb des integrierten Prozesses und eine grosse Herausforderung aufgrund der inhärenten Instabilität des Biokatalysator unter erhöhter Temperatur.

Abschliessend wurde das integrierte Prozesskonzept auf ein Multi-Enzymsystem angewandt. Dafür mussten zwei weitere Enzyme (Invertase, D-Xylose Isomerase) verwendet und charakterisiert und die SMB Trennung auf ein 3-Komponenten Gemisch erweitert werden. Der erfolgreiche experimentelle Betrieb des komplexen, integrierten Prozesses mit mehreren Enzymen stellt die erste Implementierung einer Reaktionskaskade dar, die mit einer Trennung integriert wurde und so eine stabile Produktion von D-Psicose in hoher Reinheit (99%) und hoher Ausbeute (96%) ermöglichte.

Table of content

1 Introduction

1.1 General introduction – carbohydrates

Carbohydrates, categorized into mono-, di- and polysaccharides according to the degree of oligo- or polymerization, are of exceptional importance in all aspects of life, ranging from an essential energy source via structural materials in plants (e.g. cellulose), animals (e.g. chitin) and microorganisms (e.g. murein) to bioactive secondary metabolites as for example aminoglycoside antibiotics [1]. It is estimated that an enormous amount of 4×10^{11} tons of carbohydrates are biosynthesized each year on the earth by plants and biosynthesizing bacteria [2]. The biggest part of this huge amount of carbohydrates, however, is made up of only seven standard hexose (C6-sugars) and pentose (C5-sugars) building blocks, namely D-glucose (C6), D-fructose (C6), D-galactose (C6), D-mannose (C6), D-xylose (C5), D-ribose (C5) and L-arabinose (C5) [3]. In contrast, the other nine standard pentose sugars as well as the remaining 20 standard hexose sugars are not available in nature in significant amounts and have therefore been defined as "rare sugars" or "rare monosaccharides" by the International Society of Rare Sugars (ISRS) [3].

1.2 Rare sugars

Although rare monosaccharides are not accessible from natural sources in significant amounts, they often hold considerable potential for various applications. Though there exists a number of interesting applications for rare pentose sugars, rare deoxygenated monosaccharides or aminated or methylated rare sugars [4], this thesis will focus mainly on rare (unmodified) hexose sugars (**Figure 1.1**). Among these, D-tagatose for instance has been suggested to be a useful low-calorie sweetener and diet supplement [5, 6] promoting weight loss [7] and mediating prebiotic properties [5]. It has also been recently investigated as a drug for treating type 2 diabetes [8, 9]. D-Psicose on the other hand was investigated as a non-calorie sweetener [10], for its antioxidant properties, and for its ability to suppress the activity of hepatic lipogenic enzymes, responsible for the fatty acid production in the liver [11]. It has also been shown to exhibit anthelmintic properties making them potential drugs against parasitic worms (helminths) [12]. D-Allose has attracted great interest due to its anti-tumor, anti-inflammatory, anti-oxidative and immunosuppressant activities [13], and L-gulose and L-galactose are precursors for the production of L-nucleosides that are potent anticancer and antiviral compounds [14]. A comprehensive summary of current and potential applications is presented in a recent review by Beerens *et al.* [4].

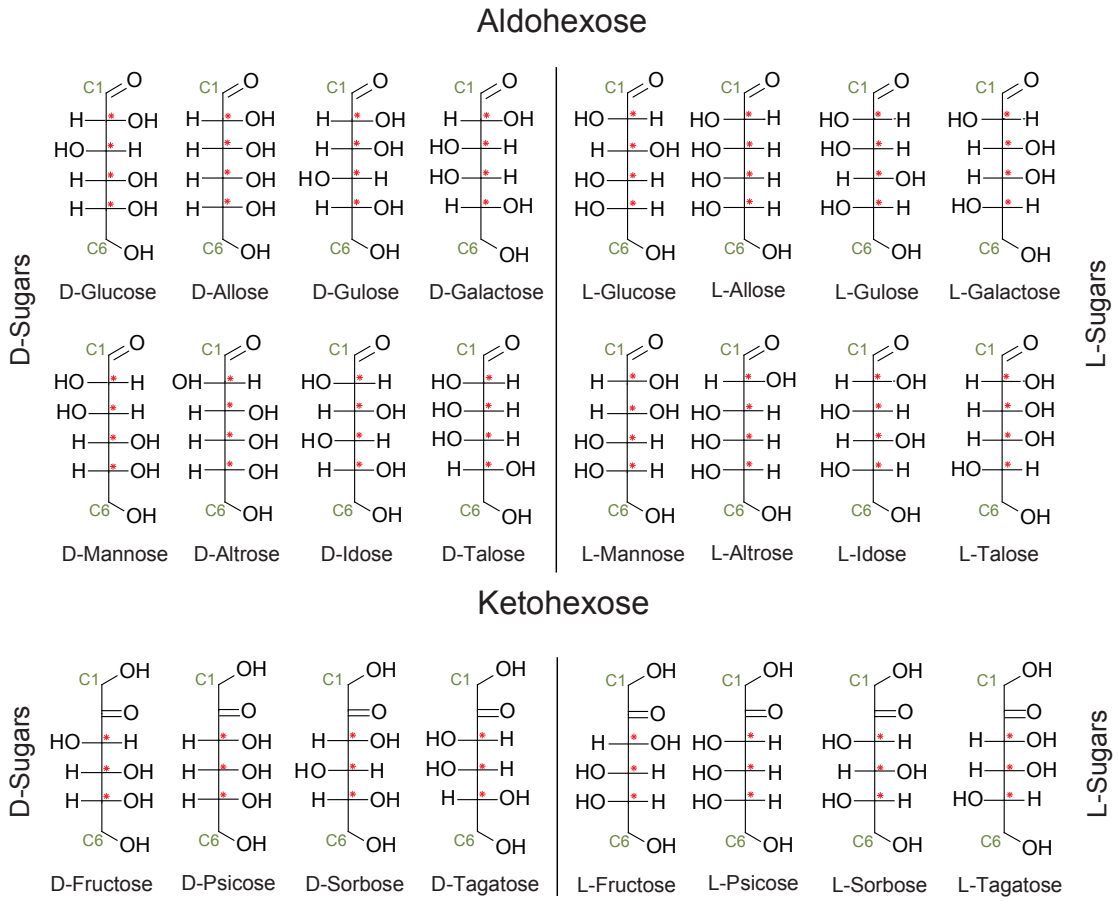

Figure 1.1. Fischer projections of all 16 (=2^4) possible standard aldohexose and 8 (=2^3) possible standard ketohexose sugars; chiral centers are indicated by red stars

1.3 Rare sugar synthesis

As the (by definition) low abundance of rare hexoses from natural sources contrasts with their great potential in the food and pharmaceutical sector, new (bio-)chemical synthesis routes of such compounds have lately gained interest in the research community. Two major strategies for rare sugar generation have been reported in literature, namely, synthesis by traditional organic chemistry and synthesis using enzymes for the biocatalytic conversion starting from abundant hexose substrates. These two approaches will be discussed in the following two paragraphs.

1.3.1 Chemical synthesis of rare hexoses

Due to the presence of multiple hydroxyl in the sugar molecule (**Figure 1.1**) the selective production of rare monosaccharides by classical chemical synthesis typically requires extensive protection group chemistry [15, 16]. These synthesis approaches usually involve multiple steps, which reduces the synthesis yields, which in turn greatly decreases the processes economy of the overall process [17] and increases the overall waste production

[18]. A notable exception in the field of rare sugar production constitutes the recently presented 5-step synthesis protocol for the production of the rare sugar L-glucose from D-glucose in high purities (99.4%) and with an acceptable process yield of 43% [19].

Further, chemical isomerization has been employed for the production of the rare sugar D-tagatose from D-galactose to a commercially significant level. D-Galactose can be derived from lactose-rich sources such as milk whey by hydrolysis into D-glucose and D-galactose, which are then separated and isomerized in the presence of an inorganic salt catalyst under alkaline conditions using calcium hydroxide as complexant [20]. Another example has been presented recently, employing the catalytic properties of Sn-beta zeolites that promote the selective epimerization of aldoses in aqueous solution at the C2 position in the presence of sodium tetraborate in a 4:1 ratio (sugar:tetraborate) [21]. However, except for the approaches using protection groups, chemical synthesis routes are limited to modifications of the C1- and C2-position (**Figure 1.1**) of the hexoses and pentoses and rely on the addition of complexing agents (boric acid, boronates or an excess of cations such as Ca^{2+}) to shift the equilibrium in favour of the desired product or to mediate selectivity, as in case of the Sn-beta zeolites, where the presence of tetraborate was found to be indispensable to avoid the corresponding isomerization taking place along with the desired epimerization reaction (see also **Figure 1.2**).

1.3.2 Enzymatic synthesis of rare hexoses

As an alternative route to the chemical routes to rare sugars the enzymatic production starting from available bulk sugars has attracted increasing attention, recently [4]. The application of biocatalysts for the synthesis of rare monosaccharides combines all the advantages of such catalysts, i.e. high stereo- and regioselectivity (obviating protection groups), operation under mostly benign reaction conditions (ambient pH, aqueous solvent, reducing the waste factor and increasing yields). Moreover, in the last decade our understanding of "tailoring" enzymes by genetic engineering has considerably increased making it possible to bring about large changes in enzyme properties (e.g. increased stability, selectivity, substrate range) [22] and thus expanding the design space of future biocatalytic processes.

In principle, 3 enzyme classes have been investigated for the enzymatic synthesis of rare sugars: (i) oxidoreductases, (ii) aldolases and (iii) iso- and epimerases. Oxidoreductases, converting carbohydrates into the corresponding sugar alcohols (polyols) were primarily used for the industrial manufacturing of rare sugar alcohols (relevant as sweetener, e.g. xylitol, mannitol) from bulk sugars [23-25]. The reduction of a bulk sugar to a sugar alcohol is however reversible, therefore these oxidoreductases were also suggested for catalyzing the transition of D-sugars to otherwise inaccessible L-sugars counterparts via D-glucitol,

D/L-galactitol, D/L-allitol or D-gulitol [26]. Izumori *et al* have suggested a strategy to reach all 24 hexoses by enzyme-catalyzed reactions using a combination of oxidoreductases [26] and iso-/epimerase (see below). For instance, the mannitol 1-dehydrogenase from *Apium graveolens* has been comprehensively studied for catalysing several interesting reactions including the transformation of galactitol to L-galactose, D-sorbitol to L-gulose and ribitol to L-ribose [27] with the latest being produced in preparative amounts achieving a productivity of 17.4 g L^{-1} day at a yield of ≈ 70% during fermentation of a recombinant *E.coli* strain [28]. Another notable biocatalyst is the recently discovered hyperthermostable D-arabitol 2-dehydrogenase from *Thermotoga maritima,* catalysing the production of the rare sugar D-ribulose starting from D-arabitol [29] or the xylitol 4-dehydrogenase from *Bacillus pallidus* which was overproduced in *E. coli* and used for the production of L-xylulose and L-xylose starting from xylitol [30]. However, the major disadvantage of the application of oxidoreductases for the production of rare sugars is their need for cofactors (NADH or NADPH), complicating reaction engineering considerably as it requires specific and efficient cofactor regeneration systems or the utilization of whole-cell biocatalysts.

Aldolase-catalyzed synthesis of rare monosaccharides from aldehydes and D—hydroxyacetone phosphate (DHAP) constitutes another approach for their manufacturing. Li *et al*. have described the simultaneous synthesis of D-psicose and D-sorbose in a ratio of 3:2 (D-psicose:D-sorbose) from dihydroxyacetone phosphate (DHAP) and D-glyceraldehyde using L-rhamnulose-1-phosphate aldolase (RhaD) and an acid phosphates (AP) [31]. In order to avoid the use of the expensive precursor DHAP, the reaction was further extended by a glycerol phosphate oxidase (GPO) and a catalase to a 4-enzyme reaction, which allowed to start from L-glycerol 3-phosphate and D-glyceraldehyde as a substrate. Recently, a first whole-cell production route was engineered based on the previously established RhaD and AP using *Corynebacterium glutamicum* as a recombinant host, which allowed to accumulate moderate amounts of D-psicose and D-sorbose when adding D-glucose and D-glyceraldehyde as a substrate [32]. In another study the thermostable enzyme L-fuculose-1-phosphate aldolase ($FucA_{T.HB8}$) from *Thermus thermophilus* was used instead of RhaD. This increased the ratio of D-psicose that could be obtained (8.4:1 for D-psicose:D-sorbose). Apart from producing D-psicose, $FucA_{T.HB8}$ has also been used for the production of L-tagatose and L-fructose starting with L-glyceraldehyde instead of D-glyceraldehyde as DHAP acceptor. However, both production routes required the application of an additional enzyme, namely an acid phosphatase to release D-psicose and D-sorbose from the originally produced D-psicose-1-phosphate and D-sorbose-1-phosphate, respectively. Although biocatalytic synthesis via aldolases can allow the synthesis of rather complex unnatural carbohydrates, it often suffers from two main drawbacks. First, most aldolases have a strict requirement for the instable and highly expensive donor substrate

dihydroxyacetone phosphate (DHAP) [33]. Secondly, they often possess imperfect stereoselectivity, resulting in a mixture of different sugar species after the reaction as demonstrated by the work of Li et al. [34], where an extensive effort was required for downstream purification.

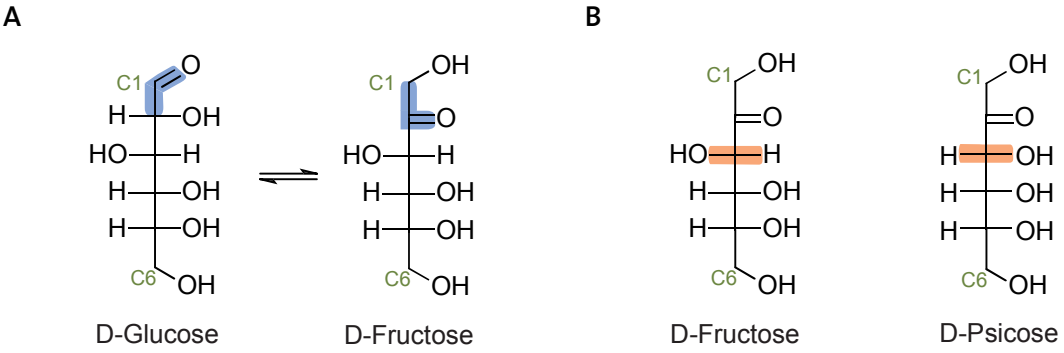

Figure 1.2. Example for (**A**) an isomerization and (**B**) an epimerization reaction

A third class of approaches for the synthesis of rare monosaccharides employs iso- and epimerase biocatalysts that can convert cheap bulk sugars into rare sugars without the necessity of cofactor regeneration or expensive starting substrates. Whereas sugar isomerases are defined as enzymes that interconvert ketoses and aldoses, exchanging the carbonyl functionality between the C1 and the C2 position (**Figure 1.2A**), sugar epimerases are able to re-orientate a single hydroxyl functionality in the molecule (**Figure 1.2B**).

In order to illustrate the structural relationship of all 24 possible hexose sugars we established a 3-dimensional representation, the so-called *sugar cube* (**Figure 1.3)**, in which neighbouring sugars can be interconverted into other by only one enzyme-catalyzed step.

The sugar cube therefore clearly suggests a generic strategy for the manufacturing of rare hexose sugars from available bulk hexose sugars by a series of simple (i.e., no cofactor regeneration required) enzyme-catalyzed steps. Such bulk sugars are the previously mentioned D-glucose (D-Glc), D-fructose (D-Frc) or D-galactose (D-Gal) that can be easily obtained from natural sources such as sugars beets, corn starch or milk. The only L-sugar that is available in large quantities is L-sorbose (L-Sor), an intermediate in the synthesis of Vitamin C via the Reichstein process, which is produced on the hundred thousand ton scale per year [35].

	Enzyme	Organism
⟷	D-Tagatose epimerase	*A. tumefaciens[36], P. cichorii [37], ..*
⟷	L-Rhamnose isomerase	*T. maritime [38], B. halodurans* [39], *P. stutzeri [40], ..*
⟷	L-Arabinose isomerase	*G. stearothermophilus [41], T. neapolitana [42], E. coli [43]*
⟷	L-Ribose isomerase	*P. stutzeri [40], Actinobacter sp. DL-28 [44]*
⟷	Ribose-5-phosphate isomerase	*C. thermocellum [45]*
⟷	D-Xylose isomerase	*T. neapolitana [46], S. murinus [47]*
⟷	UDP-Galactose-4-epimerase	*E. coli [48]*
⟷	D-Arabinose isomerase	*B. pallidus[49]*

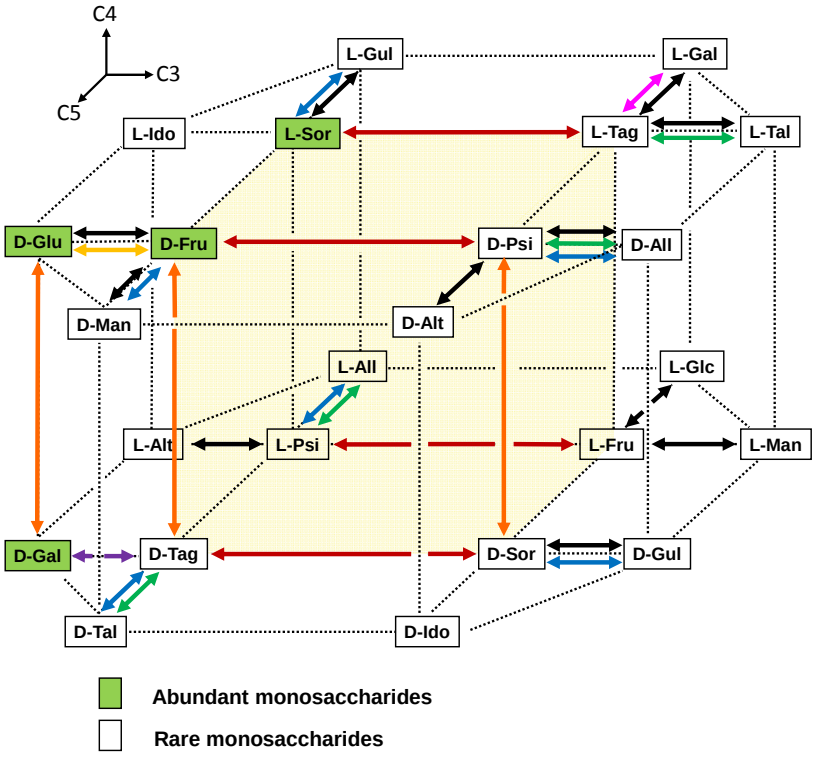

Figure 1.3. Sugar cube and known epimerases and isomerases (*courtesy of Andreas Bosshart*): Each hexose in the sugar cube differs from the adjacent/neighbouring hexose sugar by the configuration of one hydroxyl group (epimer) or the aldo-/keto functionality (isomer). The X-axis hence represents a change in conformation at the C3 position (for ketohexoses) or a change at the C2 position (between ketohexoses and aldohexoses), the Y-axis a change in conformation at the C5 position or a change at the C2 position (between ketohexoses and aldohexoses), and the Z-axis a change at the C4 position.

Starting from these 4 abundant bulk sugars, 13 of the 20 rare monosaccharides can be obtained in principle using a maximum of three iso- and epimerase enzymes [26]. Even though not all theoretically possible iso-/epimerizaion reaction are in fact catalysed by known enzymes (**Figure 1.3**), the set of available enzymes already allows accessing most of these highly interesting rare hexoses.

A key enzyme for the projected conversion constitutes the recently discovered D-tagatose epimerase (DTE) that catalyzes the reversible reaction from D-fructose to D-psicose [50], D-tagatose to D-sorbose [51], L-fructose to L-psicose [52] and L-tagatose to L-sorbose [52]. Thus, DTE accepts all 8 possible ketohexoses as substrates which positions it right in the centre of the sugar cube. D-Tagatose epimerase was first discovered in *Pseudomonas cichorii* ST-24 (PcDTE, [53]), and the gene was cloned and recombinantly expressed in *E. coli* [37, 54]. DTEs of diverse bacterial origins have been reported since then (see **Figure 1.3** for details).

On the isomerase side, many different enzymes from a variety of organisms were described to accept non-phosphorylated hexose substrates (**Figure 1.3**). Some isomerases that are responsible for the isomerization of phosphorylated pentose sugars *in vivo* such as e.g. ribose 5-phosphate isomerase from *Clostridium thermocellum*, have been described to accept also unphosphorylated hexose sugars [45].

1.3.3 Mass production of rare and bulk sugars via iso-/and epimerase reactions

The large-scale application of isomerizing biocatalysts has a long history in the sugar industry, dating back to 1967 [55], when enzymatic glucose isomerization was first accomplished on an industrial scale for the manufacturing of high-fructose corn syrup (HFCS). D-Xylose isomerase (DXI, also referred to as D-glucose isomerase), used for the interconversion of D-glucose and the sweeter-tasting D-fructose, was identified in a large number of bacteria and actinomycetes with commercial producers being patented *inter alia* from *Streptomyces murinus*, *Bacillus coagulans*, *Streptomyces rubiginosus* [55]. DXI is still one of the most important enzymes applied in food industry with HFCS production volumes in excess of 10^6 tons per year [56]. However, the maximum D-fructose content that can be directly obtained in HFCS by isomerization is restricted to approximately 42 %, thus syrups of higher fructose content (e.g. HFCS55) commonly require blending with purified D-fructose.

A first attempt to produce rare sugars in preparative amounts along the isomerase and epimerase route was conducted by Takeshita and coworkers, producing D-psicose from D-fructose using immobilized crude extract of *E.coli* recombinantly expressing PcDTE in a plug-flow-reactor (PFR) resulting in an initial conversion of 25% [57], which was further diminished as PcDTE was degraded during long-term operation at 45°C. Morimoto et al. reported on the conversion of 16.6 kg of the rare sugar D-psicose to the 1.67 kg rare sugar D-allose using an immobilized L-rhamnose isomerase from a mutant strain of *Pseudomonas stutzeri* LL172 in a PFR set-up. The reactor was operated at 42°C and conversion was kept at 30 % by reducing the flow-rate as soon as the enzyme activity was found to decline [58].

The low yields exemplified in the above examples reveal a major limitation of the rare sugar synthesis concept via iso-/epimerases, namely the often severely unfavourable position of the thermodynamic equilibrium between sugar isomers and/or epimers. Such limitations are not only encountered in iso-/epimerase reactions but are observed as well for aldolase-catalysed reactions or racemases [59].

One option to shift the yield towards the product side was recently suggested by Kim et al. for the enzymatic production of D-psicose from D-fructose. By adding stoichiometric amounts of borate (0.6:1, borate:D-fructose) to a batch reaction performed at 50°C, the overall conversion yield (60% D-psicose) could be increased 2-fold compared to the reaction performed without borate (30% D-psicose) [60]. An obvious drawback of this method is the use of a stoichiometric amount of borate, which is undesirable both in terms of waste production (borate removal) and in terms of food safety. In Europe, boric acid (E 284) and sodium tetraborate (E 285) are only authorised as food preservatives, which currently restricts their use to very small amounts (up to 4 g boric acid kg^{-1} food). At the moment, the general use of borate and tetraborate in food is re-evaluated by the European Food Safety Administration (EFSA) [61]. Additionally, this approach results in yields that are still not reaching levels that could be considered satisfactory for large-scale synthesis, and the final reaction product still constitutes a hard-to-purify mixture of two highly similar hexoses.

1.4 Integration of reaction and separation

Another solution for overcoming the thermodynamic yield limitation constitutes the integration of reaction and separation, currently representing a key strategy in the field of process rapid removal of the product upon its formation, thus allowing the reaction to continue and to use the starting material entirely or, at least, more effectively. In the field of chemical process development the integration operation of reaction and separation has been comprehensively studied [62-65] and successfully implemented on the industrial level, as demonstrated by the Eastman Kodak`s reactive distillation process for the production of methyl acetate [66, 67].

Adapting the concept of process integration for the synthesis of rare sugars could serve as a generic solution for overcoming the yield limitation in epimerase and isomerase reactions and, thus, could enable a more effective use of epimerases and isomerases in future industrial production processes. However, the potential yield improvement has some implications on the design of such integrated processes. Firstly, as substrate and product in (bio)catalysis typically exhibit a high degree of structural and chemical similarity, a highly selective and powerful separation technique is required. Secondly, the selected separation method has to be interoperable with the enzyme reaction, restricting the overall operating conditions predominately to aqueous solution. Chromatography

constitutes a highly versatile separation method that can be, depending on the selected stationary phase, operated under enzyme-compatible conditions (i.e. aqueous mobile phases). In particular ligand exchange chromatography using Ca^{2+}-substituted ion exchange materials as stationary phase (SP) and deionized water as mobile phase is widely recognized as a suitable method for the separation of mono- and disaccharides on the multi-kg to multi-ton scale, e.g. for the processing of barley syrup allowing for the production of 770 kg D-fructose per m^3 SP and day with a purity of 95% [68], the separation of HFCS (170 kg per m^3 SP and day, enrichment of fructose to around 90% [69]) or the enrichment of D-fructose (≈ 90%) from cashew apple juice with a productivity 160 kg per m^3 SP and day [70]. Additionally, continuous chromatography, technically realized as simulated moving bed (SMB) chromatography, has been studied for decades and meanwhile has evolved as a standard tool for large-scale separations [71], typically providing significantly higher productivity than batch chromatography using the same amount of desorbent [72, 73].

In principal three different process options have been discussed for the coupling of biocatalysis and SMB chromatography [59], namely, the simulated moving bed reactor (SMBR, [74]), the Hashimoto SMB process [75] and a coupled SMB-recycling concept with an external reactor (SMB&R, [59]) (**Figure 1.4**).

Most of the realized examples integrating SMB chromatography and biocatalysis belong to the first group (**Figure 1.4A**). In SMBR processes (**Figure 1.4A**) the biocatalyst is commonly added in the SMB eluent and/or the SMB feed stream. As a consequence, the biocatalytic reaction can principally take place in all sections of the SMB, which makes it particularly beneficial for biocatalytic reactions where A reacts to B and C. By continuously separating B and C, either to the extract or the raffinate outlet of the SMB, respectively, the backward reaction is prevented and the starting material can be completely converted into the products. In order to gain full advantage of the process concept the retention of the starting material A on the stationary phase should be between those of products B and C [62]. For instance, the SMBR process has been used for overcoming the thermodynamic yield limitation in lipase-catalysed esterification removing water from the reaction [76]. Additionally, the same SMBR concept has been successfully applied for addressing the problem of product inhibition at high sugar concentrations during the enzymatic inversion of sucrose [77] or lactose [78].

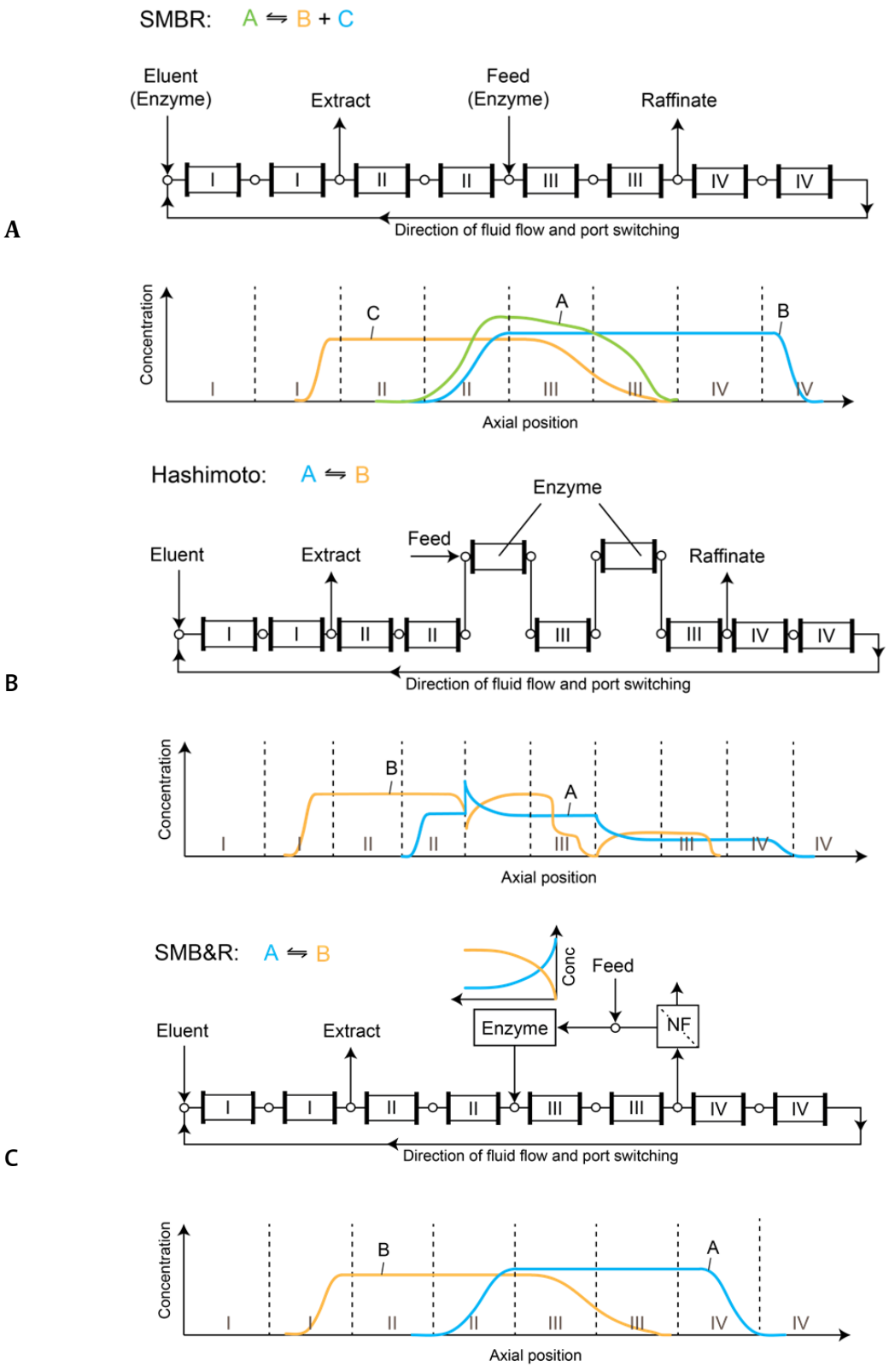

Figure 1.4. Integrated process concepts combining biocatalysis and SMB separation: (**A**) Simulated moving bed reactor (SMBR) for a reversible reaction of the type A to B and C, (**B**) Hashimoto SMB process and (**C**) coupled SMB with external bioreactor (cSMB&R) for the reversible conversion of A to B. Adapted from [59].

Clearly, the SMBR integration concept exhibits the highest degree of integration among the three discussed options, which is typically reducing the feasible design space [74] and thus resulting in reduced productivities compared to the corresponding stand-alone SMB operation [62].

In the Hashimoto process [75] the biocatalyst is immobilized in side reactors which are located only in specific SMB sections (**Figure 1.4B**) and thus prevent the enzyme reaction from taking place in the entire SMB unit. The benefit of the Hashimoto process compared to a conventional SMBR set-up becomes clear when considering reactions of the type A to B, such as the isomerization of D-glucose to D-fructose for which the process was originally developed [75]. As depicted in **Figure 1.4B** the enrichment of the more retained compound B is achieved by installing side reactors only in the section where compound A is accumulated predominantly (i.e. in this case section III). In that way, the remaining compound A is stepwise converted into the desired compound B that is separated in the direction of the up-stream located extract outlet. In sections where the product B is enriched, no side reactors are placed as they would only jeopardize the previously achieved resolution.

A coupled SMB-recycling concept (SMB&R, **Figure 1.4C**) on the other hand, consisting of an external enzyme membrane reactor (EMR), an SMB plant and a nanofiltration (NF) device, was suggested by our group as an opportunity to obtain high yields and high purities from thermodynamically limited racemase [79] and aldolase reactions [80]. In the SMB&R concept the reaction mixture is separated in the SMB and the unconverted material can be recycled via the NF device that counteracts the dilution in the SMB and re-concentrates the (diluted) raffinate stream. In such a set-up theoretically 100% yield should be possible as the product can be obtained in purities comparable to the standalone SMB.

1.5 Scope of this thesis

In this work we intend to study an integrated process strategy that combines biocatalysis in an EMR, SMB chromatography and NF for the high-yield synthesis of rare sugars. Such a process concept allows overcoming the yield limitation of equilibrium-limited biotransformations, e.g. for the investigated iso- and epimerization reaction, based on the selective removal of the product (*in situ* product removal = ISPR, **Figure 1.5A**) and the continuous recycling of the unconverted substrate, thus enabling a theoretical yield of 100% rare sugar starting from a bulk sugar substrate.

In the implementation realized in this thesis, the substrate sugar feed stream is directed to the EMR, where it is partially converted by the enzyme(s) (**Figure 1.5B**). The resulting mixture of sugars that leaves the EMR is fed to the SMB module, where the product is removed and the substrate (and intermediate) sugar(s) is (are) recycled via the NF device

back to the EMR. Such an NF concentration step is required to counterbalance the inherent dilution of the SMB operation, thus allowing the full closing of the recycling loop and therefore the complete conversion of the starting substrate into the product.

We started with a single-enzyme reaction (conversion of D-fructose to D-psicose using the key enzyme DTE, Chapter 2) and increased the complexity in the course of the work towards a multi-enzyme cascade reaction (**Figure 1.5B**, Chapter 5).

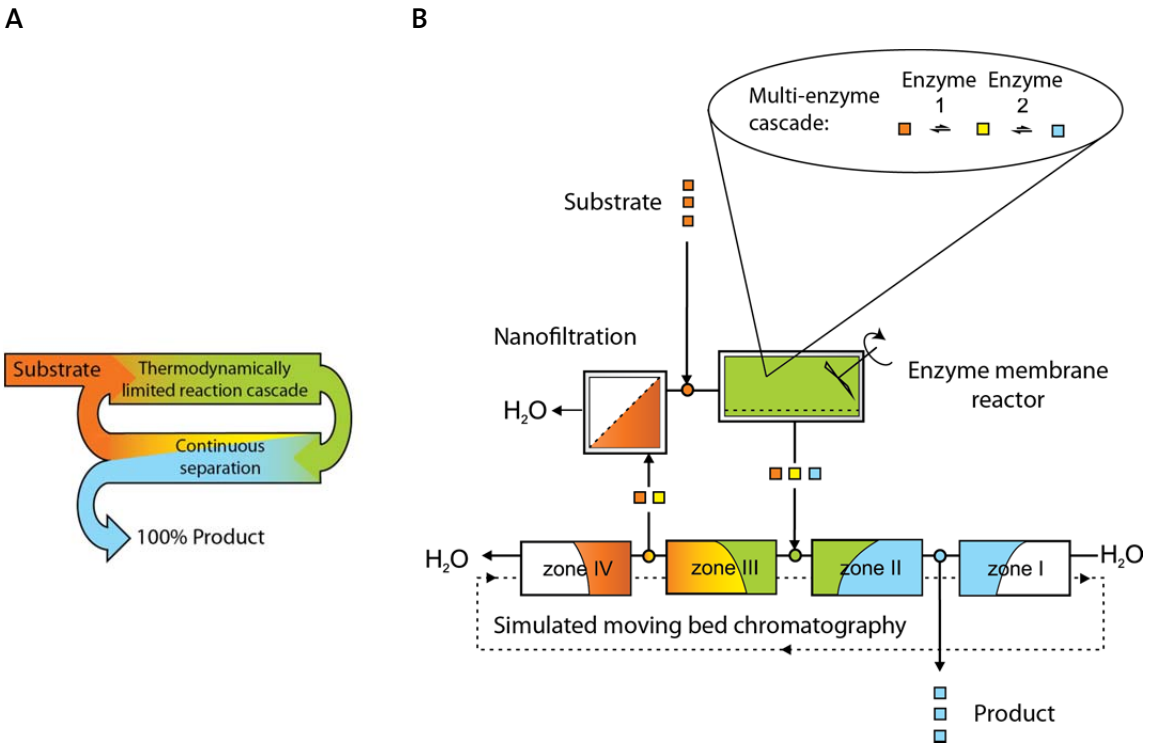

Figure 1.5. (**A**) Schematic representation of the ISPR (*in situ* product removal) principle**,** (**B**) reaction-separation integrated process consisting of an enzyme membrane reactor, simulated moving bed chromatography and nanofiltration for the production of rare sugars using a multi-enzyme reaction cascade

A major challenge that was encountered during this project was the limited stability of the applied DTE. A highly thermostable enzyme was required as elevated temperatures (> 50°C) in the process setup were considered desirable for multiple reasons: (i) prevention of microbial contamination, (ii) reduction of viscosity of the liquid stream at very high substrate concentrations, (iii) shifting the thermodynamic reaction equilibrium towards the product (as applied e.g. for the production of high fructose corn syrup (HFCS)) or (iv) increasing the enzyme reaction rate [55].

Initially, we worked with the DTE enzyme variant from the mesophilic bacterium *Agrobacterium tumefaciens* (AtDTE), which showed poor thermostability at elevated temperatures. To compensate for this circumstance, a great excess of AtDTE biocatalyst had to be supplied to the enzyme membrane-reactor to keep a constant conversion ratio

over the whole investigated runtime (see Chapter 2). Such an overloading of the reactor is unfavourable both in terms of operational reasons (overloading of the EMR might lead to a prohibitively high backpressure due to fouling of the membrane) as well as in terms of economics (most of the catalytic potential of the biocatalyst remains unused most of the time). As one of the aims of this work is the optimization of the economic and productive operation of the biocatalyst in the context of the integrated process, DTEs from another organism were investigated, namely DTE from *P. chicoriii* (PcDTE). Although this enzyme exhibited a higher thermostablility compared to AtDTE, it was still well below the requirement for a productive integrated process for the production of rare monosaccharides.

Therefore, concomitantly with this project, a significantly thermostabilized variant of PcDTE was generated in our lab, termed PcDTE Var8 that finally allowed to operate the EMR at 50°C for several days without a significant decrease in the conversion of D-psicose from D-fructose [81]. This variant allowed us to investigate the biocatalytic reaction over a wide range of temperatures and to take advantage of the higher productivity at elevated temperatures in our experimental runs (see Chapter 4). Another important aspect of the current work was the modular, model-based optimization approach that was pursued based on experimental analysis of the individual modules and the *a priori* optimization of single units, such as the optimization of the SMB in Chapter 3. This single-module optimization was followed by incorporation of all three modules in an integrated process model that allowed optimizing the complete process *per se* (see Chapter 4).

Chapter 2 constitutes a proof-of-principle study for this novel process concept, investigating the one-step epimerization of the bulk sugar D-fructose into the rare sugar D-psicose using AtDTE. Next to the first successful experimental implementation of the presented process concept, the chapter reports on important practical aspects of lab-scale process operation such as the start-up times, operational stability and the robustness of the involved unit operation. The maximum feed concentration investigated was rather low at 18 g L^{-1} D-fructose.

Chapter 3 reports on the model-based design and stand-alone optimization of the chromatographic SMB unit for the separation of the rare sugar D-psicose from its epimer D-fructose on Ca^{2+} substituted SMB columns. The inverse method was applied for parameterizing the adsorption and kinetic behaviour of the solid phase up to high feed concentrations (180 g L^{-1}) and over a wide temperature range (20-70°C). The obtained parameterization was used for SMB design based on a true moving bed (TMB) model and was verified by a series of experimental SMB runs. It was further used as a starting-point

for a Pareto optimization study addressing two cost-relevant performance parameters in SMB separation, the productivity (*PR*) and the desorbent requirement (*DR*).

Chapter 4 presents the first model-based optimization of the complete integrated process for the production of rare sugar D-psicose from D-fructose. First, an integrated process model consisting of the previously described TMB model, an EMR model and an NF model was implemented. The process model was used for the *in silico* optimization of the entire process, employing a multi-objective cost-function that accounts for the cost contributions of each involved unit operation. As biocatalyst costs are strongly depending on the projected reactor temperature, we further established a model-based procedure for characterizing the biocatalyst in terms of operational stability and catalytic activity as a function of the reactor operating temperature. Based on these estimations we analysed the process in terms of a suitable reactor temperature. Finally, we implemented the results of the simulated optimization in our existing lab-scale plant, that allowed producing significant amounts of D-psicose (95 g day^{-1}) at high purity (≈ 98%) and with very high yield (96%) using a lab-scale process implementation (60 mL SMB, 10 mL EMR).

Chapter 5 expands the integrated process concept for the first time to a multi-enzyme cascade reaction. Consequently, the previously introduced process for the production of D-psicose from D-fructose (Chapter 2 and Chapter 4) was used as a starting point and extended by two more biocatalysts in order to allow the use of the abundant and cheap disaccharide sucrose as a starting substrate. Two new enzymes were characterized and implemented into the reaction cascade, firstly an invertase, hydrolysing the disaccharide sucrose into D-glucose and D-fructose, and secondly a D-xylose isomerase, catalyzing the reversible reaction from D-glucose to D-fructose. We show that we could identify a suitable EMR operating point for such a complex system that consists of three enzymes with different stabilities and kinetics based on our previously established characterization procedure. Another challenge was the extension of the SMB separation to a 3-component mixture, which was accomplished based on an empirical approach. Finally, the successful experimental operation of the integrated process employing a multi-enzyme cascade process is presented.

Chapters 2-5 are treated as independent studies and are therefore presented with their own introduction and conclusion section. Concluding remarks on all results are given in Chapter 6, references are summarized in chapter 7.

2 Practical aspects of integrated operation of biotransformation and SMB separation for fine chemical synthesis

2.1 Introduction

Integration of product formation and separation constitutes an attractive solution for overcoming the yield-limitation of reactions with an unfavourable position of the thermodynamic equilibrium. Selective *in situ* recovery of the product (ISPR) from the reaction space in principle allows for complete conversion of substrate to product and hence 100% yield [82-84]. Such a process intensification strategy could potentially shift novel reaction routes from the academic arena into the realm of industrial application [85]. Prime candidates for such an approach are aldolase- and isomerase-catalyzed reactions that provide direct access to interesting molecule classes such as rare or unnatural saccharides and saccharide-like compounds. Classical chemical synthesis of these compounds requires frequently intensive protection group chemistry [15], motivating the development of alternative and in particular biocatalytic routes, where enzyme regioselectivity can facilitate the synthesis. However, the thermodynamic equilibrium of those direct biocatalytic reactions frequently favours the substrate [86] and the resulting limitation in product yields clearly offsets the advantages of regioselectivity and also of sustainable reaction conditions (mild temperature and pH, aqueous solvent).

In order to increase the yield in such reactions with unfavourable equilibrium selective removal of product from the reaction space while retaining the substrate is required. Since the product and substrate of a single biotransformation often do not differ substantially with respect to their physico-chemical properties, their separation requires either a highly selective auxiliary phase or a separation technology that exploits multiple equilibrium stages. The former option often cannot be realized due to the lack or the price of such a phase [82] while for the latter option a proven technology - column chromatography - is available [87]. Application of column chromatography does not permit *in situ* separation in the strict sense since a reactive chromatography approach is not applicable to the reaction types of interest, which are isomerizations and additions for isomerases and aldolases, respectively [59]. Therefore, a spatial separation of reaction and separation is required.

In principle, such a spatially separated ISPR scheme can be realized by sequential batch or continuous operation. Sequential operation of reaction and separation batches requires a number of repetitive cycles for obtaining high yields [88]. In contrast, continuous operation potentially provides directly the product in high yield and high purity (**Figure 2.1**). Additionally, simulated moving bed technology (SMB) as the technical realization of continuous chromatography, typically provides higher productivity than batch chromatography at comparable levels of solvent consumption [72] and has evolved into a standard tool for large-scale separations [89]. Furthermore, current industrial examples demonstrate the feasibility and benefit of continuous operation of biotransformations which is considered as emerging key technology in white biotechnology [90, 91]. However,

integration of these advanced technologies poses some unique challenges to the selection of material and process design. The direct coupling requires the use of the same solvent in all unit operations which is by no means a trivial constraint as established preparative chromatography often relies on organic solvents [92]. Hence, selection of an inter-operable mobile phase / reaction medium constitutes an important optimization variable for such a process.

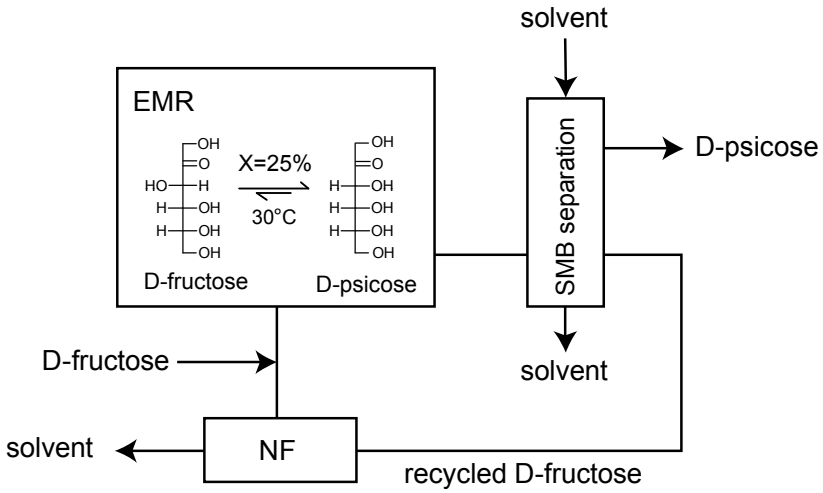

Figure 2.1. Locally separated in-situ product removal scheme for the production of D-psicose from D-fructose. The reaction takes place in the enzyme membrane reactor (EMR). The mixture of D-fructose and D-psicose is separated via simulated moving bed (SMB). D-fructose is concentrated in a nanofiltration (NF) device before re-entering the EMR. This setup enables theoretically a chemical yield of 100%.

Arguably, the production of rare sugars by enzyme-catalyzed epimerization and isomerisation reactions constitutes presently one of the most promising areas of application for such a process integration strategy: Conveniently, chromatographic separation of sugars is already based on the use of ion exchangers employing enzyme compatible aqueous solution as mobile phase [45, 69]; rare sugars like D-psicose, D-allose or D-tagatose have lately attracted considerable interest as functional food component (e.g. low-calorie sweeteners and prebiotics [93, 94]) or precursors for pharmaceuticals [95, 96]; and the currently available set of isomerases and epimerase enzymes enables to obtain most hexose stereoisomers (including those mentioned above) from cheap starting materials such as D-glucose, D-fructose, D-galactose or L-sorbose [26].

In the scope of this work a lab-scale process installation was developed and implemented that realizes integrated operation of bioreactor, SMB and nanofiltration to manufacture the rare but commercially attractive sugar D-psicose [97] from D-fructose. To our knowledge this is the first report on such an integrated process. Next to demonstrating the proof of principle, other practical aspects that equally determine the applicability of a

process such as stability, start-up and process robustness were evaluated. D-Psicose formation from D-fructose was selected as a model biotransformation, because next to the commercial interest for D-psicose, suitable enzymes – the D-tagatose epimerases (DTEs) - from different sources [36, 37] as well as a suitable chromatography material [45] were reported before.

2.2 Materials and methods

2.2.1 Chemicals

D-Psicose of high purity was produced in-house by epimerization of D-fructose using DTE and subsequent purification of D-psicose by stand-alone SMB separation (using a similar design approach as described in the results section). D-Psicose was crystallized from the collected SMB extract by first concentration by evaporation and subsequent drowning out by addition of ethanol. Crystals were washed with ethanol and dried in the exsiccator. D-Psicose purity of >99.5% was confirmed by HPLC analysis. All other chemicals were of analytical grade and purchased from Sigma-Aldrich (Buchs, Switzerland). Ultrapure water was obtained from a GenPure Water system (TKA Thermo, Germany).

2.2.2 Enzyme preparation

DTE (E.C. 5.3.1.-) from *Agrobacterium tumefaciens* was overexpressed in *Escherichia coli* BL21(DE3) from the expression plasmid pET-30a after growth in M9 medium supplied with glucose as the carbon source and induction with 0.05 mM IPTG at 18°C. Cells were harvested by centrifugation, resuspended in aqueous buffer (containing 50 mM 2-amino-2-hydroxymethyl-
propane-1,3-diol (Tris) adjusted to pH8.0 with HCl, and 1 mM $MnCl_2$) and disrupted in a high-pressure homogenizer (Haskel Hochdrucksysteme, Wesel, Germany) at 1200 bar pressure drop over the orifice. The cell free extract (CFE) was clarified from cell debris by centrifugation at 6000 g for 30 min at 4°C and stored at -80°C. In order to guarantee complete saturation of the enzyme´s active site with Mn^{2+}-ions all aliquots of thawed CFE were incubated with 1 mM $MnCl_2$ at 4°C for 180 min prior to further use. Before use in the integrated process the activity of each aliquot was determined by measuring D-psicose formation using 200 mM D-fructose as initial substrate concentration in 50 mM Tris buffer (pH 8.0) at 30°C. The initial substrate concentration was chosen to be significantly above the previously estimated K_m of 24 mM [36]. One unit (U) of DTE was defined as the amount of enzyme producing 1 µmol min^{-1} of D-psicose at 30°C and pH 8.0.

2.2.3 Operation of the enzyme membrane reactor (EMR)

Biocatalysis was performed in a jacketed 10 mL continuous stirred tank reactor (Julich Fine Chemicals, Julich, Germany) equipped with an AMICON regenerated cellulose membrane (nominal cut-off of 10 kDa) purchased from Millipore Cooperation (Bedford, USA). Unless stated otherwise, the EMR was operated at 30°C with a magnetic stirrer rotating at 200 rpm and using 100 mM D-fructose in 15 mM Tris pH 8.0 as substrate solution. The reactor was loaded with 500 U of DTE.

2.2.4 SMB columns

DOWEX 50 WX4-400 was purchased in H+-form from Sigma Aldrich (Buchs, Switzerland) and converted to the Ca2+-form by incubation with a 300 mM Ca2Cl solution for 1 h. The pretreated material was packed into PEEK columns (150 x 7.5 mm2) obtained from Omnilab (Mettmenstetten, Switzerland). The external bed porosity of all columns was measured using dextran (average molecular weight = 100-200 kDa) as non-adsorbing tracer. An average porosity of 0.41 ± 0.01 was determined. Adsorption isotherms were determined by analysis of finite injection HPLC experiments using different sample concentrations [80] of D-psicose and D-fructose (0.05 – 1.4 M) and water as mobile phase.

2.2.5 SMB set-up

The implementation of a laboratory-scale SMB-plant based on the Amersham ÄKTAbasic-10 system (GE Healthcare, Uppsala, Sweden) was described in detail previously[80]. The SMB was operated in open loop arrangement with 8 columns in a 2-2-2-2 configuration (**Figure 2.2**).

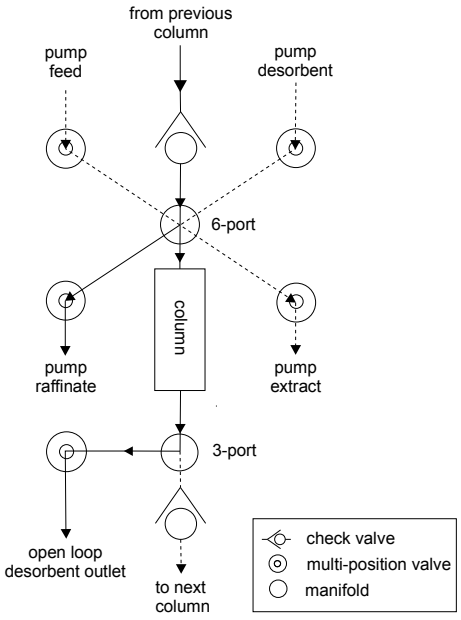

Figure 2.2. Set-up for a single column in the 2-2-2-2 SMB displaying all possible flow paths (dotted arrows). The solid arrows indicate the flow path for a column located in zone 4 (solid arrows) when no desorbent recycling is employed (open loop).

At the inlet of each column a six-port manifold was placed which connected the columns to each other and to multi-position valves that directed the SMB inlet and outlet flows, namely feed, eluent, extract and raffinate. Check valves (CV-3000, Upchurch Scientific, Oak Harbor, USA) were installed between columns to ensure correct flow direction. Back pressure relief valves (1000 psi, Upchurch Scientific, Oak Harbor, USA) were implemented

downstream of the feed and eluent pump in order to accommodate for local pressure build-up during valve switching. An additional multi-position valve that was connected to a 3-port manifold installed at the outlet of each column was dedicated to direct the waste outlet stream from zone IV in order to realize the open loop arrangement. The SMB installation including eluent reservoirs was thermostated at 25°C by housing the system in a refrigerated incubator. The SMB unit was controlled with a modified version of the UNICORN software (GE Healthcare, Uppsala, Sweden) [98, 99]. SMB design was performed based on the concept of the triangle theory [100].

2.2.6 Operation of the nanofiltration (NF)

Concentration of sugars was carried out using a custom designed cross-flow NF device (MMS AG, Urdorf, Switzerland) with an integrated gear pump (Scherzinger, Furtwangen, Germany). The NF membrane NF-90 (FilmTec Cooperation, Minneapolis, USA), a polyamide membrane with a nominal cutoff of 90 Da [101], was positioned in the jacketed annular membrane compartment providing a surface area of 28 cm^2. The NF feed was supplied by a MERCK L-6200A HPLC pump (VWR, Nyon, Switzerland). Constant flux through the membrane was achieved by using a LIQUI-FLOW flow-controller (Bronkhorst, Reinach, Switzerland) which was installed at the outlet of the retentate stream. The NF unit and the flow-controller were controlled by a Labview program (National Instruments, Austin, USA) that was provided by the NF manufacturer. For regeneration the membrane was washed for 2-3h with pure water.

2.2.7 Quantification of concentrations

Samples were analyzed on an Agilent 1200 series HPLC system equipped with a RI-101 detector using a self-packed DOWEX50 WX4-400(Ca^{2+}) column (150 x 7 mm^2) or an AMINEX Fast Carbohydrate (Pb^{2+}) column with a Carbo-P guard column (Biorad, Reinach, Switzerland). The former column was employed with pure water as mobile phase at 85°C and a flow-rate of 2 mL min^{-1} and was used exclusively for D-fructose quantification. D-Psicose quantification was conducted with the latter column using the same mobile phase at 25°C and 0.5 mL min^{-1}. Next, a DIONEX LC DX-300 system equipped with a guard column CarboPac PA1 column (50 x 4 mm^2) and a CarboPac PA1 (50 x 4 mm^2) was used for confirming purities when high accuracy was required. Samples were eluted employing an isocratic concentration of 25 mM aqueous NaOH at a flow-rate of 2.5 mL min^{-1}. They were detected via triple pulsed amperometry using an ED detector with a gold electrode (all Dionex, Sunnyvale, USA).

2.2.8 Performance parameters

In order to evaluate the performance of the integrated system and its respective subunits different parameters were applied. Conversion *X* in the reactor was defined as the ratio of concentrations of product (here, D-psicose) $c_{Psi,EMR,out}$ leaving the reactor and substrate (D-fructose) $c_{Fru,EMR,in}$ entering the reactor.

$$X = \frac{c_{Psi,EMR,out}}{c_{Fru,EMR,in}} \; [-] \qquad \textbf{Equation 2.1}$$

The purity PU_{Raff} of the SMB raffinate stream was defined as ratio of the concentration of the less retained component (D-fructose) to the total concentration of the binary mixture (D-fructose and D-psicose) in the raffinate. The extract purity PU_{Ex} was defined with respect to the more retained component, D-psicose.

$$PU_{Ex} = 100 \; \frac{c_{Psi,Ex}}{c_{Psi,Ex} + c_{Fru,Ex}} \; [\%] \qquad \textbf{Equation 2.2}$$

$$PU_{Raff} = 100 \; \frac{c_{Fru,Raff}}{c_{Fru,Raff} + c_{Psi,Raff}} \; [\%] \qquad \textbf{Equation 2.3}$$

The ability of the membrane to retain the applied monosaccharides was expressed by the rejection *REJ* that denoted the distribution of concentrations between the retentate (c_{Ret}) and the permeate side (c_P). Since the task assigned to the nanofiltration was concentration of the substrate, the rejection was expressed in terms of D-fructose concentration.

$$REJ = 1 - \frac{c_{Fru,P}}{c_{Fru,Ret}} \; [-] \qquad \textbf{Equation 2.4}$$

The total throughput *TP* of the integrated system was calculated from the extract port by:

$$TP = Q_{Ex} \; c_{Psi,Ex} [mg \; h^{-1}] \qquad \textbf{Equation 2.5}$$

The yield *Y* was calculated from the ratio of throughput and fed substrate-mass flow:

$$Y = 100 \; \frac{Q_{Ex} c_{Psi,Ex}}{Q_S c_{Fru,S}} \; [\%] \qquad \textbf{Equation 2.6}$$

2.2.9 Process simulation

SMB operation was simulated using a SMB node model combined with a transport chromatography model [92] implemented in Matlab (Mathworks, Natick, USA). Simulations of coupled EMR and SMB operation were performed applying a CSTR model for the EMR [79] and the SMB node model combined with a transport dispersive model [45]. These combined models were implemented in gProms (PSE, London, UK). The applied process parameters are summarized in **Table 2.1** and **Table 2.2**.

Table 2.1. Summary of performance parameters of each unit in integrated process

Operational unit	Performance parameters		
EMR	Equilibrium constant [-]	0.33	
SMB		D-fructose	D-psicose
	Henry constants [-]	0.99	2.55
	HETP at 1 ml min^{-1} [cm]	0.3	0.43
NF	Hexose rejection [%]	98	

Table 2.2. Flow rates used in integrated operation throughout this work and steady-state concentrations of D-fructose and D-psicose measured in the proof-of-concept-run

Stream	Flow rate [ml min^{-1}]	Concentrations	D-fructose [g L^{-1}]	D-psicose [g L^{-1}]
Q_S	0.08	c_S	18	0
$Q_{EMR,in}$	0.26	$c_{EMR,in}$	18	0
$Q_{EMR,out}$	0.26	$c_{EMR,out}$	13.5	4.5
$Q_{SMB,in}$	0.25	$c_{SMB,in}$	13.5	4.5
Q_{Raff}	0.44	c_{Raff}	7.67	0
Q_{Ex}	0.47	c_{Ex}	0	2.37
$Q_{D,in}$	1.10	$c_{D,in}$	0	0
$Q_{D,out}$	0.44	$c_{D,out}$	0	0
Q_P	0.25	c_P	0.25	0
Q_{Ret}	0.18	c_{Ret}	18.3	0

2.3 Results and Discussion

2.3.1 Process description

Integrated operation of SMB, bioreactor and NF holds great potential for the production of fine chemicals from thermodynamically limited reactions. In order to demonstrate the principle feasibility of this novel process concept, an integrated setup was realized with lab-scale equipment. Specifically, the process setup consisted of three major unit operations: (i) a 10 mL enzyme membrane reactor (EMR); (ii) a lab-scale SMB based on an Amersham ÄKTAbasic system; and (iii) a custom-made cross-flow nanofiltration unit (NF) (**Figure 2.3**).

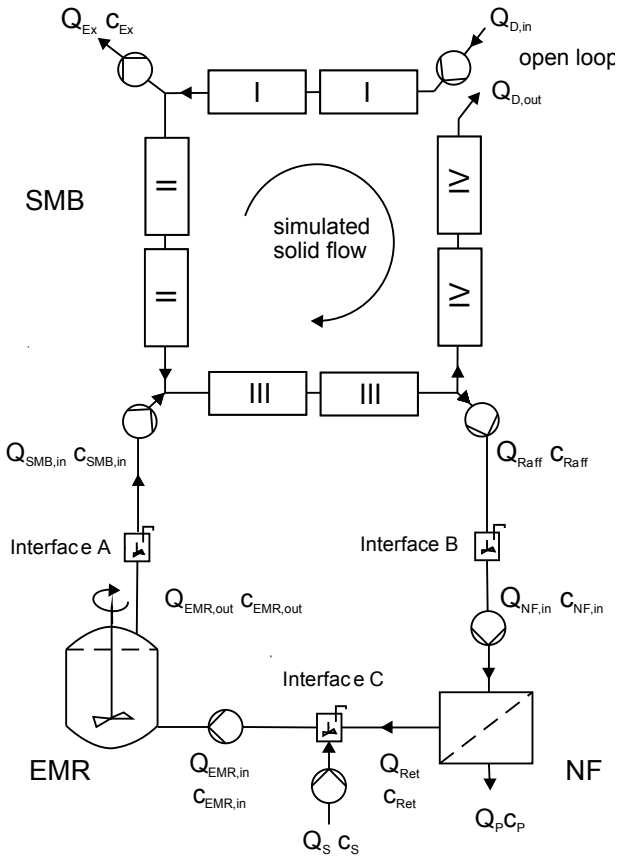

Figure 2.3. Flow scheme of the fully integrated process employing enzyme membrane reactor (EMR), open loop simulated moving bed chromatography (SMB) and substrate recycling over the nanofiltration device (NF).

In detail, the devised process concept works as follows. In fully integrated mode the substrate feed entering the system Q_s is combined with the recycled retentate stream from the NF unit Q_{Ret} and fed to the enzyme reactor Q_{EMR}. The substrate is partially converted into product in the EMR (depending on the adjusted residence time, supplied enzyme amount

and enzyme kinetics) and the obtained reaction mixture of product and substrate is directed to the SMB as stream $Q_{SMB,in}$.

The SMB unit then allows separation of binary mixtures into two outlet streams at opposing locations relative to the inlet flow. The more retained component is obtained as stream Q_{Ex} at the extract port located upstream (with respect to the fluid flow) of the inlet port. The less retained component is collected as stream Q_{Raff} at the raffinate port downstream of the inlet. Fresh eluent as stream $Q_{D,in}$ is supplied to zone I assigned to column regeneration. For the model process no solvent recycling was implemented (open loop configuration). Therefore a fraction of eluent left the system from zone IV of the SMB as stream $Q_{D,OUT}$. For a detailed description of the SMB process and the tasks assigned to the different zones please refer to reference [102].

The substrate stream (assigned to the raffinate stream in **Figure 2.3**) is directed to a NF unit in order to counterbalance the dilution introduced in the SMB separation. Depending on the rejection of the D-fructose and D-psicose by the applied membrane, the substrate mass flow is divided into a concentrated retentate stream Q_{Ret} and a diluted permeate stream Q_P. Concentration factors can be adjusted by controlling the retentate flow Q_{Ret} in order to ensure that the substrate concentration in the retentate c_{Ret} meets the design criteria. In this case it was specified to equal the feed concentration c_S.

Small stirred vessels were implemented at the interfaces before and after each unit in order to assess the concentration profiles. Therefore, the input flows were adjusted to slightly higher rates (0.05-0.10 mL min^{-1}) than the outlet flows. This demanded the use of additional feed pumps for each unit operation (**Figure 2.3**).

2.3.2 Proof of concept

Identification of suitable operating points for the integrated process requires a detailed characterization of each unit operation. Adsorption isotherms and plate numbers (as an indicator for column efficiency) were determined by analysis of HPLC elution profiles. For both components, D-fructose and D-psicose, linear isotherms were determined for the projected concentration ranges. D-Fructose was much less retained than D-psicose (**Table 2.1**) which is in line with the previously reported adsorption behavior for this system [45]. Application of the triangle theory [100] allowed identification of a safe SMB operating point with flow rate ratios m_I = 2.50, m_{II} = 1.12, m_{III} = 1.85, and m_{IV} = 0.56 and a switch time of 10 min. The significant safety margin with respect to the theoretical optimum at the vertex of the triangle can be explained by the low efficiency of the applied columns. Detailed SMB simulation accounting for the observed slow mass transfer predicted complete separation for the selected operating point. This was also confirmed in a run of the SMB alone using a

feed of 75 mM D-fructose and 25 mM D-psicose, which yielded absolute purities at both SMB outlets.

Preliminary investigations using DTE in the enzyme membrane reactor indicated that the enzyme was partially inactivated in the projected operation period of a number of days. In order to ensure constant conversion a large amount of CFE containing 500 U of DTE, was supplied to the EMR. At this loading, loss of 75 % of the enzyme activity would lead only to a reduction in the degree of conversion from 98 to 95 %. Effectively, the mixture of D-fructose and D-psicose that left the reactor was virtually at equilibrium for 10 days. Consequently EMR operation could be adequately characterized by the equilibrium constant of the epimerization (**Table 2.1**).

Initial NF experiments had demonstrated that the applied membrane retained hexoses almost completely (**Table 2.1**) and that no significant fouling occurred when operated under similar conditions as projected for integrated operation. Based on the rejection, the concentration factor and the corresponding permeate and retentate flow rates were determined (**Table 2.2**) in order to concentrate D-fructose to the process feed level.

Based on the obtained descriptions and the operating points that had been validated in stand-alone operations, appropriate flow rates were determined for a fully integrated operation (**Table 2.2**). The obtained elution order in HPLC experiments assigned the raffinate stream to the less retained D-fructose and the extract to the more retained D-psicose. Hence, the recycle was implemented at the raffinate port (**Figure 2.3**). The concentration of substrate D-fructose in the feed was set to 100 mM (18 g L^{-1}) – a relatively low concentration for sugar production but representative for fine chemical synthesis [103] and fully sufficient for this proof of principle.

Next, the fully integrated process was implemented and operated at steady state (as judged by the overall mass balance of inlet and outlet flows) for 87 h. D-Psicose could be produced in very high purity (> 99.5%, which was our analytical limit) (**Figure 2.4**). Due to the incomplete rejection (98%) in the NF unit, small amounts of D-fructose were lost in the permeate leading to a D-psicose yield based on D-fructose of 97%. The adjusted flow rates of the NF yielded - as projected - a concentration of D-fructose to the feed level proving the feasibility of the recycling strategy. The throughput for the system was 67 mg h^{-1} of D-psicose. However, please note that the throughput was not optimized and could be easily increased by a larger substrate feed and optimized design in the future.

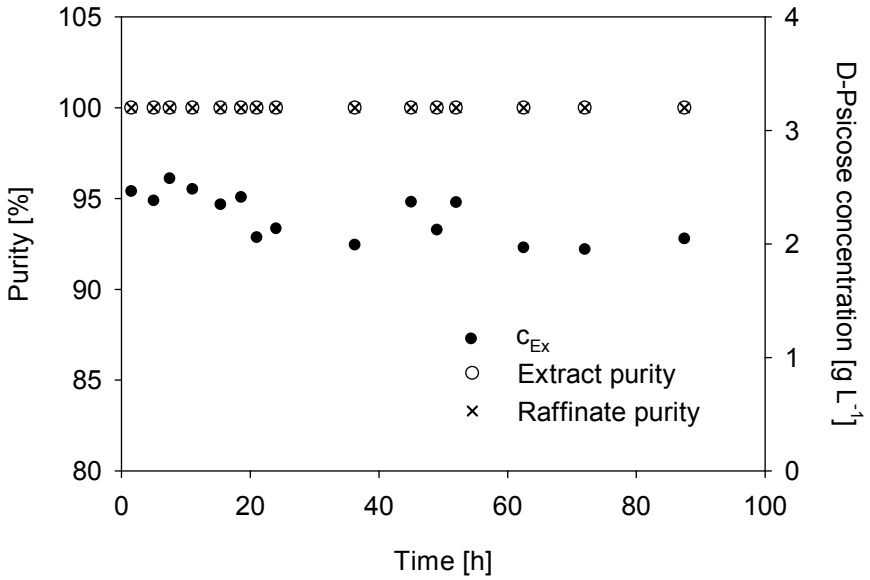

Figure 2.4. Proof-of-concept run in fully integrated mode. The product concentrations (c_{Ex}) and raffinate and extract purities were determined experimentally over 87 hours. T=0 represents the start of full process integration.

Interestingly, the pH-values measured at the interfaces A, B and C and the extract fractions differed moderately, with the pH lowered in the raffinate to 7.0 and increased in the extract to 8.5. This indicated that Tris (pK_a of 8.3), the compound that we used for buffering the system at pH 8.0, was in fact to some extent retained in its non-charged form by in the ion-exchange stationary phase, leading to an acidification of the raffinate side (SMB zones III and IV). This would have escaped our attention as Tris is poorly detectable in the used matrix with RI or UV-Vis detectors. To maintain a pH-value above 7.0 in the EMR, the Tris-buffered process feed flow (Q_S) was adjusted to pH 9 resulting in a pH of 7.4 in the EMR feed. In this way, integrated operation could successfully be conducted for three days without notable shift in pH in the respective sections. However, in order to obtain D-psicose in high purity with respect to the buffer agent we are currently screening for a suitable buffer system that is not retained by the stationary phase.

2.3.3 Start-up procedure

Next to the principle aspect of achieving close to maximum yield, the applicability of such an integrated process is further defined by the time required for the system to reach steady state or at least to obtain the product in high purity at relevant concentrations. Start-up of such a system with all units initially devoid of substrate and product and integrated from the start will take significantly longer than the sum of the individual equilibration times of the involved units. This argument can be easily made by assuming that concentration steps propagate as ideal fronts through the system depending on the residence times of

each unit. In an integrated setup the process feed becomes initially diluted when combined with – at that time - substrate-free solvent from the NF. This front of reduced concentration will propagate through the system and eventually reach the retentate recycle. In this way, a new and less diluted concentration front is generated at the interface of process feed and recycle that again propagates through the system. This step-wise increase in retentate concentrations will continue until the feed concentrations is reached.

Obviously more efficient strategies would be preferred for start-up. Initial experiments clearly indicated that the start-up of the substrate-free NF constituted a limiting factor with very long equilibration times (> 20 h with a feed of 100 mM D-fructose and a concentration factor of 5). The considerable start-up period of the concentration device is due to the high dead volume (approx. 40 mL) and the inherently slow equilibration of crossflow filtration with a partial retentate recycle. Even though the concentration factor applied in the integrated operation was only about half that value (*VCF*=2.4), NF start-up times in this order of magnitude are clearly not feasible when the entire processing time is only on the order of a number of days. Therefore we chose to pre-fill the retentate side of the NF unit with a D-fructose solution adjusted to the concentration projected for steady state operation of the integrated process (in this case, 100 mM D-fructose). The rationale behind this approach was that the retentate recycle could be instantly established when connecting the thus pre-equilibrated NF to the sequence of EMR and SMB after start-up. Obviously this can be only sustained if the set concentration factor yields the projected retentate concentration from the SMB raffinate in stationary operation which seems perfectly feasible with careful design.

Having identified a short-cut start-up for the NF unit, different strategies for EMR-SMB start-up were evaluated. Sequential start-up of EMR and SMB was tested by connecting the SMB to the EMR after uniform concentration profiles at the EMR outlet were obtained for a prolonged period of time (**Figure 2.5**). Roughly both units produced close to steady-state concentrations after 120 min of operation. After constant extract and raffinate concentrations were obtained (after 600 min) the recycle loop with the pre-equilibrated NF unit was implemented. Integration was established by connecting the retentate flow Q_{RET} to the interface vessel C and simultaneously reducing the feed stream Q_S from 0.26 to 0.08 mL min^{-1}.

As expected the implementation of the pre-equilibrated NF did not perturb the stationary state of the EMR-SMB sequence as judged by the invariant purities (**Figure 2.5**) and concentrations (data not shown) at the SMB outlets. The evolution of EMR and SMB outlet concentration profiles is characterized by an initial lag phase with little of either of the involved species in the outlet, then a steep increase in concentrations followed by a slow approximation of the eventual steady state concentration (**Figure 2.5**).

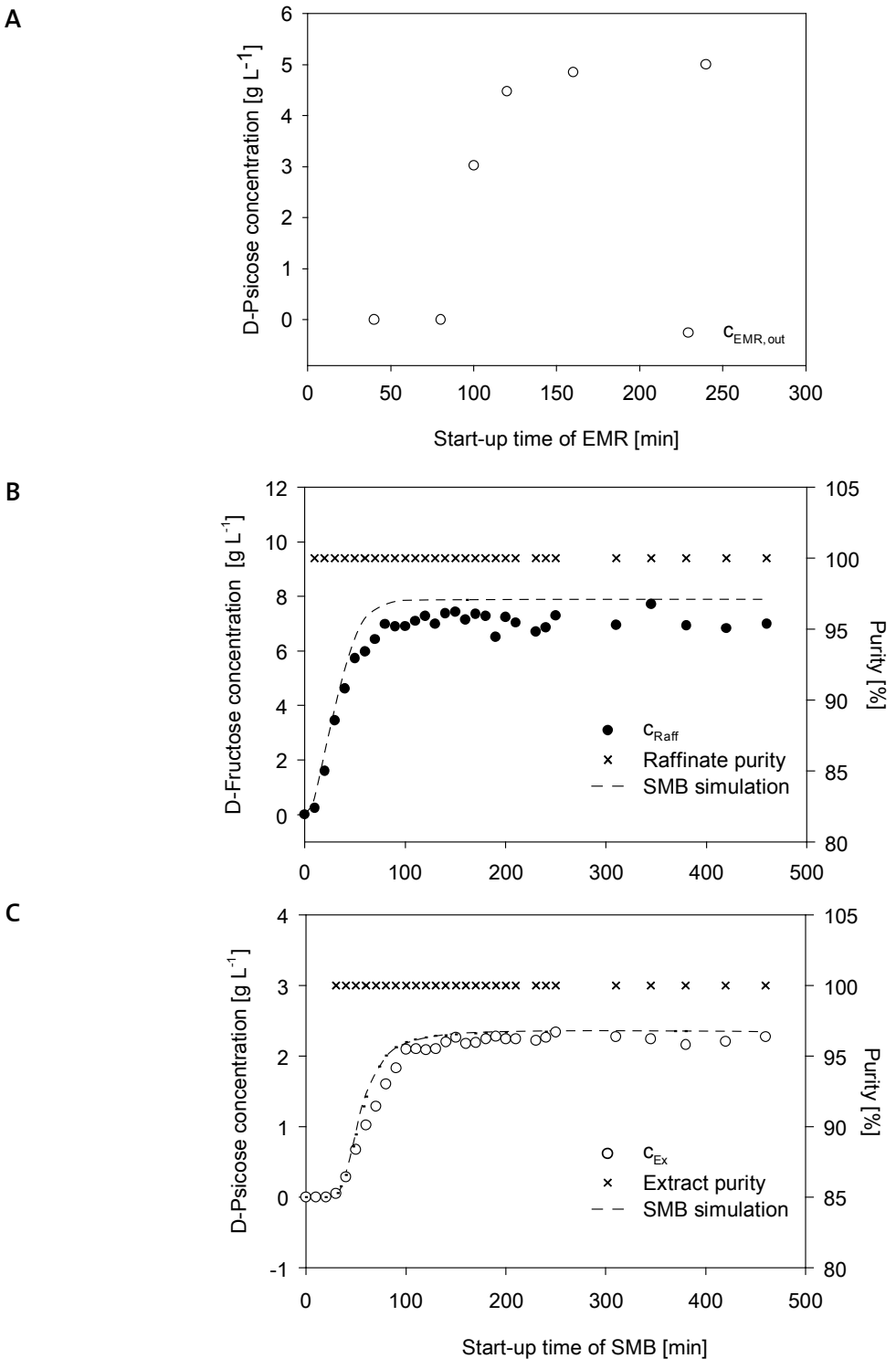

Figure 2.5. Concentration profiles and purities obtained after sequential start-up of EMR and SMB and coupling after 300 minutes. Profiles for (**A**) D-psicose concentration in the outlet stream of the EMR, (**B**) D-fructose concentration and purity of the SMB raffinate stream, (**C**) D-psicose concentration and purity of the SMB extract stream. Dashed lines represent the model prediction using a detailed SMB model.

Arguably, the transition between steep increase and slow approximation constitutes the appropriate time point for coupling the EMR to the SMB and collection of D-psicose at relevant concentrations at the SMB extract. For both units this transition occurred after approximately 120 min yielding a minimal start-up time of roughly 240 min. Please note that SMB purities were not compromised during the whole start-up procedure.

Next, starting the process with initially coupled EMR and SMB constitutes another promising option that in principle enables fast equilibration as the evolving concentration profile from the reactor would support SMB start-up. Simulation of coupled EMR-SMB operation supported this argument, suggesting an equilibration time of approximately 300 min, at which time point the deviation from the steady state mass balance was predicted to be smaller than 2%. The extract should reach usable extract concentration (arbitrarily set at 90% of the steady state concentration) after approximately 200 min.

In summary, there are a number of options for efficient start-up of the integrated process that allow a reduction of the start-up period to less than the sum of contributions of SMB and EMR. For the investigated system, the start-up could be performed in 200-300 min depending on the strategy, which is definitely acceptable for the projected operation time. In general, similar start-up strategies should be applicable to large-scale operation.

2.3.4 Robustness

For industrial application it is important that the process can withstand at least to some extent fluctuations in the operating variables. Such fluctuation can originate from deteriorating materials such as the NF-membrane or the stationary phase resulting in reduced rejection in NF operation or changes in the adsorption behavior of the SMB. Next, enzyme inactivation at some point results in decreasing conversion in the reactor leading to gradually changing SMB feed concentrations. In order to derive a general impression on how fluctuations propagate through the system and how they affect the performance of the integrated process, the feed concentration profile was subjected to a step gradient.

Based on the derived equilibration times we assumed that perturbations would migrate slowly through the systems and hence the effect of the recycle could only be accessed by excessively long experimentation times. Thus, for the sake of simplicity EMR, SMB and NF were operated in sequence without recycle and the response to a two-fold increase in feed concentration was recorded for almost 9 h. Due to the excess of supplied biocatalyst the conversion in the reactor remained unaffected by the concentration step and consequently the concentrations at the reactor outlet gradually increased to twice the initial value over approximately 200 min (**Figure 2.6**). Please note that the difference to the start-up equilibration time is due to presence of interface C in this experiment (**Figure 2.3**).

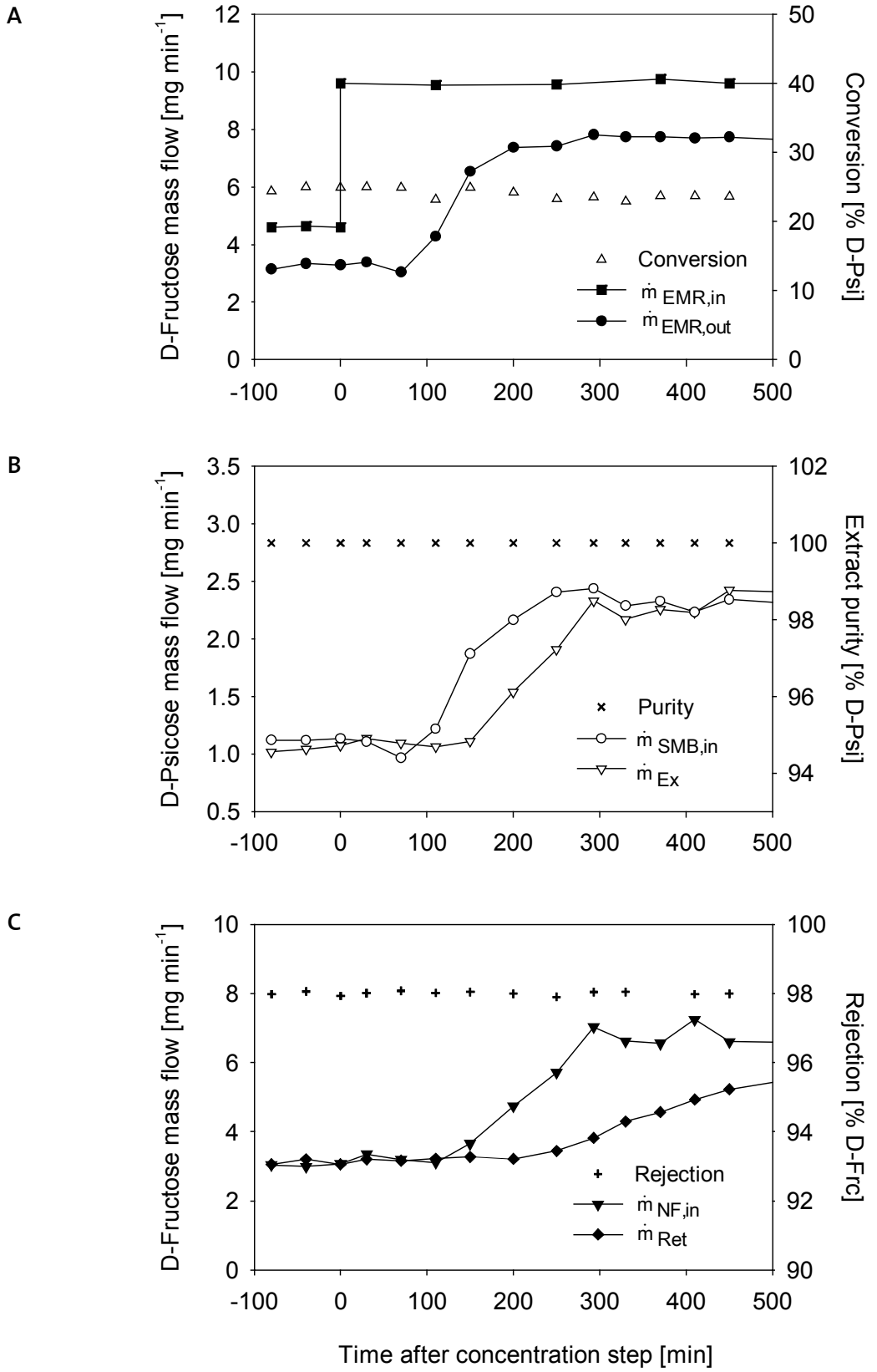

Figure 2.6. Response of the coupled EMR-SMB-NF system to a concentration step in the process feed introduced at t=0. For better comparison, the state at the respective outlets is characterized by the mass flow (**A**) EMR (**B**) SMB and (**C**) NF.

The SMB unit reached a steady-state with the new concentration regime after approximately 300 min without changes in the purity of extract or raffinate. Since the applied chromatographic system relies on linear isotherms (meaning there is no competition between D-fructose and D-psicose at the stationary phase binding sites and no capacity limitation) both species move independently of each other and of their respective concentration [87]. Consequently, the obtained constant extract and raffinate purities upon a change in feed concentration are fully supported by linear chromatography theory. The gradually increasing concentrations in the raffinate resulted in a slow increase in retentate concentrations. Due to the slow dynamics of the crossflow filtration, the concentration unit did not reach steady-state to the new concentration regime within the timeframe of the experiment, confirming our initial assumption. However, the obtained results can be transferred to predict the response of the fully integrated process upon a similar shift in the process feed. In fully integrated operation the shift in the process feed will initially be diluted by the retentate recycle resulting in a moderate increase in D-fructose concentration in the EMR feed (130 mM calculated from the flow rates given in **Table 2.2** and assuming 100 mM D-fructose in the retentate feed).

The EMR feed concentration will eventually converge to the process feed concentration according to the mechanism described for the start-up with a fully integrated system. This final state represents exactly the state of the EMR and SMB that was probed in the experiment, hence uncompromised purities can be expected also for the integrated case. Considering that roughly after 5 h the first traces of the concentration step were observed in the retentate, the time to approach the new steady state will be presumably in the range of days, demonstrating the inertia of such integrated systems.

2.3.5 Process stability

The economic feasibility of such an integrated process heavily depends on the time the process can be run without down-time. All involved unit operations are in principle prone to different sources of performance reduction. Enzymes, in particularly in cell free extracts, are potentially subject to numerous irreversible inactivation mechanisms such as proteolysis, oxidation, aggregation, loss of cofactor or shear stress induced by vigorous stirring [104]. Therefore the pool of active enzyme becomes gradually depleted which can be balanced by supplying sufficient initial amounts of enzyme to the reactor. Nevertheless, all enzyme reactions will show decreasing performance over a certain time scale depending on the enzyme´s stability. High concentrations of compounds and buffering agents potentially cause swelling of the stationary phase leading to altered velocities of the compounds and increased back pressures [105]. Next, aging effects can occur as irreversible adsorption of contaminants or chemical modifications, both of which reduce

the number of available adsorption sites resulting in changes in the adsorption behavior [92]. Membrane fouling due to irreversible adsorption of matter typically increases the pressure drop over the membrane resulting in lower rejections and higher energy consumption [106]. In order to estimate the stability of the overall process, the respective stand-alone units were investigated applying conditions similar to the integrated process. The EMR supplied with 500 U of enzyme provided constant conversion for a period of 10 days. However, the back pressure of the EMR ultrafiltration membrane steadily increased which might be due to degraded proteins causing membrane fouling. Due to pressure limitation of the membrane and the reactor the reaction was stopped at a pressure drop of 25 bar over the membrane after 10 days. During the course of the whole study the same NF-90 membrane was used and no irreversible changes in membrane performance were observed. The observed pressure increase during operation was rather moderate indicating a potential for operation of at least 10 days. Furthermore, please note that the reactor was heavily overloaded with enzyme (suggesting potential for much smaller protein loadings) and we have not yet applied molecular biology methods to increase enzyme stability. Adsorption behavior of the SMB columns was frequently assessed by determination of Henry constants over a period of several weeks that included a number of multiple-day SMB runs. The results indicate that retention decreased for both D-fructose and D-psicose under prolonged SMB conditions. However the columns could be regenerated by flushing them with a solution of 0.1 mM $CaCl_2$ for 24 h. After the regeneration step, the Henry constants were back to their original level. Using the current material we conservatively estimate potential process time to approximately 5 days due to the limited stability of the enzyme and the associated pressure drop increase over the membrane. However most of the bottlenecks can be addressed with available technologies such as enzyme immobilization [107] or enzyme engineering [108, 109] for biocatalyst stabilization or SMB cleaning in place approaches for regenerating the columns during SMB operation [99].

2.4 Conclusions

We have demonstrated for the first time the experimental implementation and successful operation of a fully integrated process consisting of a bioreactor, SMB separation and concentration by nanofiltration. The yield obtained in integrated operation (97 %) constitutes a drastic improvement compared to reactor standalone operation (max. 25 %). Furthermore, the product is obtained in high purity (> 99.5 % with respect to D-fructose) facilitating further work-up. The principle feasibility of this process with respect to critical properties such as stability, robustness and start-up time was further demonstrated. In summary, we provide here a proof of concept for this integration strategy. Obviously the applied conditions were not optimized. In order to judge the full potential of this strategy with respect to cost or productivity process optimization relying on model-based design needs to be performed. Preliminary data on the performance of DTE suggests that the process can be operated at much higher feed concentrations, up to the molar range, and an economic process can be derived by engineering a more stable and active DTE variant. This view is supported by literature examples on operation of comparable isomerase reactions at high substrate and product concentrations [110] and successes in enzyme engineering for stabilization [108, 109].

The obtained results can in principle be translated to all SMB-EMR-NF process schemes such as the integration of SMB enantioseparation and enzymatic racemisation for high-yield production of a single enantiomer from a racemate (the unifying topic of this special issue). Albeit, it has to be noted that SMB performance of chromatographic systems with more complex isotherms (e.g. Bi-Langmuir typically observed for chiral separations) depends largely on the applied process feed concentration [100]. Therefore, such systems would be more prone to non-compliance with specifications upon process disturbances, in particular upon concentration changes.

3 Multi-objective optimization for an economic production of rare sugars using simulated moving bed chromatography

3.1 Introduction

Less abundant (or "rare") sugar stereoisomers [26] are attracting interest for potential pharmaceutical and food applications, e.g. as chiral building blocks, low-calorie sweeteners with low glycemic indexes, and in view of their anti-plaque [5], anti-ischemic [111], anti-diabetic [8] and neuroprotective effects [30]. However, their limited natural occurrence makes recovery from natural sources economically unattractive and favors enzymatic or chemical manufacturing routes starting from cheap bulk sugars [3, 4]. The biocatalytic one step-conversion of bulk into rare sugars by iso- or epimerization is particularly attractive due to the requirement for only one (bio)catalyst and the absence of protection group chemistry. However, this strategy suffers from an unfavorable position of the thermodynamic equilibrium [59, 86, 112] and thus requires combination with a subsequent separation of the resulting isomeric mixture.

A case in point is the production of the hexose sugar D-psicose, which represents an interesting target molecule due to a number of future clinical applications, e.g. as metabolic regulator of glucose and lipid metabolism [113, 114], as neuroprotector [30] and as scavenging molecule for reactive oxygen species [115]. D-Psicose can be easily produced by C3-epimerization from D-fructose, catalyzed by the enzyme D-tagatose epimerase (DTE,[50, 57]). In this specific example the enzymatic route is strongly favored as, in contrast to other rare sugars that have been recently addressed by chemical iso- or epimerization using Sn-beta zeolites in the presence of sodium tetraborate [21], to the best of our knowledge no inorganic catalyst for C3 epimerization has been discovered yet. Importantly, the epimerization of D-fructose leads to fructose/psicose mixtures, which need to be separated before application. For example, a reaction at 50°C was found to equilibrate at a ratio of approximately 72/28 D-fructose/D-psicose (this work), while the equilibrium is shifting further towards D-fructose with decreasing reaction temperatures (e.g. 75/25 at 25°C [116]).

Two fundamental strategies have been suggested for separating the two epimers, extraction and chromatography. Solvent extraction with derivatized boronic acid carriers was primarily investigated for the purification of sugars from complex biological matrices like lignocellulose or hemicellulose hydrolysates [117, 118] as well as for the selective extraction of D-tagatose from mixtures with D-galactose [119]. However, this method suffers currently from high costs, leakage of inedible boronic acids, and low extraction rates [118, 120]. Alternatively, chromatographic processes have been suggested for several rare sugar separations and were demonstrated on the analytical scale using batch chromatography [50-52, 121]. Predominantly, ligand exchange chromatography [122, 123] was used employing sulphonated polystyrene-divinyl-benzene polymer resins loaded with Ca^{2+} and water as mobile phase [50-52, 121, 124]. Such systems provide small to medium selectivity at low resin costs. Their operation can be further intensified by continuous

chromatographic processes such as simulated moving bed (SMB) chromatography, which has been found to deliver high resolution for low-selectivity separations due its countercurrent operation and has been demonstrated to be particularly favorable for the low efficiency found in bulk sugar chromatographic separations [125]. As SMB chromatography can be rapidly scaled up from lab via pilot to production-scale [71] and displays increased productivities (*PR*) combined with reduced solvent consumption compared to comparable batch separations [89, 126], it constitutes an economically promising process option to obtain suitable quantities of rare sugars. Correspondingly, SMB chromatography is already used for the separation of bulk quantities of sugar mixtures, including the separation of glucose and fructose for the production of high-fructose corn syrup and the purification of sucrose from sugar beet molasses, with product volumes in excess of 10^6 and 10^5 tons per year, respectively [56]. It is also being investigated for the manufacturing of the pentose L-ribose from L-arabinose and D-psicose from D-fructose [45, 127]. However, although in both examples high purities (*PU*) could be the achieved, the *PR*'s of the investigated rare sugar separations turned out only moderate, mainly due to the standard nature of the applied design routines and leaving much room for improvement. Next to *PR*, which constitutes a major aim in SMB design, desorbent requirement (*DR*) was revealed to have a great impact on the overall SMB operating costs [128]. Therefore, especially in sugar processes, where the costs for the solid phases are relatively low in comparison to, for example, processes employing chiral stationary phases, reducing the required amount of desorbent has become a major interest [125]. Since the aim of optimizing for high *PR* and low *DR* describes opposite trends, Pareto optimization was used as a valuable tool to incorporate a trade-off into SMB optimization [72].

Here, we implemented and validated a model-based design for an SMB plant for the separation of a rare sugar which we subsequently used for a multi-objective Pareto optimization of the SMB separation of D-fructose and D-psicose. We included temperature as a variable, which influences both, thermodynamics and kinetics of the separation process and emerged as one of the key process parameters for process optimization. Finally, in view of possible separation-integrated production processes, we also investigated the potential of reduced purities in the non-product stream.

3.2 Theory

This section contains all equations used for the determination of the parameters and for the true moving bed (TMB) simulation and optimization. Where appropriate, the equations are discussed in more detail in the Results section.

3.2.1 Parameter determination using the inverse method (IM)

3.2.1.1 System peaks

The system peaks, representing numerical descriptions of the inlet boundary concentrations c_{sys} over time, were produced by fitting experimental inlet concentration profiles with Gaussian functions:

$$c_{sys} = \frac{A}{\sqrt{2\pi\sigma}} exp\left(\frac{(t-t_p)^2}{-2\sigma^2}\right) \qquad \textbf{Equation 3.1}$$

where A denotes the peak area, σ the peak variance, and t_p the elution time of the peak maximum. In case of long injection pulses (e.g. 2 min) the system peaks usually reached a concentration plateau which was then approximated using a sequential function in which the front (*FR*) and rear (*RE*) section of the concentration plateau were described by half-Gaussian functions **Equations 3.2 and 3.4** and the middle section by the linear function of **Equation 3.3**, respectively:

$$t < t_1 \colon c_{sys} = \frac{A_{FR}}{\sqrt{2\pi\sigma_{FR}}} exp\left(\frac{(t-t_1)^2}{-2\sigma_{FR}^2}\right) \qquad \textbf{Equation 3.2}$$

$$t_1 < t < t_2 \colon c_{sys} = m\,t + c_0 \qquad \textbf{Equation 3.3}$$

$$t_2 < t \colon c_{sys} = \frac{A_{RE}}{\sqrt{2\pi\sigma_{RE}}} exp\left(\frac{(t-t_2)^2}{-2\sigma_{RE}^2}\right) \qquad \textbf{Equation 3.4}$$

Here, t_1 and t_2 are the chosen time points at the start and end of the plateau.

3.2.1.2 Chromatographic and adsorption model

A transport-dispersive chromatography model (TDM) was used accounting for a finite rate of mass transfer between liquid and solid phase, axial dispersion, and convection in the liquid phase where *i* denotes for each compound (*i*= 1, 2 with 1= D-psicose, 2= D-fructose),

$$\frac{\partial c_i}{\partial t} + u\frac{\partial c_i}{\partial x} + F\,k_i a\,(q_i^* - q_i) = D_i\frac{\partial^2 c_i}{\partial x^2} \qquad \textbf{Equation 3.5}$$

$$\frac{\partial q_i}{\partial t} = k_i a\,(q_i^* - q_i) \qquad \textbf{Equation 3.6}$$

Transforming to dimensionless numbers using $u_i = Q/\varepsilon A_C$, $t_o = L/u$, $\tau = t/t_o$, $\xi = x/L$, $St = k_i a t_o$, $Pe = uL/D$:

$$\frac{\partial c_i}{\partial \tau} + \frac{\partial c_i}{\partial \xi} + F\,(q_i^* - q_i) = \frac{1}{Pe}\frac{\partial^2 c_i}{\partial \xi^2} \qquad \textbf{Equation 3.7}$$

$$\frac{\partial q_i}{\partial \tau} = St\,(q_i^* - q_i) \qquad \textbf{Equation 3.8}$$

Linear isotherms were assumed:

$$q_i^* = H_i c_i \qquad \textbf{Equation 3.9}$$

Here, u is the linear flow velocity of the liquid phase, x describes the spatial coordinate, q^* is the equilibrium concentration in the solid phase, k is the mass transfer coefficient between the mobile and solid phase, H is the Henry coefficient and F represents the phase ratio $(1-\varepsilon)/\varepsilon$, with ε being the extraparticle porosity, A_C represents the column cross-section and Q the fluid flow-rate. The axial dispersion coefficient D represents all discrepancies of the fluid dynamics from plug flow behavior and is theoretically composed of contributions of molecular and Eddy diffusion [129]. However, in practice the contribution of molecular diffusion has been shown to be negligible compared to the Eddy diffusion [130] leading to:

$$D_i \approx u\, d_p \lambda_i \qquad \textbf{Equation 3.10}$$

with d_p denoting the average particle diameter of the solid phase and the dimensionless parameter λ characterizing the packing quality of chromatographic beds.

3.2.2 TMB model

TMB models were previously demonstrated to provide an accurate representation of SMB separations while requiring only reduced computing efforts [131]. The single-column model introduced in section **3.2.1.2** can be easily extended to a multi-column TMB model,

$$\frac{\partial c_i}{\partial t} + u_j \frac{\partial c_i}{\partial x} + F\,k_i a\,(q_i^* - q_i) = D_i \frac{\partial^2 c_i}{\partial x^2} \qquad \textbf{Equation 3.11}$$

$$\frac{\partial q_i}{\partial t} - u_{SP}\frac{\partial q_i}{\partial x} = k_i a\,(q_i^* - q_i) \qquad \textbf{Equation 3.12}$$

where j represents the SMB section number ($j = 1,\ 2,\ 3,\ 4$) and u_{SP} the velocity of the solid phase. A node model is used to connect the different SMB sections [132].

The pressure drop ΔP along one column length L is given by Darcy's law:

$$\frac{\Delta P}{L} = \alpha\, u\, \eta \qquad \textbf{Equation 3.13}$$

with α as the specific bed resistance depending on the properties of the packing and η as the dynamic viscosity of the fluid phase.

In case of multi-column chromatography the total SMB pressure drop ΔP_{SMB} needs to be expressed as the sum of single section pressure drops as different flow rates are established in the different SMB sections [133, 134]. As column packings, valves and pumps of the SMB unit are specified for a certain pressure regime, ΔP_{SMB} needs to be smaller than or equal to a maximum permissible pressure drop ΔP_{max} (**Equation 3.14**) which was used to impose a lower limit to the switch time t_{sw} for a given set of m-values and a given column length [133]:

$$\Delta P_{SMB} \leq \Delta P_{max} \qquad \textbf{Equation 3.14}$$

$$t_{sw} \geq \frac{\varepsilon L^2 \alpha\, \eta}{\Delta P_{max}} \sum_j \left(1 + F m_j\right) \qquad \textbf{Equation 3.15}$$

The volumetric flow-rate $Q_{SMB,j}$ [73] in each section j of the SMB is described by:

$$Q_{SMB,j} = \frac{m_j\, V_j(1-\varepsilon) + V_j \varepsilon + V_{j,D}}{t_{sw}} \qquad \textbf{Equation 3.16}$$

where m_j is the dimensionless flow-rate ratio, describing the ratio between the net fluid flow rate and the net solid flow rate, V_j is the empty column volume per section, and $V_{j,D}$ denotes for the plant dead volume per section, which can be computed from the dead volume per column (previously determined to be 0.1 mL per column [135]) and the number of columns.

3.2.3 Performance parameters

PU's at the SMB outlet streams were defined as

$$PU_{Ex} = 100 \frac{c_{1,Ex}}{c_{1,Ex} + c_{2,Ex}} [\%] \qquad \textbf{Equation 3.17}$$

$$PU_{Raff} = 100\, \frac{c_{2,Raff}}{c_{1,Raff} + c_{2,Raff}} [\%] \qquad \textbf{Equation 3.18}$$

with the suffixes *Ex* and *Raff* denoting the SMB extract or the raffinate stream.

PR is defined as mass of product recovered per total column volume (V_T) and time

$$PR = \frac{Q_{Ex} c_{1,Ex}}{V_T} \left[\frac{g}{L\ h}\right] \quad \textbf{Equation 3.19}$$

where $Q_{Ex}c_{1,Ex}$ is the through-put (*TP*) of the SMB plant. *DR* is defined as the volume of mobile phase entering the SMB in the desorbent stream (*D*) per recovered mass of product

$$DR = \frac{Q_D}{Q_{Ex} c_{1,Ex}} \left[\frac{L}{kg}\right] \quad \textbf{Equation 3.20}$$

The volumetric concentration factor (*VCF*) of the product is defined as the ratio of the concentration of the product in the extract stream and the concentration of the product in the feed stream (*F*):

$$VCF = \frac{c_{1,Ex}}{c_{1,F}} [-] \quad \textbf{Equation 3.21}$$

Yield *(Y)* is defined as amount of product recovered from the extract stream per amount of product fed within a switching period:

$$Y = \frac{Q_{Ex} c_{1,Ex}}{Q_F c_{1,F}} [-] \quad \textbf{Equation 3.22}$$

3.2.4 Optimization and objective function

Numerical optimization of the TMB model was carried out by minimizing the objective function *f*:

$$MIN \rightarrow \quad f = \omega \frac{1}{PR} + (1 - \omega)\, DR \quad \textbf{Equation 3.23}$$

Allowing the decision variable ω to take values between 0 and 1 enables a comprehensive coverage of all possible trade-off scenarios between *PR* and *DR*. The boundaries ω = 0 and ω = 1 corresponded to optimization of only a single objective, either minimizing *DR* or *PR*.
The optimization was performed using Δm (positive values) instead of *m*-values in order to exclude infeasible *m*-value sets. Thus, the five free variables for optimization summarize as m_1, t_{sw}, Δm_1, Δm_2 and Δm_3:

$$m_2 = m_1 - \Delta m_1 \quad \textbf{Equation 3.24}$$

$$m_3 = m_2 + \Delta m_2 \quad \textbf{Equation 3.25}$$

$$m_4 = m_3 - \Delta m_3 \quad \textbf{Equation 3.26}$$

3.3 Materials and methods

3.3.1 Chemicals

All chemicals were purchased in highest purity grade from Sigma Aldrich (Buchs, Switzerland) unless mentioned otherwise. Water was deionized using a TKA-Genpure machine.

3.3.1.1 Preparation of mixtures of D-fructose and D-psicose

Sugar solutions used as SMB feeds were produced by enzyme-catalyzed epimerization of D-fructose (Carbosynth, Compton, UK) employing a thermo-stabilized enzyme variant of DTE from *Pseudomonas cichorii* [81]. A solution of 2 M D-fructose in 10 mM sodium phosphate buffer, pH 7.0, was converted at 50°C in a continuous process using an enzyme membrane reactor and a previously described set-up [116]. The reaction delivered mixtures of the two sugars close to equilibrium (equilibrium conversion at 50°C ≈ 28%). A one-step desalting procedure was employed to remove the buffer from the solution prior to SMB using the mixed bed resin DOWEX Marathon MR-3A. Presumably due to the short residence time in the enzyme membrane reactor (20 min or less), the formation of undesired side products previously reported [45] could be avoided and no further purification steps were required.

3.3.1.2 Purification of D-psicose

Purified D-psicose used for parameter estimation was obtained from SMB extracts (PU_{Ex} ≥ 98%) by evaporation of water as the solvent at 45°C and 40 mbar until a D-psicose concentration of about 80% (g g^{-1}) was reached. D-Psicose was crystallized from these solutions by adding an equal volume of ethanol (abs ≥ 99.5%). Subsequently, crystals were recovered, washed with ethanol and their purity was analyzed as described below.

3.3.2 Sugar analytics

Sugar samples were analyzed on an Agilent 1200 series HPLC system (Agilent Technologies, Palo Alto, USA) equipped with an refractive index detector (RI) using a 100 mm x 7.8 mm AMINEX Fast Carbohydrate (Pb^{2+}) column at 85°C with a Carbo-P guard column (both, Biorad, Reinach, Switzerland) and water with a flow rate of 2 mL min^{-1} as the mobile phase. Where higher accuracy was required (e.g. when confirming concentrations at SMB outlets or purity of crystallized psicose), high-performance anion-exchange chromatography was used employing a Dionex LC DX-300 system (Dionex, Sunnyvale, USA) equipped with a CarboPac PA1 analysis column (250 mm x 4 mm). Samples were eluted at 30°C employing isocratic conditions of 25 mM aqueous NaOH at a flow rate of 2.5 mL min^{-1}. Detection was

done by triple pulsed amperometry using an electrochemical detector with a gold electrode.

3.3.3 Stationary phase in SMB columns

The cation exchange material DOWEX 50 WX4-400(H^+) was converted to Ca^{2+} - form by incubating with 300 mM $CaCl_2$ for 1h prior to packing into stainless steel columns (150 mm x 8 mm, Morvay Analytics, Basel, Switzerland). Eight columns were used in the SMB, while a ninth column was used for isotherm determination. An average bed void fraction of ε= 0.24 ± 0.005 was determined for all columns by using dextran (Mw= 550,000 g mol^{-1}) as non-penetrating and non-retained tracer [130].

3.3.4 Column characterization

The Agilent 1200 series HPLC system equipped with an SMB column and a diode array detector was employed for all column analysis as well as for the pressure experiment using water as eluent.

3.3.4.1 Generation of concentration profiles and experimental system peaks for IM

Various injections of 2 M D-fructose or 2 M D-psicose solutions were done for parameter estimation at 20, 30, 40, 50, 60, and 70°C. Different volumes (ranging from 0.5 to 2 mL) were injected using the gradient delivery system of the HPLC pump. Overloaded injections were accomplished by switching from channel A (delivering eluent) to channel B (delivering sugar solution) and back. The maximum amounts injected were 720 mg and 270 mg for D-fructose and D-psicose, respectively. The eluent flow-rates were varied between 1 and 4 mL min^{-1}. For more experimental details see **Supplementary Table 3.1** in **3.6**. The UV signals were taken at 230 nm. We used the less-sensitive signal at 230 nm instead of the one at 210 nm, because the signal response as a function of loaded amount was linear up to the highest overload profile investigated in this study and still showed sufficient sensitivity for the detection of the smallest investigated sample volumes. All experiments were repeated with the column by-passed in order to generate the corresponding system peaks.

3.3.4.2 Determination of column pressure drop

The pressure drop caused by a single SMB column was determined as a function of the eluent flow-rate between 0.25 and 5 mL min^{-1} at 20°C. Measurements were performed both, with the SMB column in-line and in by-pass in order to subtract the contributions of the HPLC system to the overall pressure drop.

3.3.5 SMB set-up and experiments.

The implementation of a laboratory-scale SMB-plant based on the Amersham AEKTA basic-10 system (GE Healthcare, Uppsala, Sweden) was described in detail previously [80, 116]. The SMB was operated in open-loop arrangement with eight columns in a 2-2-2-2 configuration. A six-port manifold was placed at the inlet of each column that connected the columns to each other and to multi-position valves that directed the SMB inlet (feed and eluent) and outlet (extract and raffinate) flows. Check valves (CV-3000, Upchurch Scientific, Oak Harbor, USA) were installed between columns to ensure correct flow direction. Back pressure relief valves (1,000 psi, Upchurch Scientific) were implemented downstream of the feed and eluent pump in order to accommodate for local pressure build-up during valve switching. An additional multi-position valve that was connected to a three-port manifold installed at the outlet of each column was dedicated to direct the waste outlet stream from zone IV in order to realize the open-loop arrangement. The SMB installation including eluent reservoirs was kept at constant temperature by housing the system in an incubator (Binder, Tuttlingen, Germany). The SMB unit was controlled with a modified version of the UNICORN software (GE Healthcare) [98, 99]. All SMB runs were performed with deionized water as mobile phase.

3.3.6 Fitting procedures, TMB simulations and optimization

The conversion of the experimentally measured system peaks into mathematical functions as well as the conversion of the UV signals of the elution peaks into dimensionless time-concentration profiles was performed in MATLAB (Mathworks, Natick, USA). A fitting procedure (based on maximum likelihood estimation objective function) used for parameter estimation and the TMB model given in section 2.2 was implemented in the gPROMS software (PSE, London, UK), which was used for all TMB simulations and optimizations in this work.

3.4 Results and discussion

3.4.1 Parameter estimation

In order to rapidly generate a suitable model description for the separation of D-fructose and D-psicose on the single column level we used the IM to estimate kinetic and thermodynamic parameters. Among the different available methods for chromatographic parameter estimation [136], elution by characteristic point (ECP) and the IM allow for parameter estimation with only small amounts of compounds, which is beneficial in the case of rare sugars where pure substances are expensive. In contrast to ECP, which is restricted to columns providing high plate numbers [137], IM has been successfully applied for parameterizing low efficient separations using the equilibrium-dispersive model [138, 139] and for estimating the effect of pore and surface diffusivity in mass-transfer limited separations from elution peaks [140, 141]. Parameter estimation based on the IM was performed in 3 steps: (i) collection of experimental elution peaks and the conversion to dimensionless time-concentration profiles; (ii) selection of a chromatographic model; (iii) the fitting of the model predictions to the experimental profiles based on maximum likelihood estimation. For scoring the goodness-of-fit for a given set of experimental and simulated profiles for different temperatures or different chromatographic models the weighted sum-of-squares errors (E) was calculated for each set.

The a priori selection of the chromatographic model in IM requires some previous knowledge on the chromatographic system [142]. Here, a transport-dispersive model was considered in order to account for axial dispersion and mass transfer limitations and a linear isotherm model was applied to describe the thermodynamics of the adsorption of D-fructose and D-psicose on Dowex 50 WX4-400(Ca^{2+}). Linear isotherm models are frequently used to describe the adsorption of neutral sugars on ion-exchange resins [69, 143-146]. In the present case, linear isotherms had been previously confirmed up to 116 g L^{-1} and 42 g L^{-1} for D-fructose and D-psicose by frontal analysis, respectively [45]. In order to account for the low efficiency in sugars chromatography, we used a TDM considering axial dispersion and mass transfer kinetics according to a linear driving force (LDF) assumption. In most studies axial dispersion is calculated applying established correlations such as the ones derived from Chung and Wen [147] or Gunn [148]. We found that the specification of the axial dispersion in advance (by applying one of the previously mentioned correlations) led to a slight but systematic underestimation of the curvature at the peak maximum for both sugars (data not shown). This deviation was not observed when we used the axial dispersion as free parameter for fitting (as described in section **3.2.1.2**) indicating that in the investigated case band broadening includes effects remaining unaccounted for by the simplified approximations. Additionally, we have investigated more sophisticated mass-

transfer assumptions such as the bi-LDF approximation suggested by Azevedo et al. [149] for describing the mass transfer kinetics of D-fructose and D-psicose on bidisperse adsorbents, but did not find further improvement in terms of *E*'s (data not shown). Each set of experimental elution profiles used for parameter estimation consisted of 8 injections for D-fructose and 5 injections for D-psicose ranging from small to large injections. A maximum load of 720 mg and 270 mg was investigated for D-fructose and D-psicose, respectively. The corresponding concentrations of 250 g L^{-1} and 70 g L^{-1} for D-fructose and D-psicose at the column outlet determined the maximum valid concentration of the estimated isotherm parameters [142].

Special attention was paid to an accurate description of the inlet concentration profiles constituting the boundary conditions for the differential mass balance equations used in the IM. Since the concentration at the column inlet evolves from the concentration profile travelling from the pump head to the column inlet, system peaks usually could not be accurately approximated using an ideal rectangular shape [150], but were better approximated by fitting experimentally produced system peaks to mathematical functions (**Equations 3.1** to **3.4**).

3.4.1.1 Chromatographic parameters and temperature

In a next step, we investigated the effect of temperature ranging from 20 to 70**°C** on the thermodynamics of the adsorption and mass transfer kinetics of both sugar species. Following the previous workflow, sets of single-solute elution profiles were recorded (for an exemplary overlay of experimentally and model-predicted D-fructose or D-psicose concentration profiles see **Supplementary Figure 3.1** in **3.6**. In general, the applied TDM was found to produce good fitting results for both sugar species at all investigated temperatures judged by the weighted-sum-of-squares error [142] calculated for the individual profile sets (for details see **Supplementary Table 3.2** in **3.6**). We observed that for both sugars better fits were obtained at elevated temperatures (between 50 and 70°C). This could be due to a reduced impact of the viscosity difference between sugar injections and mobile phase at high temperature, which is known to affect both retention time and band resolution [151] and is not accounted for in the applied model.

The development of the free model parameters with temperature is depicted in **Figure 3.1**. Due to reduced retention at elevated temperature, in case of linear isotherms the Henry coefficients of both sugars decrease. The stronger retained D-psicose was affected to a larger extent, which resulted in significantly decreased selectivity at elevated temperatures. The reduction in selectivity with increasing temperature was countered by an improved mass transfer: the mass transfer coefficients for both sugars were calculated to significantly increase over the investigated temperature range. The bed packing factor **λ**

was widely unaffected by temperature, therefore we concluded that the effect of temperature on axial dispersion in the investigated system is exclusively depending on the mobile phase viscosity (**Equation 3.10**). Similar trends for mass transfer and axial dispersion had been found earlier by Beste et a.l. [125] for the temperature-dependence of the kinetic parameters of the mass transfer of D-glucose and D-fructose.

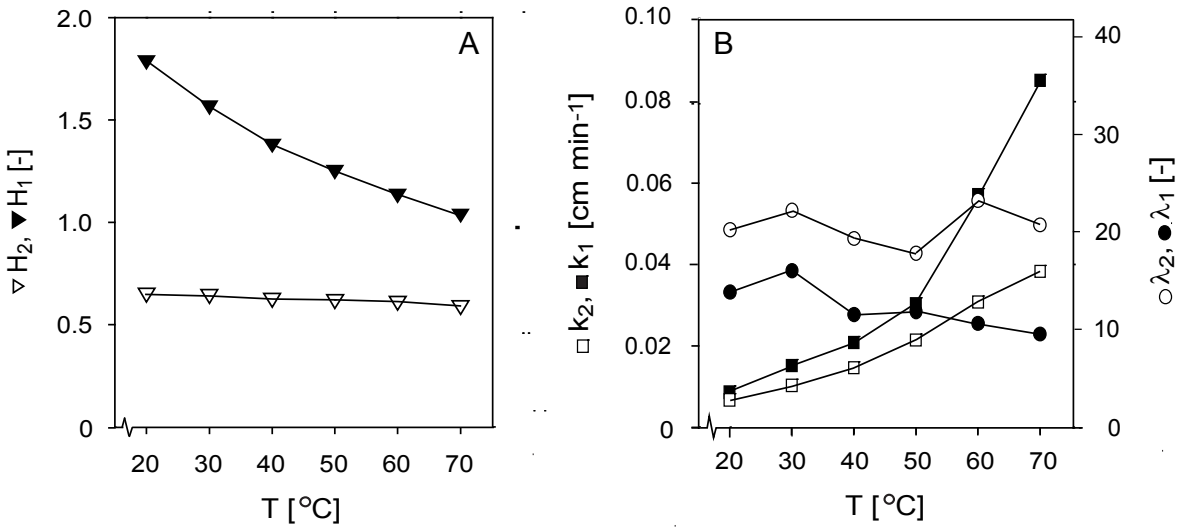

Figure 3.1. Results of parameter estimations based on the inverse method: Effect of temperature **(A)** on thermodynamics of the adsorption and **(B)** on the kinetics of the mass-transfer for D-fructose (empty symbols) and D-psicose (filled symbols).

3.4.1.2 Pressure determination

An operational constraint that has to be taken into account for lab-scale as well as industrial SMB is the maximum permissible pressure drop [129], which is defined by the structural integrity of the packed stationary phase, the pressure resistance of the pumps or the valves. In order to achieve high productivities SMB plants are best operated slightly beneath this pressure limit [73]. Therefore we studied the column backpressure related to fluid phase velocity of single columns in order to experimentally determine the specific bed resistance α. A value of $2.34*10^8$ cm^{-2} was determined for α when considering experimental slopes from the pressure experiments at 20°C and a dynamic viscosity η for water of 1.00 cP [152]. The experimentally measured α was in line with values obtained from Carman-Kozeny estimation [129] and used to calculate the specific flow resistance ϕ at different temperatures. More detailed data is available in **Supplementary Table 3.3** in **3.6**.

3.4.2 TMB design and SMB experiments

The parameters obtained from the single column experiments were used for SMB design. It was previously shown that TMB models can be used in order to approximate SMB

operation [132]. For the purpose of model validation we conducted a number of SMB experiments. The conditions were chosen to include operating points leading to high purities (≥ 99.9%) in both streams (extract and raffinate), in only one stream, or in neither of the two streams. Even though the last option might not include meaningful operating points in terms of rare sugar production using a stand-alone SMB, it provides valuable information in terms of model assessment. The applied flow-rate ratios and switch-times are summarized in **Table 3.1** together with the simulated and experimental purities determined from SMB extract and raffinate streams.

Table 3.1. Comparison of experimental (exp) and simulated (sim) extract and raffinate purities obtained for different operating points and different temperatures. The switch times refer to the experimental SMB runs and are already divided by a factor of 2 to align them to the experimental set-up.

Run	T	Flow rate ratios				Switch time	Experimental purities		Simulated purities	
	[°C]	m_1 [-]	m_2 [-]	m_3 [-]	m_4 [-]	t_{sw} [s^{-1}]	$PU_{Ex,exp}$ [%]	$PU_{Raff,exp}$ [%]	$PU_{Ex,sim}$ [%]	$PU_{Raff,sim}$ [%]
A_1	20	2.43	0.51	1.54	0.3	335	62.9	99.9	64.7	99.9
A_2	20	2.44	0.76	1.78	0.35	335	99.7	94.5	99.9	95.2
A_3	20	2.43	0.61	1.63	0.3	335	86.0	99.1	86.1	99.9
B_1	30	1.85	0.8	1.61	0.51	144	99.6	96.5	99.9	98.2
B_2	30	1.73	0.61	1.33	0.37	197	82.4	996	82.3	99.9
C_1	40	1.66	0.73	1.41	0.51	148	99.5	95.8	99.9	98.5
C_2	40	1.67	0.82	1.51	0.44	148	99.7	92.4	99.9	93.6
D_1	50	1.42	0.71	1.17	0.45	145	98.2	99.9	99.9	99.9
D_2	50	1.46	0.71	1.61	0.37	145	99.7	95.9	99.2	95.4
E_1	60	1.33	0.69	1.07	0.55	111	96.0	99.9	98.2	99.9
E_2	60	1.56	0.97	1.37	0.77	111	99.2	99.8	99.9	99.9
F_1	70	1.25	0.72	1.06	0.33	86.6	98.0	99.9	99.0	99.9

Comprehensive SMB experiments revealed that the simulated purities were remarkably consistent with experimental purities at all temperatures, which confirmed the suitability of the applied transport-dispersive TMB model in approximating the SMB operation. The TMB simulations tended to slightly overestimate the experimental purities, which is probably due to the fact that the number of columns per section in the explored configuration was limited to two. It was shown previously that experimentally derived internal concentration profiles in an SMB align better with TMB predictions for larger column numbers per section [130]. For TMB simulations and optimizations the model

equations described in 2.2 were numerically solved for a constant section length of 30 cm in order to mimic the experimentally used 2-2-2-2 lab-scale SMB installation with 15 cm column. Correspondingly, the switch time used in the simulations was two times the switch time used in SMB experiments.

3.4.3 Multi-objective SMB optimization

After having broadly confirmed the validity of our TMB model, we optimized SMB operation for two important performance parameters, namely, maximizing *PR* and minimizing *DR*, which have been identified as the main costs contributors in SMB chromatography [128] and therefore need to be considered at an early stage of process design. However, the two performance parameters exhibit opposite trends, i.e. highest *PR* is obtained at maximum desorbent expenditure and vice versa. In such cases, the optimal operating point can be determined from an SMB cost optimization, which constitutes a trade-off between these two competing objectives. A two-objective optimization based on the function presented in **Equation 3.23** allowed us to include both parameters in the optimization using one objective function, producing so-called Pareto sets of *PR* and *DR*. The full parameterization set used for simulation is summarized in **Supplementary Table 3.4** in **3.6**.

3.4.3.1 Impact of the operating temperature

In a first step, we investigated the influence of the operating temperature on *PR*/*DR* Pareto sets. Temperature constitutes an important variable for optimization; since it affects a number of process parameters such as retention time, selectivity, mass transfer kinetics and viscosity of the eluent translating into altered pressure drop along the SMB columns.

For the simulations we have selected a total sugar concentration of 180 g L^{-1}, which was selected not to exceed the valid range of the estimated adsorption isotherm parameters (determined by the maximum concentrations obtained during parameter estimation at the column outlet). The feed composition of 72/28 D-fructose/D-psicose was chosen equal to the composition investigated in the experimental runs in Section 4.4. Overall, the feed composition has a considerable impact on the *PR*/*DR* optimization, which is exemplarily demonstrated for an SMB optimization at 50°C in **3.6** (**Supplementary Figure 3.2**). In case of linear chromatography, higher contents of D-psicose in the SMB feed stream directly translate into higher *TP*s, which are clearly beneficial in terms of *PR* and *DR*. However, the use of feed solutions of higher D-fructose/D-psicose ratios is also supposed to be more expensive as it necessitates higher conversion temperatures during preparation demanding increased amounts of biocatalyst. The purity for both streams, PU_{Ex} and PU_{Raff}, was constrained to 99.5 % and maximum permissible pressure drop (ΔP_{max}) of 80 bar was

considered for the SMB optimization (representing the maximum pressure drop advised for the ÄKTA SMB system used in this study). As very short port switching intervals have been previously discussed to be associated to disturbances in the fluid flow interfering with stable SMB operation [72, 73], we required t_{sw} to be larger than a minimum value of 30 s as an additional constraint, as suggested in a previous study [72] (equivalent to $t_{sw} \geq$ 60 s in the TMB simulations with 30 cm section length).

The Pareto sets (**Figure 3.2**) clearly indicate that temperature has a strong impact on the operating points optimized only for *PR* ($\omega \rightarrow 1$). In fact, the maximum feasible *PR* is increased by 50 % (from 140 to 210 g L^{-1} h^{-1}) when raising the operating temperature from 20 to 70°C. In contrast, only minor improvements in desorbent expenditure can be observed for the operating points optimized only for DR ($\omega \rightarrow 0$).

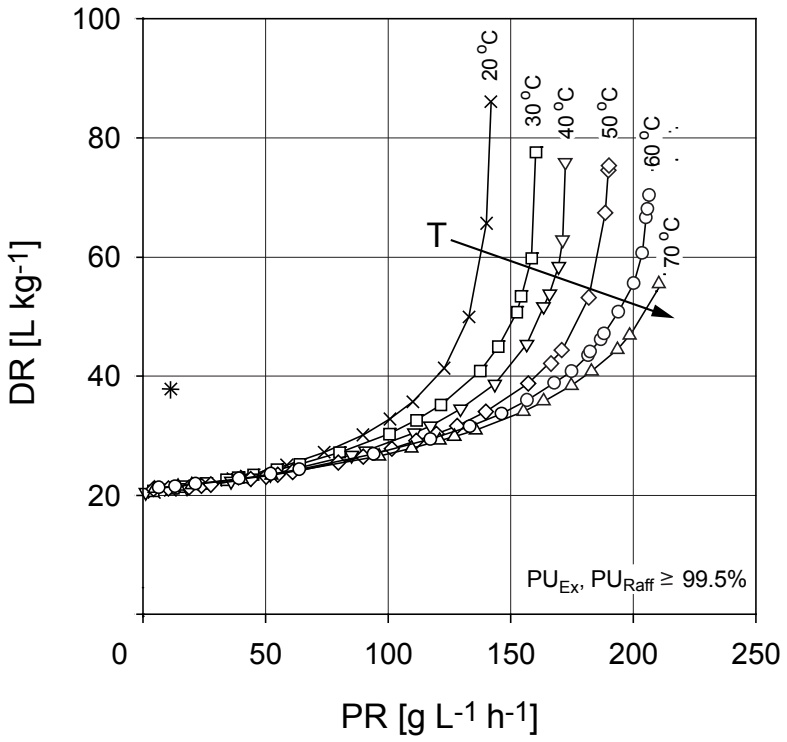

Figure 3.2. *PR*/*DR* Pareto sets for different temperatures; the *PR*/*DR* of a previously published optimization result [45] for the D-fructose/D-psicose separation using SMB is marked by a star.

The development of the corresponding operational parameters m values and t_{sw} for all temperatures with increasing decision variable ω is given in **Figure 3.3**. As expected, large differences can be found in the operational parameters of operating points optimized for either *PR* or *DR*. Desorbent-saving operating points are characterized by *m* values converging to the vertex of the triangle and by very long t_{sw}. In contrast, for obtaining high productivities the switch times have to be decreased. Moreover, in order to compensate for

the significant mass transfer limitation under these conditions the *m* values need to be adapted in order to keep up with the purity requirements of the separation [153]. This is mainly accomplished by increasing m_1 and m_2 and decreasing m_3 and m_4. Considering intermediate points in the Pareto plot allows introducing specific constraints into the analysis, e.g. constraining desorbent expenditure per unit product and thus limiting dilution of the product (**Supplementary Figure 3.3** in **3.6**), which is an inherent consequence of the increased internal flow-rates when optimizing for *PR* in mass-transfer limited SMB processes [125]. The analysis shows that increasing the temperature in such intermediate scenarios still allows increasing the *PR* by a substantial factor: for instance, for a fixed *DR* of 30 L kg^{-1} the PR improvement is 75% (from 80 to 140 g L^{-1} h^{-1} for a temperature increase from 20 to 70°C).

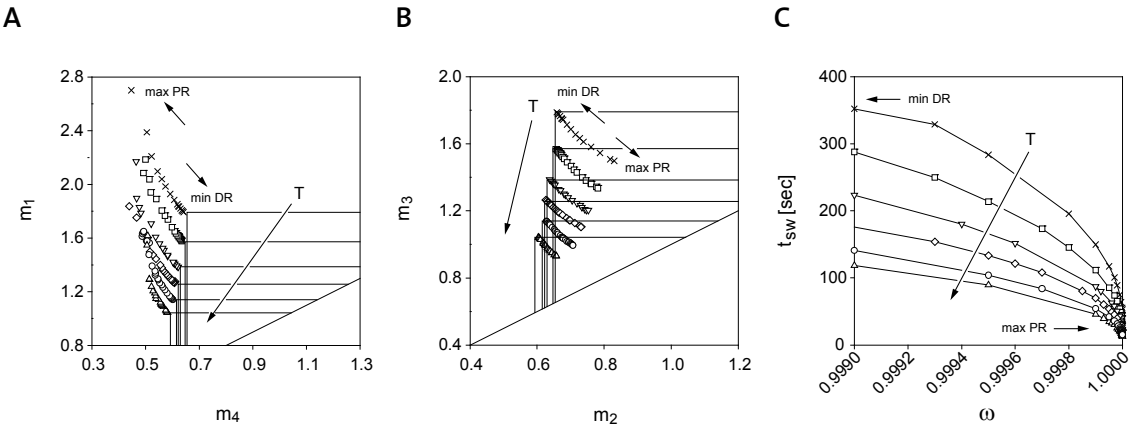

Figure 3.3. Development of SMB design parameters with temperature for the different Pareto sets of **Figure 3.2**. (**A**) Development of m-values in the m_1/m_4 and (**B**) m_2/m_3 (panel, middle) plane, and (**C**) development of the switch time t_{sw} (panel, right). 20°C (cross), 30°C (square), 40°C (triangle, down), 50°C (diamond), 60°C (circle) 70°C (triangle, up); the solid triangles represent the theoretical separation area according to the equilibrium theory [100]; the depicted values for t_{sw} were already divided by a factor of 2 to align them to the experimental set-up.

The potential impact of this analysis becomes clear when comparing the performance of the Pareto-sets in **Figure 3.2** with a previously described D-fructose/D-psicose SMB separation processes performed at 50°C ([45]; *PR*/*DR* of this operating point were outlined by a star in **Figure 3.2**). The previously described SMB process yielded a maximum *PR* of 11.4 g $(L\ h)^{-1}$ requiring 37 L kg^{-1}, while the Pareto analysis clearly suggests that for the same *DR* a 13- to 15-fold higher *PR* should be possible (155 g L^{-1} h^{-1} for 50°C, 175 g L^{-1} h^{-1} for 70°C). Overall, the Pareto optimization revealed that the decreased selectivity at higher temperatures (represented by the decreased difference between m_2 and m_3 in case of SMB separation) can be fully compensated by the gain in mass transfer affording an overall

higher *PR*. In the investigated example, the maximum obtainable *PR* at 60 and 70°C was clearly limited by the switch time constraint (**Supplementary Figure 3.4**). The corresponding maximum feasible operating points therefore exhibited ΔP_{SMB}*'s* significantly below the theoretically feasible ΔP_{max} (ΔP_{SMB}'s of 62 and 48 bar for 60 and 70°C). At lower temperatures (20 to 50°C) the minimum possible value for t_{sw} was not reached during the optimization.

3.4.3.2 Impact of reduced purities in the non-product stream

One option for further increasing the *TP* in mass-transfer limited separations is lowering the purity constraints on the outlet streams. While purity of the product stream is typically specified, reduced purity requirement of the non-target stream constitutes an interesting option when the loss of product in the non-target stream is acceptable (e.g. when the production of the feed stream is relatively cheap) or when the non-target stream is anyways converted to the SMB feed mixture (in this case the partial conversion of D-fructose to D-psicose).

For investigating the influence of such an asymmetric purity scenario on *PR* and *DR*, we conducted a Pareto optimization applying high purity specifications on the extract port ($PU_{Ex} \geq 99.5\%$) and relaxed purity specification on the raffinate port ($PU_{Raff} \geq 99\%$, $PU_{Raff} \geq 95\%$, $PU_{Raff} \geq 90\%$). Again, we adopted ΔP_{max}= 80 bar as upper limit for the permissible pressure drop with the lower boundary for the t_{sw} set to 30 s.

Comparing the differences between the Pareto sets derived from the reduced purity scenarios at 50°C (**Figure 3.4**) with the previously investigated scenario where stringent purity constraints were specified on both streams (PU_{Ex}, $PU_{Raff} \geq 99.5\%$) clearly demonstrates the great potential of reduced purity operation for the D-fructose/D-psicose example. Optimizing for *PR* ($\omega \rightarrow 1$), the maximum feasible *PR* virtually doubled (from 180 to 325 g L^{-1} h^{-1}) when decreasing the *PU* requirements on the non-product stream (from ≥ 99.5% to ≥ 90%).

The improvement in *PR* arises from significantly higher m_3 values, which become possible due to relaxed *PU* constraints (for details see **Supplementary Figure 3.5** in **3.6**), providing an additional margin for increasing the difference between m_2 and m_3 heading towards a higher *TP* in mass transfer limited separations. Of course, with reduced purity requirements on the non-product stream the possible *Y* in a stand-alone SMB significantly reduces (for PU_{Raff} of 99%, 95% and 90% to *Y* of 0.97, 0.87 and 0.71, respectively) making reduced *PU* operation in particular interesting for process integration strategies.

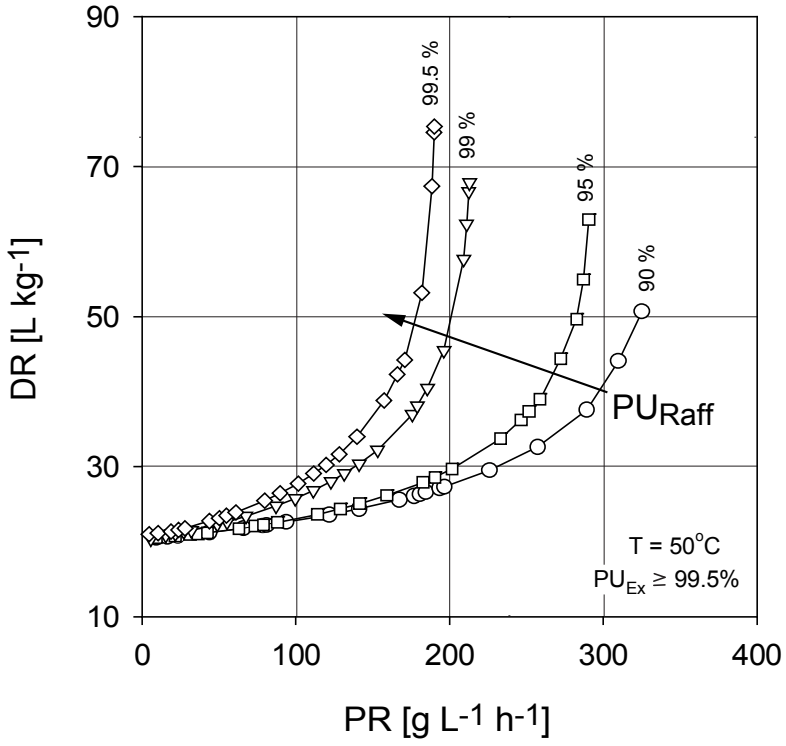

Figure 3.4. Development of Pareto plots with temperature allowing for reduced purities in the raffinate stream PU_{Raff}: ≥ 90% (circle), ≥ 95% (square), ≥ 99% (triangle, down), ≥ 99.5% (diamond)

3.4.4 Experimental validation of the optimization results

In order to demonstrate the usefulness of the model-based optimization results obtained in **3.4.3**, three SMB runs were conducted at different temperatures with operating points taken from the Pareto set of the respective temperature. For better comparability the operating points were chosen to require equal amount of desorbent. Specifically, experiments were performed at 30, 50, and 70°C with the *DR* set to 27 L desorbent per kg D-psicose. The *DR* was deliberately chosen to be in the Pareto set region that is most sensitive with respect to *PR*. Operating parameters and performance parameters are summarized in **Table 3.2**.

Both outlet streams showed reasonably good purity - well within the difference expected between TMB modeling and SMB operation with two columns per section – and consequently all performance parameters aligned very nicely with the predictions from the optimization. As expected, a certain safety margin needs to be applied in order to obtain absolute purity at both ports.

In summary, the predicted performance improvement at higher temperatures could be quantitatively reproduced in experimental SMB runs clearly demonstrating the benefit of the applied optimization procedure.

Table 3.2. Operating and performance parameters for the optimized runs

		Operating parameters					Performance parameters			
Run	T [°C]	m_1 [-]	m_2 [-]	m_3 [-]	m_4 [-]	t_{sw} [s^{-1}]	PU_{Ex} [%]	PU_{Raff} [%]	PR [g $L\ h^{-1}$]	DR [L kg^{-1}]
Opt1 *)	30	1.68	0.69	1.49	0.60	223	98.0	99.3	80.2	27.2
Opt2 *)	50	1.33	0.66	1.21	0.58	120	98.5	99.1	101.5	27.2
Opt3 *)	70	1.10	0.62	1.01	0.56	79	97.6	98.9	109.5	27.2

*) $c_F \approx 130/50$ g L^{-1} D-fructose/D-psicose

3.5 Conclusions

Multi-objective optimization producing *PR/DR* Pareto plots was demonstrated to serve as promising tool for providing an extensive insight into the economically relevant aspects of rare sugar SMB separation. Based on a parameterization obtained from the IM, a TDM was established allowing for an accurate SMB design proved by the good agreement between model simulations and experimental SMB runs. To our knowledge this study represents the first comprehensive design strategy presented for the separation of the bulk sugar D-fructose and the rare sugar D-psicose, resulting in both, the highest *PR* and the lowest *DR* reported for this separation. Temperature emerged as the main factor for increasing the *PR* of the separation, clearly suggesting that decreasing selectivity at elevated temperatures can be compensated by a significant increase in mass transfer kinetics. Furthermore, a separation characterized by such a mass transfer limitation could be better operated when allowing for significantly reduced *PU* requirements in the raffinate stream. The full economic potential of relaxed *PU* constraints compared to stringent for the SMB stand-alone operation has not been evaluated in this work, as this would require entering the spent substrate as a third cost-relevant performance parameter for optimization.

The presented optimization study confirms the great potential of SMB separation for the economic production of the rare sugar D-psicose from epimeric mixtures with D-fructose, as already a lab-scale SMB experiment allowed the production of 157 g of rare sugar per day at an expenditure of only 4 L desorbent. Projecting these findings to a medium-sized industrial unit (e.g. SMB with 10 cm column ID) production of multiple tons D-psicose per year seems absolutely feasible.

3.6 Supplementary material

Supplementary Table 3.1. Experimental details on the generation of elution and system peaks for parameter estimation via IM; Overloaded injections were performed by switching from channel A (delivering eluent) to % channel B (delivering sugar solution) and back using the gradient mixer of the HPLC, A-H refer to the profiles depicted in **Supplementary Figure 3.1**

	D-Psicose profiles				D-Fructose profiles			
#	Flow rate [ml min^{-1}]	Channel B [%]	Volume loaded [mL]	Loaded D-psicose [mg]	Flow rate [ml min^{-1}]	Channel B [%]	Volume loaded [mL]	Loaded D-fructose [mg]
A	1	25	0.5	45	1	25	0.5	45
B	1	50	0.5	90	1	50	0.5	90
C	1	100	0.5	180	1	100	0.5	180
D					1	100	1.0	360
E					1	100	2.0	720
F	2	100	0.5	180	2	100	0.5	180
G	3	50	1.5	270	3	50	1.5	270
H					4	50	2.0	360

Supplementary Table 3.2. Weighted sum-of-squares errors calculated for experimental and simulated profile sets of D-psicose (E_1) and D-fructose (E_2) according to [142] at several temperatures (T). For the simulation the TDM described in **3.2.1.2**. was applied. To allow for direct comparison between E_1 and E_2, E's were normalized by the number of profiles used (i.e. 5 for D-psicose and 8 for D-fructose)

T [°C]	E_1 [-]	E_2 [-]
20	0.013	0.005
30	0.011	0.003
40	0.011	0.002
50	0.006	0.002
60	0.006	0.003
70	0.005	0.002

Supplementary Table 3.3. Experimentally determined specific bed resistance α at 20°C and calculated specific flow resistance $\varphi = \alpha * \eta$ as function of temperature

T [°C]	η [cP]	α [bar s]	$\varphi = \alpha * \eta$ [bar s cm^{-2}]
20	1.00*)	2.34 x 10^{8}	3.3
30	0.8*)		2.6
40	0.65*)		2.1
50	0.55*)		1.8
60	0.47*)		1.5
70	0.40*)		1.3

*) dynamic viscosity of water adopted from [152]

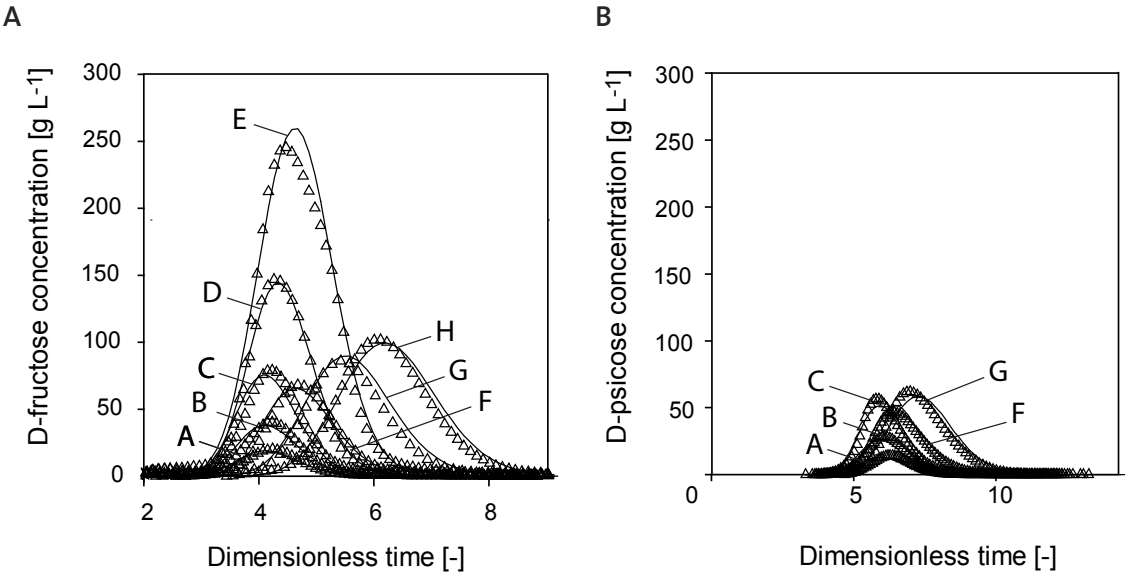

Supplementary Figure 3.1. Model-predicted profiles (continuous line) based on a TDM and linear isotherms and experimentally observed profiles (triangles) of (**A**) D-fructose and (**B**) D-psicose injections at 50°C, for experimental details see **Supplementary Table 3.1**.

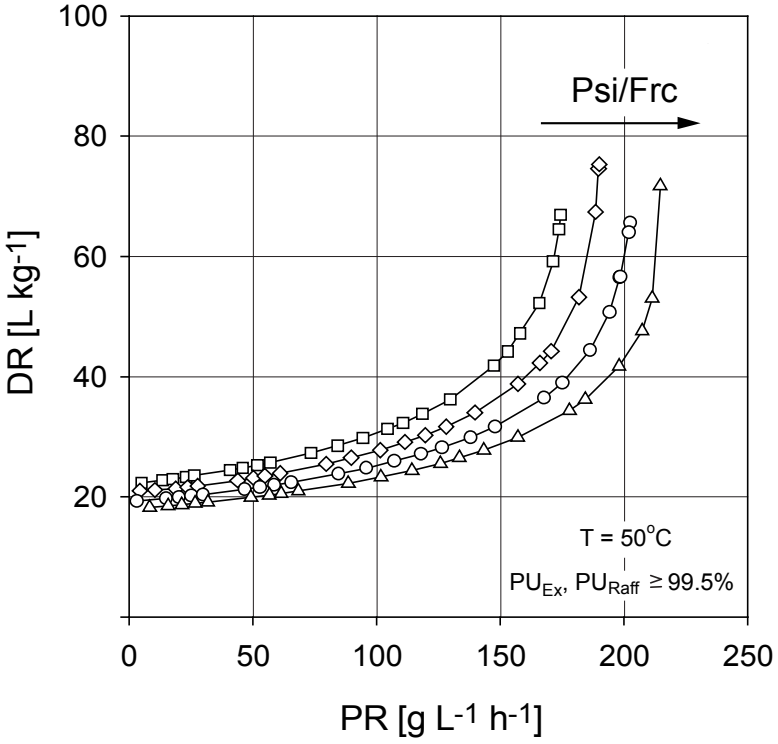

Supplementary Figure 3.2. Pareto sets of rare sugar SMB at 50°C assuming different feed compositions X_{Feed}: 0.26 (square), 0.28 (diamond), 0.3 (circle), 0.32 (triangle, up)

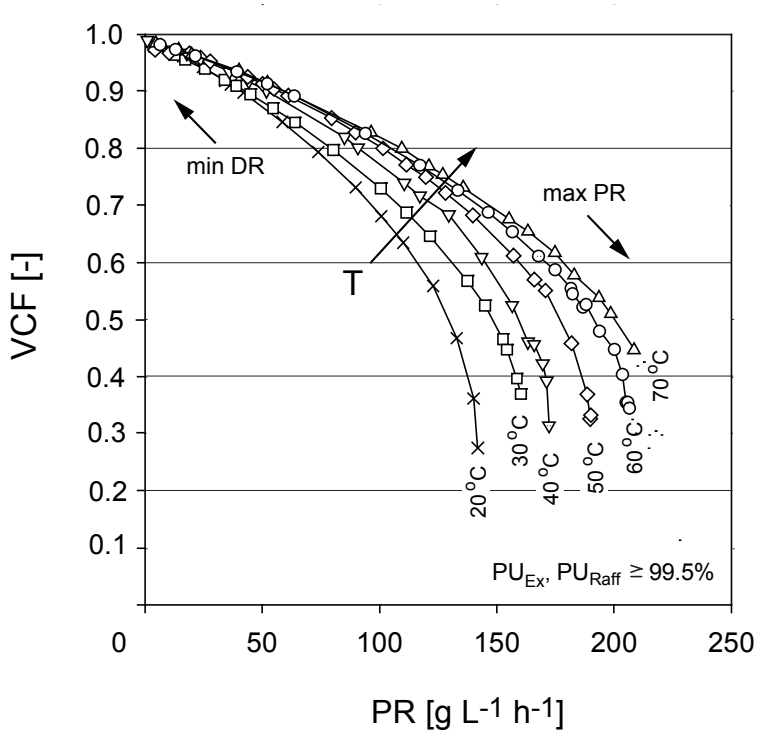

Supplementary Figure 3.3. Development of the product concentration factor (*VCF*) in the SMB extract stream at different temperatures with increasing *PR*.

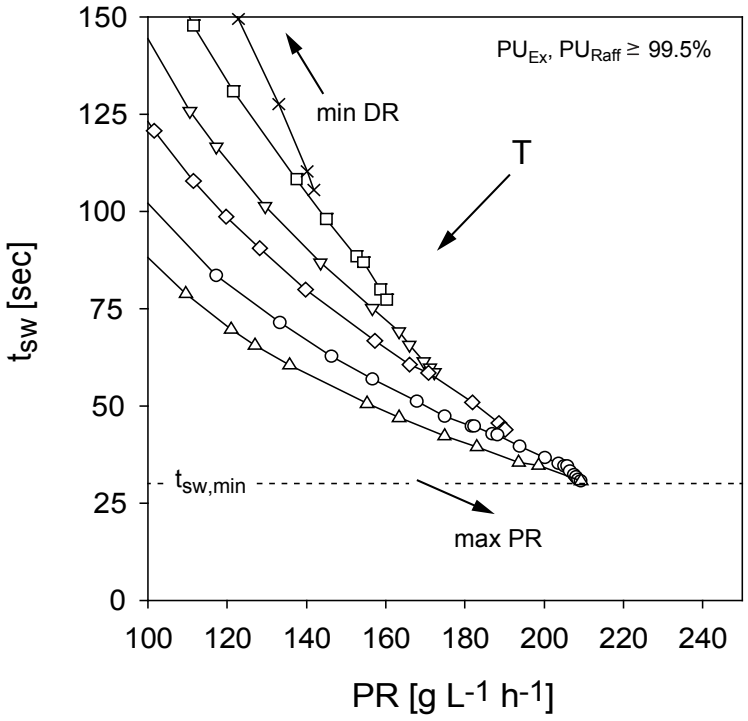

Supplementary Figure 3.4. *PR* and t_{sw} for Pareto sets at different temperatures: 20°C (cross), 30°C (square), 40°C (triangle, down), 50°C (diamond), 60°C (circle), 70°C (triangle, up); values for t_{sw} were already divided by a factor of 2 to align them to the experimental set-up

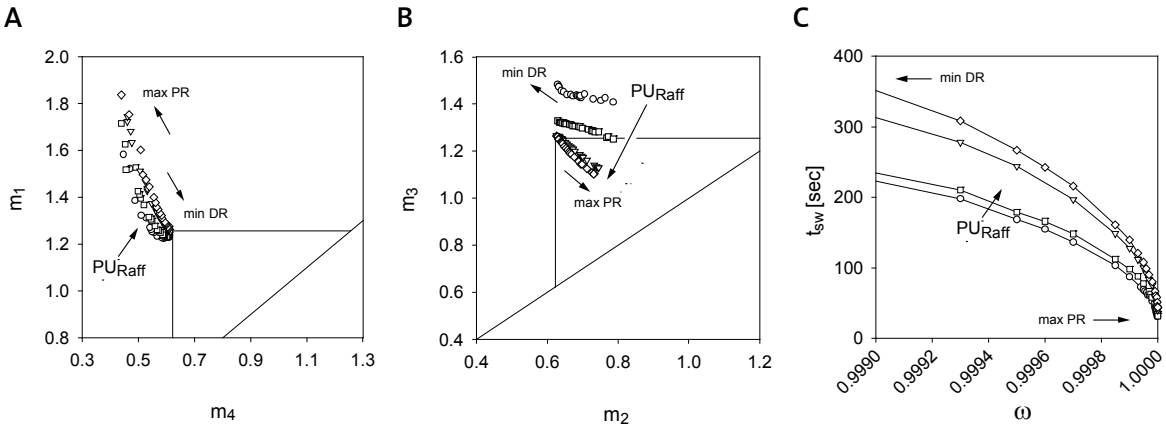

Supplementary Figure 3.5. Development of SMB design parameters for *PR*/*DR* Pareto sets of **Figure 3.4** allowing for reduced purity in the non/product stream (PU_{Raff}). (**A**) Development of *m*-values in the m_1/m_4 and (**B**) m_2/m_3 plane and (**C**) development of t_{sw} (panel, right) with ≥ 90% (circle), ≥ 95% (square), ≥ 99% (triangle, up), ≥ 99.5% (diamond); the solid triangles represent the theoretical separation area according to the equilibrium theory [100]; the depicted values for t_{sw} were treated as described above.

Supplementary Table 3.4. Parameter set used for *PR*/*DR* Pareto optimization

Temperature independent parameters			
Section length	L_c	30	[-]
Column porosity	ε	0.24	[cm]
Radius particle	r_p	4×10^{-3}	[cm]
Density solid phase	ρ_{SP}	736.8	[g L^{-1}]
Specific bed resistance	α	2.34	[cm^{-2}]
Feed concentration	(Psi+Frc)	1	M
Feed composition	(Psi/Frc)	0.28	[-] except for simulations in **Supplementary Figure 3.2**

Temperature dependent parameters								
		20°C	30°C	40°C	50°C	60°C	70°C	
Dynamic viscosity (desorbent)		1.0	0.8	0.65	0.55	0.47	0.40	[cP]
Thermodynamic Parameter	H_1	1.79	1.57	1.38	1.26	1.14	1.04	[-]
	H_2	0.65	0.65	0.63	0.62	0.62	0.59	[-]
Kinetic parameter	k_1	6.8	10	15	22	31	38	x 10^{-3} [cm min^{-1}]
	k_2	8.7	15	21	30	57	85	x 10^{-3} [cm min^{-1}]
	λ_1	13.8	16.0	11.5	11.8	10.6	9.5	[-]
	λ_2	20.2	22.2	19.3	17.8	23.2	20.7	[-]

4 Model-based cost optimization of a reaction-separation integrated process for the enzymatic production of the rare sugar D-psicose facing enzyme degradation at elevated temperatures

4.1 Introduction

Biocatalysis constitutes a promising route for the production of high-value fine chemicals and pharmaceuticals, which can be largely attributed to the excellent chemo-, enantio-, and regioselectivity of enzymes, which reduce by-product formation and therefore facilitate downstream processing [154]. Additionally, enzyme reactions are typically performed under environmentally benign conditions, such as near-neutral pH and ambient temperatures, which happens to be *in line* with the 12 principles of green chemistry [155].

Some enzyme classes such as oxidoreductases and hydrolases are frequently used in industrial applications, whereas others such as lyases and isomerases are less well established, although they are theoretically able to catalyse a number of potentially highly relevant reactions [156, 157]. A general property that makes the latter biotransformations less attractive for industrial-scale application is the frequent unfavourable position of the thermodynamic equilibrium of the catalysed reactions, typically restricting possible product yields in batch reactions to between 20 and 70 % [158]. However, instead of performing reaction and separation in subsequent steps, integrated operation of both steps can help to significantly enhance the process yield [159]. This is achieved by directly separating the product upon its formation from the reaction mixture, allowing to shift the equilibrium to the product side and running the equilibrium reaction close to completion [160]. A promising example is represented by the combination of biocatalysis and continuous chromatography, typically operated as SMB chromatography [59]. In principle, all realized approaches of this kind of integrated processes can be divided into three concepts: (i) chromatographic reactors ("SMBR", [78]), where the biocatalyst is added to the eluent (and feed stream) of the SMB; (ii) SMB with additional biocatalytic side reactors ("Hashimoto process", [75]); and (iii) an SMB-recycling concept with an external reactor (SMB&R [59]). Whereas the first two approaches are attractive for enhancing the yield and productivity, they are not suitable when it comes to high purity of the product stream [59]. The third option on the other hand is particularly suitable when high purity of the product is required.

An integrated process consisting of an enzyme membrane reactor (EMR), an SMB chromatography unit for separation and a nanofiltration (NF) unit for concentration of the raffinate recycling stream was proposed previously [59]. As a proof-of-principle, we recently demonstrated that such a process is able to provide highly pure (99.9%) product at significantly increased yield: in the thermodynamically limited biocatalytic production of the rare sugar D-psicose from its cheap C3 epimer D-fructose, it allowed shifting the yield from 25% (batch reaction) to 97% [116]. Rare monosaccharides like D-psicose have recently attracted a great deal of attention due to their potential role as low calorie sweetener, chiral building blocks or active pharmaceutical ingredients [4]. Their synthesis by

traditional organic chemistry is cumbersome due to demanding protection group chemistry [161], making production of rare monosaccharides from bulk sugars (D-glucose, D-fructose, L-sorbose, and D-galactose) by means of iso- and epimerase enzymes in an integrated process the route of choice [116]. Apart from implementing a potentially powerful strategy to increase the product yield (D-psicose from D-fructose in this case) in an equilibrium-limited reaction, this recent report of an integrated process showed also a high degree of robustness against perturbation in terms of substrate and product concentration and product purity (99.5%), which strongly suggested a high degree of robustness of the specific implementation. However, the operating point was not optimized and consequently, the achieved SMB productivity (appr. 30 g D-psicose per L SMB column volume and day^{-1}) was rather low and large amounts of desorbent were required (desorbent requirement (DR) of 0.6 L water per g D-psicose produced), even when assuming closed loop operation. Moreover, for the proof-of-concept run the reactor was provided with an excess of D-tagatose epimerase from the mesophilic organism *Agrobacterium tumefaciens* in its wild type form. This allowed counteracting the poor stability of the enzyme under process conditions and running the EMR under constant conversion. We overall concluded that this process still left much room for improvement in terms of productivity and production economy.

First, we suggest that the utilization of a more thermostable D-tagatose epimerase enzyme might help to improve the overall process performance significantly. To this end, we recently improved the thermostability of a D-tagatose epimerase from the mesophilic bacterium *Pseudomonas cichorii* by more than 20°C (PcDTE Var8, [81]), and this improved variant is now applied in the process.

Secondly, simulation tools and a process model can help to analyse and assess suitable operating points in such complex process concepts at an early stage and reduce the experimental effort during process development. Obviously, optimization of an integrated process is governed by minimization of the overall costs per amount of product yielded. Thus, the cost contribution of the individual unit operation should be reliably estimated as a function of their operating conditions. For a meaningful estimation of the different cost contributors to the overall process costs, the quality of the cost estimation for the different modules is of decisive importance [162]. For most consumables and equipment, a reliable estimation of the cost contribution is possible [163] with information obtained from online data resources (alibaba.com), text books [164] or directly from suppliers. However, the cost contribution stemming from biocatalyst consumption is particularly difficult to estimate as, next to cost variability in the enzyme manufacturing process due to the scale of expression, expression level and required purity (addressed in [165]), it is strongly dependent on the functional half-life, which in turn is a function of the reactor

temperature. Whereas the reaction rate is accelerated at increasing temperatures according to the well-known Arrhenius law, increasing temperature is likewise a predominate reason for enzyme inactivation [166]. Additionally, a change in temperature may also cause a shift in the reaction equilibrium of reversible reactions [166]. Taking into account that in an SMB&R configuration the reactor temperature basically constitutes a free parameter (i.e. it is independent of the temperature in the separation unit), the temperature of the reactor is a key parameter to be considered during cost optimization.

In this work we report the first comprehensive model-based design for the enzymatic production of the rare sugar D-psicose in an SMB&R process design and confirmed the power of this design by implementing a highly productive experimental run on our existing lab-scale plant. Next, an *in silico* procedure was established for optimizing this novel process concept for all scales using a cumulative cost function. As outlined above, a major focus of the current work was on the characterization and the estimation of the cost contribution of the biocatalyst in the context of the SMB&R process concept. A model-based characterization procedure was used to parameterize the reactor performance at temperatures between 20°C and 70°C and a comprehensive procedure for the lifetime assessment of the thermostable D-tagatose epimerase is presented.

4.2 Theory

For process optimization we implemented an integrated process model consisting of a steady-state reactor model for the EMR, a true moving bed (TMB) model for the description of the SMB separation and a simple mass balance-based model for the description of the NF. A node model was used to interconnect the individual single unit models.

4.2.1 EMR model

A continuous stirred tank reactor (CSTR) model with reversible Michaelis-Menten (MM) kinetics was used to describe the concentration *c* of each compound *i* (S= D-fructose, P= D-psicose) at the reactor outlet:

$$\frac{dc_i}{dt} = \frac{c_{i,EMRin} - c_i}{t_{EMR}} \pm \frac{c_E \frac{k_{cat}}{Km_S}\left(c_S - \frac{c_P}{K_{eq}}\right)}{1 + \frac{c_S}{Km_S} + \frac{c_P}{Km_P}} \qquad \textbf{Equation 4.1}$$

Here, $c_{i,EMRin}$ represents the inlet substrate concentration, t_{EMR} the residence time, c_E the concentration of active enzyme in the EMR, k_{cat} the catalytic rate constant of the forward reaction (D-fructose to D-psicose), and Km_S and Km_P the MM constants of the forward and backward reaction, respectively. The thermal dependence of the equilibrium constant of the chemical reaction K_{eq} (**Equation 4.2**) and of the reaction rate constant k_{cat} (**Equation 4.3**) is described by a van`t Hoff and an Arrhenius correlation, respectively:

$$K_{eq} = \frac{c_{P,eq}}{c_{S,eq}} = K_{eq,ref}\ exp\left(\frac{\Delta H_{eq}}{R}\left(\frac{1}{T} - \frac{1}{T_{eq,ref}}\right)\right) \qquad \textbf{Equation 4.2}$$

$$k_{cat} = \frac{k_B T}{h} exp\left(\frac{\Delta G_{act}}{RT}\right) \qquad \textbf{Equation 4.3}$$

Here, $c_{S,eq}$ and $c_{P,eq}$ are the equilibrium concentrations of D-fructose and D-psicose, respectively, *R* denotes the universal gas constant, ΔH_{eq} the reaction enthalpy, k_b Boltzmann`s constant, *h* Planck`s constant, and ΔG_{act} the Gibbs' free energy of activation of the enzyme reaction. The temperature dependence of the MM constants can be expressed similarly to the equilibrium constant by a van't Hoff correlation but is not considered in this work.

4.2.1.1 Enzyme deactivation

We assumed a Lumry-Eyring equilibrium model (**Equation 4.4**, [167]) for the enzyme with an infinitely rapid equilibration between the active (*E*) and unfolded (*U*) enzyme fraction and an irreversible, first-order decay of the unfolded to the denatured enzyme fraction (*D*) (**Equation 4.4**).

$$E \overset{K_{EU}}{\longleftrightarrow} U \overset{k_{inact}}{\longrightarrow} D$$ **Equation 4.4**

In this case, enzyme degradation in a stirred tank with variable temperature (representing e.g. conditions in an EMR with temperature adjustment for constant conversion) can be described by the equilibrium-constant between the folded and the unfolded state of the enzyme K_{EU}, the first-order decay constant k_{inact} and the total amount of supplied enzyme $c_{E,tot}$:

$$\frac{dc_E}{dt} = \frac{c_{E,tot}}{(K_{EU}+1)}\left(-k_i K_{EU} - \frac{dK_{EU}}{dT}\frac{dT}{dt}\right)$$ **Equation 4.5**

with

$$K_{EU} = 1\ exp\left(\frac{-\Delta H_{EU}}{R}\left(\frac{1}{T} - \frac{1}{T_m}\right)\right)$$ **Equation 4.6**

$$k_i = \frac{k_B T}{h}\ exp\left(\frac{-\Delta G_{inact}}{RT}\right)$$ **Equation 4.7**

where ΔH_{EU} denotes the reaction enthalpy of reversible protein unfolding and ΔG_{inact} Gibbs' free energy of enzyme deactivation. By convention the reference state of the van`t Hoff equation is selected at equal concentrations of both species ($K_{EU,ref}$ = 1 for [*E*]=[*U*]) with the corresponding temperature T_m referring to the melting temperature. In order to estimate the enzyme's operational lifetime a specific operation regime – constant conversion facilitated by temperature adjustment until virtually all active enzyme is depleted – is considered. **Equation 4.1** is therefore solved for conversion *X*

$$\frac{dX}{dt} = -X + t_{EMR}\ \frac{c_E \frac{k_{cat}}{Km_S}\left((1-X) - \left(\frac{X}{K_{eq}}\right)\right)}{1 + \frac{(1-X)c_{i,EMRin}}{Km_S} + \frac{Xc_{i,EMRin}}{Km_P}} = 0 \quad , X = \frac{c_P}{c_{i,EMRin}}$$ **Equation 4.8**

Rearrangement yields

$$f = (1-X)c_E k_{cat} - X\frac{C_E k_{cat}}{K_{eq}} = \frac{XKm_S\left(1 + \frac{(1-X)c_{i,EMRin}}{Km_S} + \frac{Xc_{i,EMRin}}{Km_P}\right)}{t_{EMR}} = const$$ **Equation 4.9**

The RHS of **Equation 4.9** contains solely parameters that are temperature independent, therefore the derivative of the LHS of **Equation 4.9** with respect to time – here expressed as dimensionless time $\tau = \frac{t}{t_{EMR}}$ is:

$$\frac{df}{d\tau} = 0 = \frac{d\left((1-X)c_E k_{cat} - X\frac{c_E k_{cat}}{K_{eq}}\right)}{d\tau}$$ **Equation 4.10**

The required temperature for maintaining constant conversion can be calculated by

$$\frac{dT}{d\tau} = \frac{-\frac{dc_E}{d\tau}\left((1-X)k_{cat} - X\frac{k_{cat}}{K_{eq}}\right)}{\left((1-X)c_E - X\frac{c_E}{K_{eq}}\right)\frac{dk_{cat}}{dT} + \left(\frac{Xc_E k_{cat}}{K_{eq}^2}\right)\frac{dK_{eq}}{dT}}$$ **Equation 4.11**

with

$$\frac{dk_{cat}}{dT} = k_{cat}(T)\left(\frac{1}{T} + \frac{\Delta G_{act}}{RT^2}\right)$$ **Equation 4.12**

$$\frac{dK_{eq}}{dT} = K_{eq}\,\frac{\Delta H_{eq}}{RT^2}$$ **Equation 4.13**

4.2.2 TMB model

A transport-dispersive TMB model assuming linear isotherms for both sugars was used for the description of SMB operation as described previously in detail (**Chapter 3**). Briefly,

$$\frac{\partial c_i}{\partial t} + u_j\frac{\partial c_i}{\partial x} + F\,k_i a\,(q_i^* - q_i) = D_i\frac{\partial^2 c_i}{\partial x^2}$$ **Equation 4.14**

$$\frac{\partial q_i}{\partial t} = k_i a\,(q_i^* - q_i)$$ **Equation 4.15**

$$q_i = H_i\,c_i$$ **Equation 4. 16**

where c_i and q_i represent the concentrations of *i* in the mobile and stationary phase of the SMB, respectively, *j* the SMB section number (*j*= 1, 2, 3, 4), u the linear flow velocity of the liquid phase, x the spatial coordinate, and *F* the phase ratio (1-ε)/ε, with ε being the extraparticle porosity. Variable q^* is the equilibrium concentration in the solid phase, *k* the mass transfer coefficient between the mobile and solid phase, *D* the axial dispersion coefficient and u_{SP} the velocity of the solid phase.
Further, the volumetric flow-rates $Q_{SMB,j}$ in each section are defined as

$$Q_{SMB,j} = \frac{m_j\,V_j(1-\varepsilon) + V_j\varepsilon + V_{j,D}}{t_{sw}}$$ **Equation 4.17**

where m_j is the dimensionless flow-rate ratio describing the ratio between the net fluid flow rate and the net solid flow rate, V_j the empty column volume per section, $V_{j,D}$ the plant dead volume per section (previously determined to be 0.1 mL per column *[135]*) and t_{sw} the periodic switch time.

4.2.3 NF model

In order to describe the concentration of the recycling stream, an ideal steady-state NF model based on the membrane rejection *REJ* (**Equation 4. 18**) and the volume concentration

factor *VCF* (**Equation 4.16**) was implemented, relating retentate concentration $c_{i,Ret}$ (**Equation 4.20**), permeate concentration $c_{i,Perm}$ (**Equation 4.21**), and NF feed concentration $c_{i,NFin}$:

$$REJ = 1 - \frac{c_{i,Perm}}{c_{i,Ret}} \quad \textbf{Equation 4.18}$$

$$VCF = \frac{Q_{i,NFin}}{Q_{i,Ret}} \quad \textbf{Equation 4.19}$$

$$c_{i,Ret} = \frac{VCF}{VCF\ (1 - REJ)\ +\ REJ}\ c_{i,NFin} \quad \textbf{Equation 4.20}$$

$$c_{i,Per} = (1 - REJ)\ c_{i,Ret} \quad \textbf{Equation 4.21}$$

4.2.4 Node model

A node model based on the individual single unit models was established using mass balances. The feed node where the feed fresh up is mixed with the recycled retentate stream is denoted as

$$c_{\,i,EMRin} = c_{S_0} + \frac{(m_3 - m_4)\left(c_{i,Ret} - c_{S_0}\right)}{VCF\ (m_3 - m_2)} \quad \textbf{Equation 4.22}$$

where c_{SO} is the fresh-up substrate concentration, and m_1 to m_4 denote the flow-rate ratios in zone 1 to 4 in the SMB. The overall concentration in the retentate ($c_{S,Ret} + c_{P,Ret}$) was chosen to equal c_{SO}.

Further, the EMR outlet concentration c_{EMRout} was assigned to equal the concentration in the SMB feed stream c_{SMBin} and the concentration in the SMB raffinate stream c_{Raff} to equal c_{NFin}:

$$c_{i,EMRout} = c_{i,SMBin} \quad \textbf{Equation 4.23}$$

$$c_{i,Raff} = c_{i,NFin} \quad \textbf{Equation 4.24}$$

4.2.5 Performance parameter and purities

The purities of the SMB extract/product (PU_{Ex}) and the raffinate/recycling stream (PU_{Raff}) were defined as:

$$PU_{Ex} = 100\ \frac{c_{P,Ex}}{c_{S,Ex} + c_{P,Ex}}[\%] \quad \textbf{Equation 4.25}$$

$$PU_{Raff} = 100 \frac{c_{S,Raff}}{c_{S,Raff}\ +\ c_{P,Raff}}\ [\%] \quad \textbf{Equation 4.26}$$

Further, the process performance parameters throughput (*TP*), process yield (*Y*), EMR productivity (PR_{EMR}), SMB productivity (PR_{SMB}), and SMB desorbent requirement (*DR*) were defined as:

$$TP = Q_{Ex} c_{P,Ex} \left[\frac{g}{g}\right]$$ **Equation 4.27**

$$Y = \frac{TP}{Q_{S0}\ c_{S0}} [\%]$$ **Equation 4.28**

$$PR_{EMR} = \frac{TP}{c_E\ V_{EMR}} \left[\frac{g}{g}\right]$$ **Equation 4.29**

$$PR_{SMB} = \frac{TP}{n_C\ V_C} \left[\frac{g}{Lh}\right]$$ **Equation 4.30**

$$DR = \frac{Q_D}{TP} \left[\frac{L}{g}\right]$$ **Equation 4.31**

where V_{EMR} and V_C are the EMR volume and the SMB empty column volume, respectively, n_C represents the total number of SMB columns employed and Q_D the flow-rate of the SMB desorbent stream.

4.3 Materials and methods

4.3.1 Chemicals

All chemicals except for D-fructose (Carbosynth, Compton, UK) and stationary phase materials were purchased from Sigma Aldrich (Buchs, Switzerland) in the highest available purities. Pure D-psicose used for enzyme characterization was crystallized from SMB extract (PU_{Ex}≥ 98 %) as previously described [116]. Deionized water was used to for the preparation of all solutions and as desorbent for the SMB.

4.3.2 Enzyme production

A thermostabilized and 6x His-tagged enzyme variant of D-tagatose epimerase from *P. cichorii* (PcDTE Var8, [81]) was overproduced in *E. coli* BL21(DE3) using the T7 expression system. After cultivation in an aerated 3 L culture to a cell wet weight concentration of approximately 80 g L^{-1}, cells were harvested by centrifugation and an aliquot of 50 g of wet biomass was suspended in lysis buffer containing 10 mM sodium phosphate buffer (pH 7.0), 30 mM imidazole, and 100 mM NaCl. The cells were then disrupted using a high-pressure homogenizer (M-110P, Microfluidcs, Westwood, USA). Cell debris was removed by centrifugation at 40,000 rcf for 20 min at 4°C, before the clarified lysate was distributed over 3 gravity-flow columns, each filled with 2 mL Ni-Sepharose 6 Fast Flow (GE Healthcare, Uppsala, Sweden). Columns were extensively washed with lysis buffer before adsorbed protein was eluted with 5 x 2 mL elution buffer (10 mM sodium phosphate buffer pH 7.0, 200 mM imidazole, 100 mM NaCl). The fractions containing pure PcDTE Var8 were pooled after SDS-PAGE analysis and dialyzed first against 10 mM sodium phosphate buffer pH 7.0 with 1 mM EDTA, then 2 times against 10 mM sodium phosphate buffer pH 7.0. The volume ratio (enzyme solution: buffer) was chosen 1:200 for each dialysis step. Dialyzed protein solution was then supplemented with a final concentration of 1 mM $MnCl_2$ to ensure excess availability of the enzyme cofactor and stored at -80°C. Enzyme concentration was determined spectrophotometrically at 280 nm using the extinction coefficient ε and the molecular weight (*Mw*) calculated for PcDTE Var8 using the online tool ProtParam [168] (ε = 46,410 M^{-1} cm^{-1} and *Mw* = 33,790 Da).

4.3.3 Experimental progress curves of PcDTE Var8

Enzyme kinetics of PcDTE Var8 were determined at 50°C by recording progress curves of the formation of D-psicose from D-fructose in 50 mM sodium phosphate (pH 7.0) at 6 different substrate concentrations (2.5 g L^{-1}, 5.2 g L^{-1}, 10.4 g L^{-1}, 21 g L^{-1}, 42 g L^{-1}, 167 g L^{-1} D-fructose) and for the reverse reaction again at different substrate concentrations (2.5 g L^{-1}, 5.2 g L^{-1}, 10.4 g L^{-1}, 21 g L^{-1}, 42 g L^{-1}, 84 g L^{-1} D-psicose). The assay was started by the addition of

purified enzyme to 13 µM. Aliquots of 20 µL were regularly removed for analysis. The enzymatic reaction was stopped by mixing the aliquot with 145 µL of 0.1 M HCl and incubating for 5 min, and the resulting solution was neutralized with 135 µL of 0.1 M NaOH. Conversion was determined by HPLC analysis using a LC ICS-3000 system (Dionex, Olten, Switzerland) equipped with a CarboPac PA1 column (250 mm x 4 mm ID) with a CarboPac PA1 guard column. Samples were eluted isocratically with 25 mM NaOH at a flow rate of 2.0 mL min^{-1} and detected by triple-pulsed amperometry using an EC detector with a gold electrode.

4.3.4 Determination of the reaction equilibrium constant K_{eq}

The thermodynamic equilibrium between D-fructose and D-psicose was experimentally determined in batch experiments at 40°C, 50°C, 60°C and 70°C using a BioShake iQ thermoshaker (Q.Instruments, Jena, Germany). The experiment was started by supplementing 1 mL of buffered D-fructose solution (180 g L^{-1} D-fructose in 10 mM sodium phosphate buffer, pH 7.0) with 54 µg PcDTE Var8. After 13h of incubation a 100 µL sample was removed and another 4 µL of 13.5 mg mL^{-1} (total of 54 µg) PcDTE Var8 were added. The procedure was repeated after 17h and 31h. All samples taken were immediately transferred to a pre-cooled Eppendorf tube at 4°C to rapidly stop the reaction. Conversion was measured on an Agilent 1200 series HPLC system (Agilent Technologies) equipped with an refractive index detector (RI) using a 100 mm x 7.8 mm ID AMINEX Fast Carbohydrate (Pb^{2+}) column at 85°C with a Carbo-P guard column (Biorad, Reinach, Switzerland) using 2 mL min^{-1} water as the mobile phase. At all temperatures, the equilibrium was already reached after either the second (13h) or the third enzyme supplementation (17h), which was judged by comparing the concentration of D-psicose and D-fructose from HPLC analysis after 0, 13, 17 and 31h.

4.3.5 Isothermal deactivation experiments of PcDTE Var8

Operational stability was analysed in an 8.6 mL heat-jacketed EMR (Julich Fine Chemicals, Julich, Germany) equipped with an Ultracel regenerated cellulose membrane with nominal cut-off of 10 kDa (Millipore Cooperation, Bedford, USA). The EMR was stirred at 800 rpm using a magnetic stirrer and the temperature was controlled using an external thermostat (Huber, Offenburg, Germany). Feed solution (180 g L^{-1} D-fructose, 10 mM sodium phosphate buffer, pH 7.0) was supplied using an Agilent 1200 series HPLC pump (Agilent Technologies) before the enzyme was injected using the autosampler of the Agilent HPLC. Experiments were conducted at 50, 60, 65 and 70°C with enzyme concentrations of 0.20 g L^{-1} (6.0 µM), 0.13 g L^{-1} (3.9 µM), 0.26 g L^{-1} (7.8 µM) and 0.13 g L^{-1} (3.9 µM), respectively. All experiments were performed at a flow rate of 0.175 mL min^{-1} except for the EMR run at

65°C that was supplied with substrate solution at 0.35 mL min^{-1}. Fractions were collected periodically at the outlet of the reactor using a Frac-920 Fraction Collector (GE Healthcare). Conversion was measured on an Agilent 1200 series HPLC system as described above.

4.3.6 EMR stand-alone experiment at elevated temperature

Based on the inactivation parameters extracted from the isothermal deactivation experiments (see **4.3.5**) we calculated the amount of enzyme that needed to be periodically replenished (2.1 x 10^{-2} mg per 30 min) at the chosen temperature and enzyme concentration (70°C and 0.1 g L^{-1} PcDTE Var8, respectively) in order to keep the level of enzyme activity constant. A stand-alone EMR run with periodic enzyme injections was performed using a manual Rheodyne injection valve (IDEX, Rohnert Park, US) equipped with a 5 mL loop for injecting the initial amount of PcDTE Var8 and the Agilent HPLC autosampler for periodically readjusting the active enzyme amount in the reactor every 30 min. A buffered substrate solution (180 g L^{-1} D-fructose, 10 mM sodium phosphate buffer, pH 7.0) was supplied initially at a flow-rate of 0.175 mL min^{-1}, and then after 25 h at 0.35 mL min^{-1}, after 45 h at 0.7 mL min^{-1}, and after 68.5 h again at 0.175 mL min^{-1}. Samples were fractionated at the reactor outlet and analyzed as described above.

4.3.7 Integrated process set-up

A representation of all unit operations in the lab-scale integrated process is provided in **Figure 4.1A**. Briefly, the set-up is composed of the 8.6 mL EMR (the detailed EMR set-up is described in **4.3.5**), a laboratory-scale SMB plant based on the Amersham AEKTA basic-10 system (GE Healthcare) with eight stainless steel columns (150 mm x 8 mm ID, Morvay Analytics, Basel, Switzerland) packed with Dowex 50 WX4-400 (Ca^{2+}) ligand exchange material, and a custom designed cross-flow NF device (MMS, Urdorf, Switzerland) with an integrated gear pump (Scherzinger, Furtwangen, Germany) and a flow-controller (LIQUI-FLOW, Bronkhorst, Reinach Switzerland) regulating the NF retentate stream. Concentration of sugars was performed at 40°C using a 28 cm^2 polyamide Filmtec NF-90 membrane area (nominal cut-off of 90 Da, Dow Chemicals, Midland, USA). The individual unit operations (EMR, SMB, and NF) were connected by 1/16" OD/ 0.020" ID PEEK capillaries or 1/8" OD/ 0.062" ID ETFE capillaries (both Ercatech, Bern, Switzerland) when used up-stream of a pump. Three 10 mL stirred vessels (labelled as A, B, C in **Figure 4.1**) were positioned in the interface of each unit operation to withdraw samples from the integrated process via a syringe. Additionally, three online degasser were used to degas the streams Q_D, Q_{SMBin}, and Q_{EMRin} (**Figure 4.1**).

A

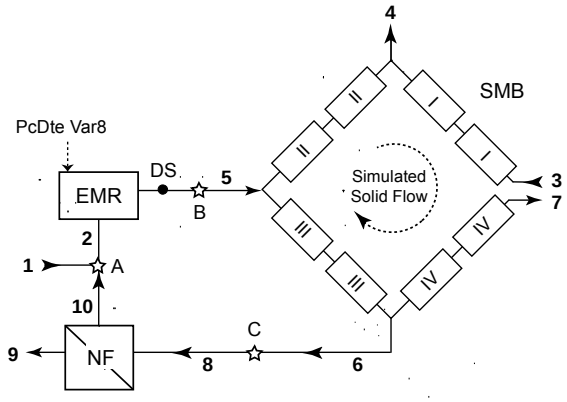

B

	Stream	Flow rate	Concentration [g L^{-1}]	
#		[ml min^{-1}]	D-Fructose	D-Psicose
1	Q_S	0.431	180	0
2	Q_{EMRin}	1.503	180	0
3	Q_D	6.435	0	0
4	Q_{Ex}	2.198	0	30.3
5	Q_{SMBin}	1.486	135	45
6	Q_{Raff}	1.863	107.5	0.5
7	Q_W	3.859	0	0
8	Q_{NFin}	1.843	107.5	0.5
9	Q_{Perm}	0.755	2.5	0
10	Q_{Ret}	1.088	180	0

Figure 4.1. (**A**) Scheme of the investigated integrated process for the production of the rare sugar D-psicose from D-fructose consisting of an enzyme membrane reactor (EMR), simulated moving bed (SMB) chromatography and nanofiltration (NF). (**B**) Flow rates and simulated steady state concentrations applied in the experimental run at the respective site. Stars indicate sampling devices (A, B, C); other abbreviations: DS= 2-column desalting installation.

In order to remove the buffer ions from the SMB feed stream a simple two column-desalting (DS) installation was implemented consisting of a two-position Rheodyne 7030 six port valve (IDEX) with a double three-way switching pattern and two VICI PEEK columns (150 mm x 7.5 mm ID, Schenkon, Switzerland) packed with mixed-bed resin (Dowex Marathon MR-3). The desalting columns, which were alternatingly switched into the flow, were already pre-equilibrated with feed solution and replaced either every hour (during start-up) or every 3 h (after integration).

4.3.8 In silico procedures

The fitting of the enzyme progress curves and the isothermal inactivation experiments was performed in MATLAB (Mathworks, Natick, USA), as described previously [169]. Model-based calculation of the operational lifetimes of the enzyme and simulation of EMR operation as a stand-alone unit operation was performed in MATLAB, whereas the analysis and optimization of the integrated process model was implemented in the gPROMS modelling environment (PSE, London, UK). The main parameters used for the latter simulations are given in **Table 4.1**.

Table 4.1. Parameters used for the integrated model optimization. Superscripts: exp: experimentally determined parameter; fit: parameter derived from model-based fitting of experimental data; sup: parameters from supplier or literature data

	Parameter		
EMR	PcDTE Var8	M_w	33,790 Da
		c_E	2.96×10^{-2} mM
	Reaction equilibrium	$K_{eq,ref}$	0.38 (exp)
		$T_{eq,ref}$	323.15 K (exp)
		ΔH_{eq}	8.22 kJ mol^{-1} (fit)
	Enzyme kinetics	ΔG_a	69.6 kJ mol^{-1} (fit)
		K_{mS}	39 mM (fit)
		K_{mP}	23 mM (fit)
	Enzyme stability	K_{EU}	1 (fit)
		T_m	353 K (fit)
		ΔH_{EU}	67.6 kJ mol^{-1} (fit)
		ΔG_{inact}	113.6 kJ mol^{-1} (fit)
SMB	Column characteristics	ε	0.24 (exp)
		r_p	4×10^{-3} cm (sup)
		L_c	2x15 cm
		δ_{SP}	736.8 g L^{-1} (sup)
		α	2.34×10^{8} cm^{-2} (exp)
		η_{H2O}	0.4 cP (sup)
	Adsorption	H_A	1.04 (fit)
		H_B	0.59 (fit)
	Kinetic parameters	k_A	38×10^{-3} cm min^{-1} (fit)
		k_B	85×10^{-3} cm min^{-1} (fit)
		λ_A	9.5 (fit)
		λ_B	20.7 (fit)
NF	Rejection	*REJ*	0.98 (exp)

4.4 Results and discussion

In order to characterize the novel D-tagatose epimerase, PcDTE Var 8 [81] for its application in the projected integrated process, we first determined the temperature-dependent activation and deactivation parameters of PcDte Var8, following a model-based characterization procedure (**4.4.1**). In a next step, an integrated process model was constructed. Therefore, the assigned models of the single unit operations (EMR, SMB, NF) were interconnected in a node model (**Equation 4.19 to 4.21**). Apart from the EMR model accounting for rMM kinetics (**Equation 4.1**), a TMB model (a mathematically less expensive representation of the SMB unit), and an ideal filtration model accounting for incomplete rejection of sugars in the NF unit (*REJ* = 0.98 [116]) were used for model-based description. The applied transport-dispersive TMB model had been established in a previous work (**Chapter 3**), which confirmed linear isotherms for both sugars.

First the model was used for implementing a highly productive, experimental integrated process run on our existing lab-scale plant (**4.4.2**). Next, a cost-based optimization procedure was established that allows for process optimization on every scale (**4.4.3**) and was used for an *in silico* study elucidating the impact of reactor temperature on the overall process economics.

4.4.1 Model-based characterization of PcDTE Var8

For parameterizing the activation and deactivation of PcDTE Var8 as a function of temperature isothermal continuous EMR experiments were fitted to model-descriptions. Numeric values for the K_m of forward and backward reactions (**4.4.1.1**) as well as the thermal dependence of the K_{eq} (**4.4.1.2**) were *a priori* determined from independent experiments in order to reduce the number of free model parameter in the subsequent fitting procedure. The temperature-dependence of the K_m values was considered to be low [170] and therefore neglected in this work.

4.4.1.1 K_m values

Assuming reversible Michaelis-Menten (rMM) kinetics, the K_{mS} and K_{mP} for substrate and product were first estimated using progress curve experiments [79]. Each experiment consisted of 6 individual progress curves for the forward and backward reaction, respectively, recording the conversion over time from D-fructose to D-psicose and *vice versa*. The experiments were performed at 50°C in order to minimize the impact of temperature-dependent deactivation. As expected, rMM kinetics provided an accurate description of all obtained experimental progress curves (**Supplementary Figure 4.1** in **4.6**) and no deviation from the model prediction was observed at high substrate concentrations indicating that PcDTE Var8 is not subject to substrate or product inhibition. K_{mS} and K_{mP}

were found to be 39 mM (7.0 g L^{-1}) and 23 mM (4.1 g L^{-1}), respectively. Please note that the extracted value of 36 s^{-1} for k_{cat} was only used for model evaluation (**4.4.1.3**) and does not constitute a direct input parameter for the *in silico* procedures.

4.4.1.2 Temperature dependency of the thermodynamic equilibrium

Due to the lack of literature data on the position of the thermodynamic equilibrium between D-fructose and D-psicose at different temperatures, we performed a number of equilibrium experiments. The experimentally determined K_{eq} values (0.35, 0.38, 0.43, 0.46 for 40°C, 50°C, 60°C, 70°C, respectively) were used for estimating the reaction enthalpy value of ΔH_{Eq}=8.22 kJ mol^{-1} ("Van't Hoff plot", **Supplementary Figure 4.2.** in **4.6**), which was used as input parameter for the process model (**Equation 4.2**).

4.4.1.3 Temperature dependency of enzyme stability and catalytic parameters of PcDTE Var8

We next performed a series of isothermal inactivation experiments (at 50°C, 60°C, 65°C, and 70°C) using a buffered feed solution containing 180 g L^{-1} D-fructose. Importantly, the amount of PcDTE Var8 supplemented was selected to ensure that even at the start of the experiment, the EMR outlet concentration was significantly below the equilibrium concentration at the respective temperature. Whereas at 50°C PcDTE Var 8 showed only minor inactivation over the investigated time span of 6,000 min, the inactivation became more dominant at more elevated temperatures (**Figure 4.2**).

Next, the thermal activation and deactivation parameters of the PcDTE Var 8 were determined by fitting the D-psicose concentration to potential inactivation models [169] using a non-linear regression method according to Levenberg-Marquardt. A three-state Lumry-Eyring model was used (**Equation 4.4**), as it already provided a sufficiently accurate description of the experimental data (**Figure 4.2**). A complete data set of activation and inactivation parameters was obtained and is depicted in **Table 4.1**. The value of k_{cat} that was obtained based on the van`t Hoff equation (**Equation 4.3**) (k_{cat} = 37.9 s^{-1} at 50°C) was in excellent agreement with the k_{cat} value that was obtained by fitting of the progress curve (36 s^{-1}, see section **4.4.1.1**) underlining the applicability of the applied model approach.

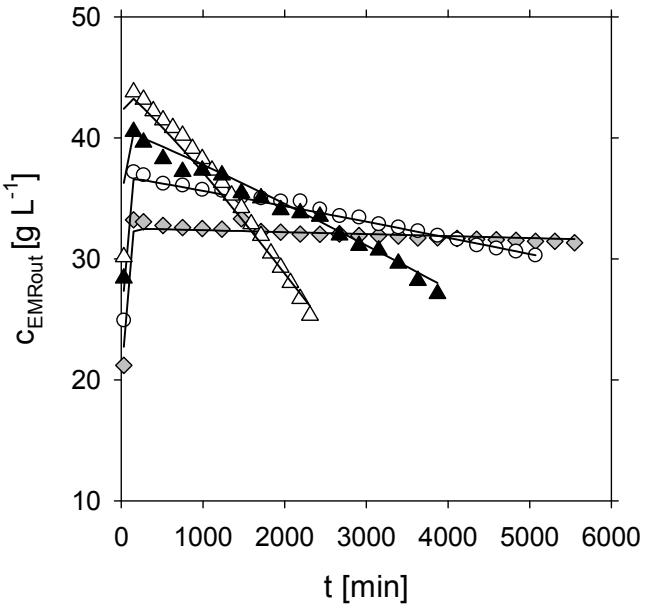

Figure 4.2. D-Psicose concentration measured at the outlet of the enzyme membrane reactor at 50°C (grey diamonds), 60°C (white circles), 65°C (black triangles), 70°C (white triangles). Solid lines indicate the best fit assuming rMM kinetics and inactivation according to a three-state Lumry-Eyring model. The less enzyme deactivation was observed (flat slope), the longer the experiments were conducted in order to obtain a visible decrease in enzyme activity.

4.4.2 Experimental model validation on a lab-scale SMB plant

To confirm the feasibility of the model-based design an integration run was performed using lab-scale process equipment, specifically, an 8.6 mL EMR, an NF with 28 cm^2 membrane area and an SMB equipped with eight 15 cm x 0.8 cm ID columns. An operating point that maximizes the *TP* in the existing plant was chosen. Briefly, the SMB was operated at 70°C adapting an operating point (**Table 4.2**) from a previous work (**Chapter 3**) imposing full purity constraints on both outlet streams (PU_{Ex}, PU_{Raff} ≥ 99.9%). Please note that the applied SMB flow-rates also represent the maximum possible flow-rates feasible with the existing equipment due to constraints of the pumps and operational limits of other parts of the lab-scale implementation (e.g. in-flow check valves). With the column dimensions, the *m*-values and the t_{sw} fixed, all SMB flow rates were set, which automatically sets the flow-rates in the entire process, as the feed flow rate for the SMB is necessarily equal to the flow rate in the EMR (**Equation 4.23**) and the NF feed flow-rate has to equal the SMB raffinate flow-rate (**Equation 4.24**). For a detailed representation and a summary of the applied flows please see also the scheme in **Figure 4.1**.

The NF flow-rates were calculated taking into account the incomplete retention of the NF membrane and the retentate flow-rate (and thus the retentate concentration) was adjusted such that it matched the concentration of the refresh-feed stream (180 g L^{-1}).
The EMR was operated at high temperature (70°C), which was necessary to cope with the short residence time (**Table 4.2**) that was imposed by the productive operation of the SMB. The EMR was operated to produce a high degree of conversion of 25%. Obviously, one has to take into account that during isothermal operation of the EMR the active enzyme would be subject to a steady depletion due to thermal inactivation, which would interfere with a stable long-term operation of the envisioned integrated process. Thus, constant conversion was achieved by maintaining the concentration of the native enzyme fraction (*E*) by periodically injecting fresh enzyme.
To test this strategy an isothermal EMR run was conducted at 70°C using a programmable HPLC autosampler for the repeated injection of fresh enzyme ("enzyme refresh strategy"). The time-dependent depletion of the active enzyme pool was estimated based on the thermal inactivation rate (**Equation 4.7**) and used to calculate the amount of enzyme that needed to be injected every 30 min (**4.3.6**). The performed stand-alone experiment revealed that this approach constituted a feasible strategy to keep the conversion in the reactor stable over long operating period (**Supplementary Figure 4.3** in **4.6**).
Accordingly, the EMR was implemented for the operation in the fully integrated process. Specifically, an initial amount of 8.7 mg (1.0 g L^{-1}) of PcDTE Var 8 was injected yielding the envisioned conversion of roughly 25% at the given t_{EMR}. In order to replace the thermally inactivated amount of PcDTE Var8, 0.2 mg of enzyme were injected every 30 min.

Table 4.2. Operation parameters applied in the experimental integration run

Operational parameters	
m_1	1.136
m_2	0.634
m_3	0.973
m_4	0.548
t_{sw}	1.3 min*
t_{EMR*}	5.8 min

*t_{SW} = 2.6 min for 30 cm section

The integrated process was started by prefilling the EMR with buffered feed solution containing 180 g L^{-1} D-fructose and 17.4 mM sodium phosphate buffer (pH 7.0) and heating the EMR up to 70°C. Unlike the previous implementation of the process design [116], the present implementation included a desalting unit located between the EMR and the SMB.

Desalting is necessary to prevent the slow displacement of the Ca^{2+} ions in the ion exchange resin by the cations in the buffer.

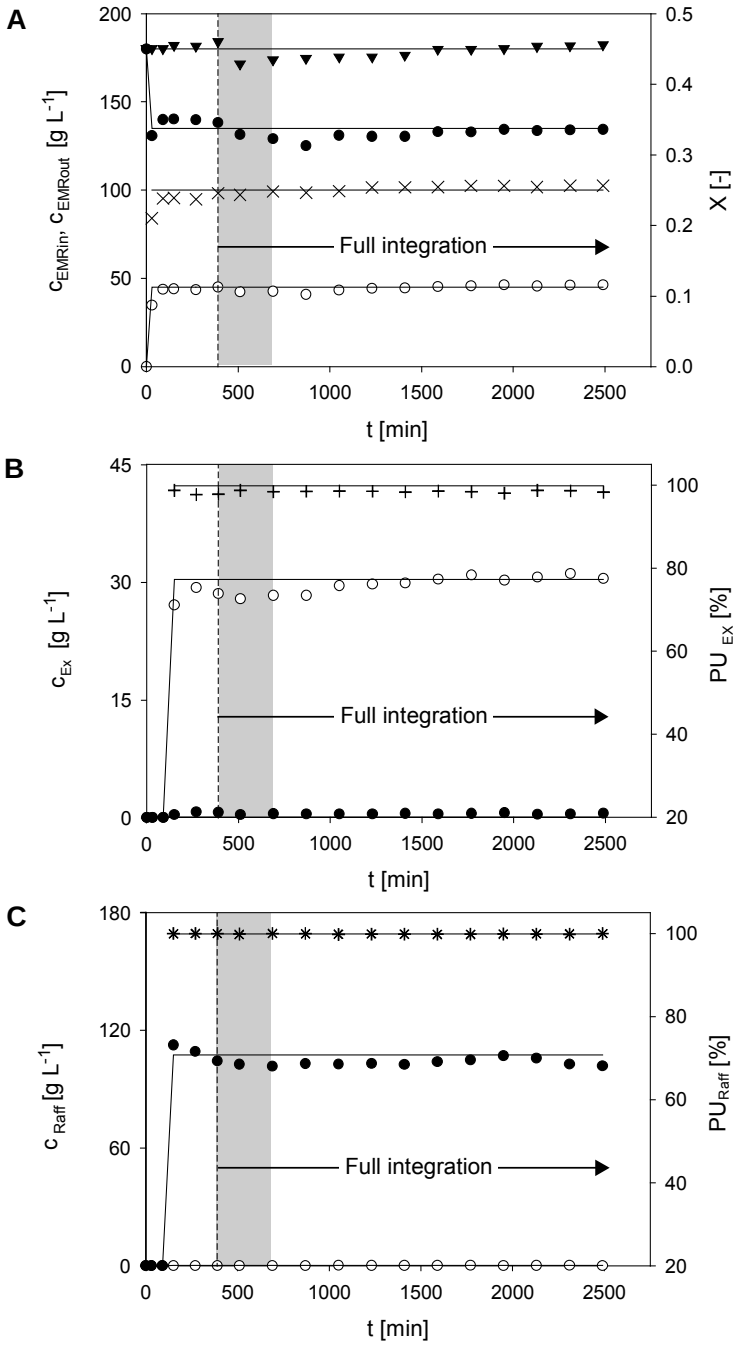

Figure 4.3. Experimental (symbols) and simulated (lines) concentrations of D-fructose (black) and D-psicose (empty) in an lab-scale integrated process run measured (**A**) at the EMR inlet (sampling device A, triangles) and EMR outlet (sampling device B, circles), (**B**) in the SMB extract (circles) and (**C**) in the raffinate stream (sampling device C, circles) ; the grey area represents the time period where the NF was adjusted in a stepwise manner to deliver accurate recycling stream flow rates. Other symbols: *X* (crosses), PU_{Ex} (+), PU_{Raff} (stars)

Next, the reactor was supplied with the initial amount of PcDTE Var, after 30 min the enzyme refresh was started by injecting the first 0.2 mg PcDTE Var8. The envisioned conversion of 25% was reached after 100 min (**Figure 4.3A**) and the EMR was connected to sampling device B, which served simultaneously as a stirred 20 mL feed reservoir for the SMB. Subsequently, the SMB was started up using the accumulated feed from the sampling device B (**Figure 4.1A**) and run until the outlet concentrations determined at the SMB extract (29.3 g L^{-1}, **Figure 4.3B**) and raffinate port (104.6 g L^{-1}, **Figure 4.3B C**) were close to the steady state concentrations (**Figure 4.1B**). After 400 min the raffinate stream was connected to sampling device C, which simultaneously acted as a feed reservoir for the NF. For an accelerated start-up, the NF was previously filled with D-fructose solution of the projected retentate concentration of 180 g L^{-1}. The procedure has been previously used to minimize the start-up time of the NF [116] and allows for immediate recycling of the Q_{Ret}. In order to fully integrate the process, Q_{Ret} was connected to the sample taking device A and the flow-rate of Q_S was reduced from 0.519 mL min^{-1} during the start-up to 0.431 mL min^{-1}.
Comparison of the experimental and the simulated concentrations revealed that they were in good overall agreement (**Figure 4.3**). After full integration a slight decline in the EMR inlet concentration profile was observed (**Figure 4.3A**) which resulted from a too low D-fructose concentration in the retentate stream recycled via the NF (as determined by HPLC analysis). Therefore, the concentration of the retentate stream was increased in a stepwise manner by manually adjusting the *VCF* over a period of 300 min (**Figure 4.3**, grey area). Apart from the minor disturbances during this time period, no significant deviation from the simulated concentrations could be detected. Overall, 20.3 mg PcDTE Var8 (of a total of 29 mg provided) were inactivated during the complete run time of 41 h. This resulted in a remarkable PR_{EMR} of 10.6 kg D-psicose per L of reactor volume and day (or correspondingly 4.5 kg D-psicose per g enzyme and day). It is worth noting that the process immediately delivered D-psicose and D-fructose in high purity in the extract (PU_{Ex} ≥ 98 %, **Figure 4.3B**) and raffinate stream (PU_{Raff} ≥ 99 %, **Figure 4.3C**), respectively.
The highly productive way to operate the SMB plant led to a PR_{SMB} of 2.3 kg of D-psicose per L of SMB column volume and day (77-fold more than in the first implementation) and in consequence to comparatively high desorbent requirement (37 L per kg D-Psicose) which was however still 16-fold less than in the first implementation of the process [116]. Overall, an experimental process yield of 96 % and preparative amounts of D-psicose (TP = 95 g day^{-1}) could be obtained, which represents, to the best of our knowledge, the highest amount of rare sugar D-psicose produced in a fully integrated set-up so far.

4.4.3 In silico optimization of the integrated process

We next used the established integrated process model for a comprehensive *in silico* optimization of the integrated process on every scale.

4.4.3.1 Objective cost function

An important aspect when optimizing integrated processes is the selection of the objective function. Ideally, the objective function should cover the most important cost contributors to identify the operating point where the product could be obtained at minimum costs. In this work, next to the major cost-contributors in SMB chromatography (desorbent (*D*), stationary phase (*SP*)) we considered the cost contribution of the enzyme (*E*) and of the substrate (*S*) loss occurring due to the incomplete rejection of the NF membrane. Please note that as the cost contribution of the NF membrane was identified as relatively small compared to the overall cost considered, it was not further considered after a first estimation.

Next, in order to cover the multiple objectives in one function a cumulated cost function (*CoFu*, **Equation 4. 32**) was established,

$$CoFu = P_S \frac{\dot{M}_S}{TP} + P_E \frac{\dot{M}_E}{TP} + P_{SP} \frac{\dot{M}_{SP}}{TP} + P_D \frac{\dot{M}_D}{TP} \rightarrow min \qquad \textbf{Equation 4.32}$$

where P_z with $z \in \{S, E, SP, D\}$ represents the specific prices of the respective consumables and ($\dot{M}_Z$) represents the mass flows of the consumables exhausted, which can be either derived directly from the operating points in case of educt feed and the solvent supply or by calculating the ratio of required amount of enzyme or stationary phase with the respective lifetime. By substituting the terms in **Equation 4.32** the cost function can be expressed as a function of the cost-relevant performance parameters (*Y*, PR_{EMR}, PR_{SMB}, *DR*),

$$CoFu = \frac{P_S}{Y} + \frac{P_E}{PR_E\ t_{E,op}} + \frac{P_{SP}}{PR_{SP}\ t_{SP,op}} + P_D DR \rightarrow min \qquad \textbf{Equation 4.33}$$

Please note that the cost term used throughout this work refers solely to the production costs originating from the consumption of auxiliaries such as solvents, stationary phase, enzyme and educt and should not be confused with total manufacturing costs. Down times necessary for exchanging the spent biocatalyst are also not considered.

4.4.3.2 Model-based estimation of the temperature-dependent operating time of PcDTE Var8

For an optimization on the basis of the proposed cost function specific prices of all consumables (*Z*) and the maximum possible operating period of the stationary phase and the enzyme need to be known or estimated. While we found relatively detailed information on the specific consumable prices by consulting literature [164], web databases (alibaba.com) and supplier`s information (e.g. for lifetime/replacement times of chromatographic phases), estimating the possible operating period of the biocatalyst was more challenging. Here, one important issue is constituted by the selected operating temperature of the reactor. This is due to the fact that temperature represents a key variable [171] in the optimization of economics in biocatalytic processes affecting enzyme activity, the equilibrium position in reversible reactions as well as enzyme degradation [166]. As stable operation (as well as the application of a steady state model for optimization) further requires that the conversion stays constant, we decided to exploit the temperature-induced activation of the reaction rate by heating up the reactor (**Figure 4.4B**) to counterbalance for the time-dependent loss of active enzyme. However, the concomitant change in the enzyme deactivation rate, the change in equilibrium between folded and unfolded enzyme fractions and the change in the thermodynamic equilibrium between product and substrate have to be considered. Therefore a model was established that takes all these parameters into account yielding an analytical solution for the temperature gradient (**Equation 4.11**) and thus, a maximum operating time of the reactor ($t_{op,E}$), assuming a certain starting temperature and constant conversion. As such a temperature gradient could be applied until virtually no active biocatalyst is left (or the steepness of the required temperature increase exceeds the technical capabilities of the thermostat), it principally reflects an ideal scenario where the entire catalytic capacity of the biocatalyst could be used for conversion of substrate into product.

We assumed a substrate concentration of 180 g L^{-1} D-fructose and an enzyme concentration of 1 g L^{-1} which was considered to be a reasonable concentration based on previous EMR experiments. Based on these assumptions we calculated $t_{op,E}$ and the reactor performance parameters for different temperatures (20°C - 70°C) and conversion rates *X* (free parameter) (**Figure 4.4**). Two trends could be confirmed in terms of PR_{EMR}: firstly, higher operating temperatures appear to be superior to low temperature operation in terms of PR_{EMR}. Secondly, the operation becomes less productive when the reactor is operated close to equilibrium (**Figure 4.4A**). Analysis of $t_{op,E}$ with respect to the starting temperature indicated that, as expected, high-temperature operation drastically reduces $t_{op,E}$ (**Figure 4.4B**). In contrast there was only little influence of *X* (see **Supplementary Figure 4.4** in **4.6**). We therefore adopted a fixed conversion of X= 0.1 for the calculation of $t_{op,E}$ and

the respective temperature gradients (**Figure 4.4B**). The exact values of $t_{op,E}$ are displayed in **Table 4.3**.

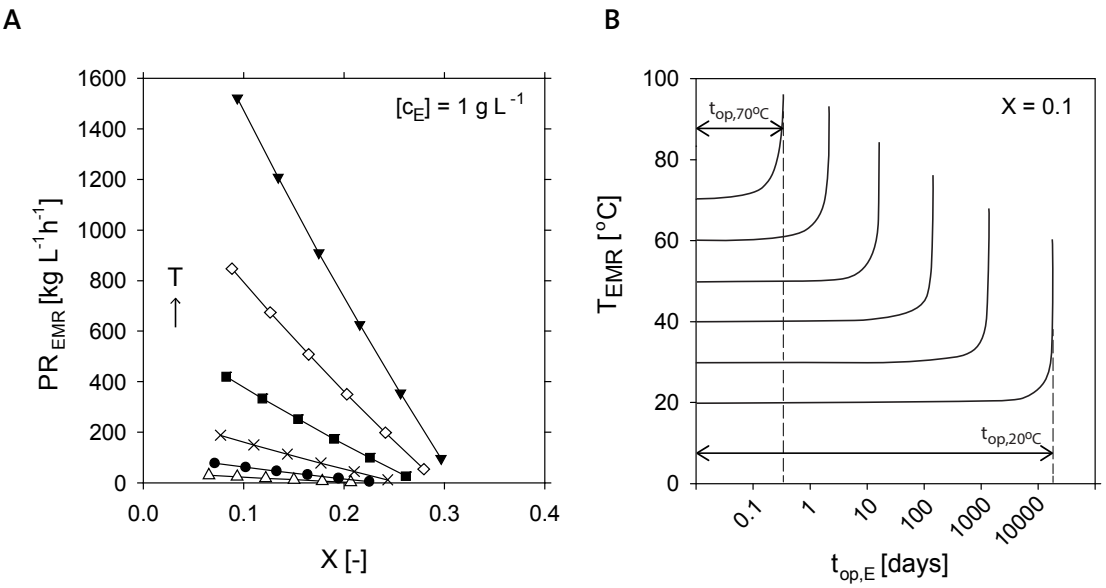

Figure 4.4. (**A**) Simulation of the temperature-dependence of PR_{EMR} for PcDTE Var8 as a function of X; symbols: T_{EMR}: 20°C (empty triangles), 30°C (black circles), 40°C (crosses), 50°C (black squares), 60°C (white diamonds), 70°C (black triangles); (**B**) Simulated temperature gradients resulting in a constant conversion of X = 0.1; the maximum possible operating time for temperature gradients starting at 20°C ($t_{op,20°C}$) or 70°C ($t_{op,70°C}$) are indicated with arrows

4.4.3.3 In silico optimization of the integrated process

From an enzyme cost perspective, operation at low temperature is clearly advantageous, however it remains unclear if this scenarios prevails when coupling the reactor to an SMB. As stationary phases are typically considered to be rather stable in the specified range of operating conditions, the dilemma between decreased stability and better performance at elevated temperature (this type of separation system works better at elevated temperatures [55]) is lifted. Consequently, we set SMB temperature to 70°C which corresponds to the optimum temperature found in the previously performed stand-alone optimization of the SMB (**Chapter 3**). Different reactor starting temperatures ranging from 20°C to 70°C were applied in the optimization runs. For the optimization we assume that the constant conversion policy introduced before is applied. As the limited enzyme lifetime is accounted for in the applied cost function and the conversion of the initial temperature is maintained, the reactor model applied in the optimization assumes steady state operation on the basis of the enzyme kinetics at the starting temperature. For the sake of simplicity and due to the fact that throughout the bulk of the operation period the reactor temperature deviates not much from its initial value (**Figure 4.4B**) we use the term reactor

temperature (T_{EMR}) when actually referring to the reactor starting temperature in the following. Moreover, a stringent purity constraint was taken into account for the product stream ($PU_{Ex} \geq 99.5\%$), whereas reduced purity requirements were admitted for the recycling stream (PU_{Raff} = unspecified). Further, a maximum pressure drop of 80 bar in the SMB plant was adopted to impose a lower limit to the switch time in the SMB (**Chapter 3**).

Table 4.3. Cost estimates of consumables *Z* and operating time $t_{op,Z}$

Z	P_x (USD kg^{-1})	$t_{op,Z}$ (days)
Substrate	1	-
Enzyme	600	17000/1400/140/16/2/0.3*
Solid phase	20	365
Desorbent	1.25 x 10^{-3}	-

* for T_{EMR} of 20/ 30/ 40/ 50/ 60/ 70°C

The feed concentration could in principle also be included as an optimization variable. However, in this work we chose the maximum feed concentration to match the one investigated in a previous work (180 g L^{-1} D-fructose) (**Chapter 3**). At a substrate concentration of 180 g L^{-1} D-fructose the enzyme kinetics are clearly in the v_{max} -region (i.e. the reaction is running at 96% of the maximum possible velocity) meaning the reaction rates are virtually independent of substrate concentration. A further increase in concentration should therefore not impact reactor performance metrics by much. However, preliminary experiments indicated that D-fructose concentrations above 200 g L^{-1} were affecting the adsorption as isotherms were found to slightly deviate from linearity, which, in turn, is impairing the robustness of the integrated process design.

Next, for each T_{EMR} an optimization of the respective operation parameters (*m* values, t_{sw}, t_{EMR}) was performed. Upon comparison of the distribution of the costs for the investigated cases it can be seen that the major contributors significantly change as function of the T_{EMR} (**Figure 4.5A**). The cost function increases exponential with increasing T_{EMR} from 0.07 \$ kg^{-1} at 20°C to 0.37 \$ kg^{-1} at 70°C demonstrating the importance of rational T_{EMR} selection. The evolution of costs with temperature can be largely attributed to the enzyme costs as the cumulative costs derived from SMB operation (stationary phase, desorbent) increase to a much lesser extent. Obviously, the potential benefit of a more favorable position of the reaction equilibrium at elevated temperature is largely offset by unfavorable enzyme cost development.

At low T_{EMR}'s, the enzyme hardly contributes to the overall costs resulting in cost-optimized SMB operation with the EMR reactor set to values that furnish optimized condition for SMB

operation. The dominating cost contribution stems from the desorbent (69.2%), followed to a much lesser extent by costs from the substrate (15.8%) and the stationary phase (13.5%). Operation at a T_{EMR} of 20°C is therefore characterized by an extremely low productivity of the enzymatic transformation and an extremely high SMB productivity with a slightly elevated desorbent requirement (**Figure 4.5B**). In contrast, at elevated T_{EMR} there is a tremendous increase in the cost contribution of the biocatalyst, which results from the decreased stability of the biocatalyst under these conditions. As a consequence of the high cost contribution of the biocatalyst at high temperatures, the enzyme reactor is operated in a cost optimized way which is reflected by an almost 300-fold improved PR_{EMR} at 70°C compared to operation at 20°C (**Figure 4.5B**). The impact of the substrate cost is generally very low, and there is almost no potential for improvement as the overall yield never dropped below 94% (**Figure 4.5B**). This leads to the conclusion that for the assumed cheap substrate (D-fructose, 1 \$ kg^{-1}) it is not necessary to incorporate the substrate costs as an individual term of the objective function. This might however be different if a much more expensive substrate is used.

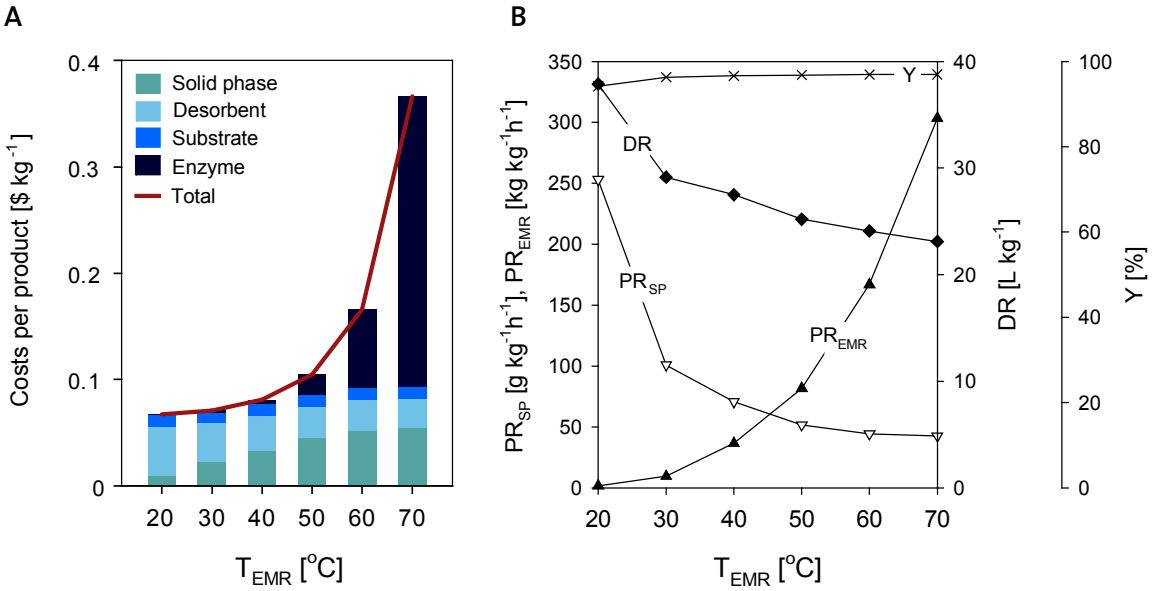

Figure 4.5. (**A**) Cost contribution at different T_{EMR} assuming a specific cost function given in Eq. 32 and (**B**) development of the cost-relevant performance parameters: PR_{EMR} (black triangles), PR_{SP} (empty triangles), *DR* (diamonds) and *Y* (crosses) as a function of the T_{EMR}

4.4.3.4 Operating parameters and concentrations

Next, we analysed the development of the 6 decision variables (m_1, m_2, m_3, m_4, t_{sw} and t_{EMR}) with increasing T_{EMR}. Taking a closer look at the SMB flow-rate ratios revealed that variable m_3 is mainly affected: at low reactor temperatures m_3 becomes very large, representing an operating point with significantly reduced purity requirements for the raffinate/recycling

stream. This is in line with the results from standalone SMB optimization (**Chapter 3**), where reduced purity requirements lead to significantly increased PR_{SMB}'s.

Moreover, the optimized operating point is characterized by relatively short t_{sw} (1 min) and long t_{EMR} (416 min, **Figure 4.6B**), which are required to compensate for the reduced catalytic activity of the biocatalyst at low temperatures.

In contrast, very short t_{EMR} (9.8 min) were found beneficial at high T_{EMR}'s and m_3 was converging towards the vertex of the triangle in the m_2/m_3 plane (**Figure 4.6A**), representing an operating point were both SMB outlet streams carry either substrate or product at full purity. Considering the long t_{sw} and the low values for m_1 such an operating point clearly represents a less productive but highly desorbent-efficient way to run the SMB. This behaviour can be explained by considering that at high EMR temperatures, where the enzyme is the main cost contributor, the system has to adjust for better enzyme usage. This can be achieved by reducing the t_{EMR} in the EMR and by minimizing the reflux of unconverted substrate via the NF. A good overview of the observed trends can be obtained by analysing the development of the actual concentration and composition of the in- and outlet streams of the individual unit operations at different T_{EMR} (**Figure 4.7**).

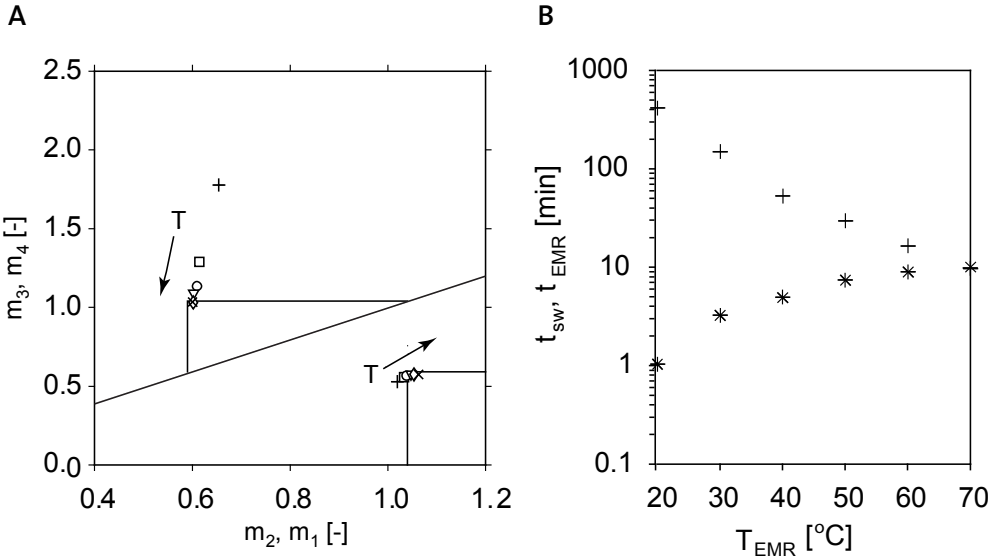

Figure 4.6. Development of the optimized operating parameter at different reactor temperatures: (**A**) optimum *m*-values in a m_2/m_3 and m_1/m_4 plane at 20°C (+), 30°C (square), 40°C (circle), 50°C (triangle), 60°C (diamond), 70°C (cross). (**B**) Optimum t_{EMR} (crosses) and t_{sw} (stars) as a function of T_{EMR}

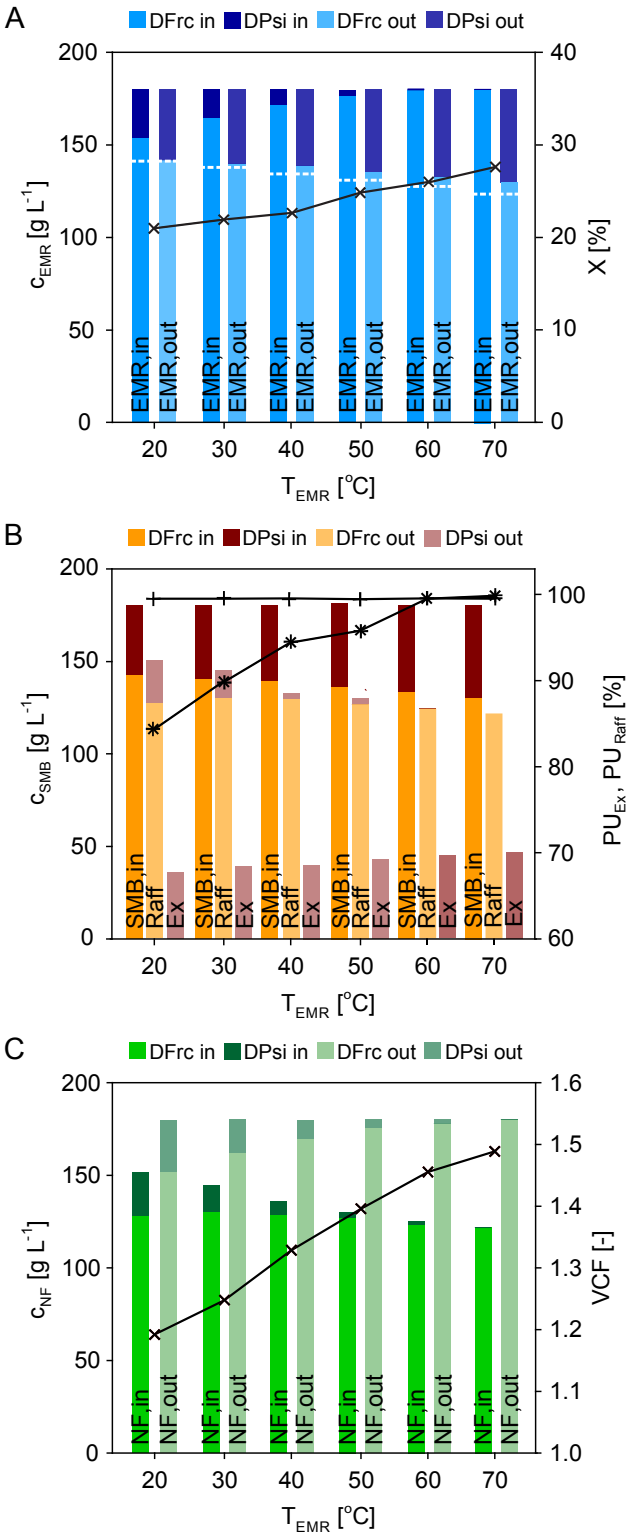

Figure 4.7. Development of the concentration and composition of the in- and outlet streams of (**A**) EMR, (**B**) SMB and (**C**) NF as a function of T_{EMR}. The theoretically possible thermodynamic equilibrium compositions between D-fructose and D-psicose were calculated for the respective T_{EMR} based on the parameterization given in **Table 4.1** and indicated by a dashed white line; right axis: (**A**) conversion *X* (cross), (**B**) purity extract PU_{Ex} (+), purity raffinate PU_{Raff} (stars), (**C**) volume concentration factor *VCF* (cross).

Figure 4.7A shows that in simulated optimized operation at low T_{EMR} a rather high fraction of D-psicose (≈ 20%) is recycled to the reactor, whereas the outlet composition is close to the thermodynamic equilibrium composition of D-fructose and D-psicose. Obviously, operating the EMR at equilibrium represents the least productive way of EMR operation as a large part of the biocatalyst is used to catalyse the reverse reaction from D-psicose to D-fructose. At high $T_{EMR,}$ though, no D-psicose is recycled and the EMR outlet stream is shifting clearly away from the respective equilibrium composition. However, due to the overall shift of K_{eq}, X is nevertheless found to be moderately increased (**Figure 4.7A**).

The higher content of D-psicose in the SMB feed stream and the high PU_{Raff} further lead to a higher overall sugar concentration in the extract stream and a lower concentration in the recycling stream (**Figure 4.7B**). Consequently, higher *VCF* are required to concentrate the recycling stream in the NF at higher T_{EMR} (**Figure 4.7C**). Higher *VCF* usually translate into lower *Y* as, due to the constant rejection of the NF membrane, more material is lost through the permeate stream. However, in the investigated case slightly higher *Y*`s could be obtained at 70°C compared to 20°C (96.9% and 94.2%, **Figure 4.5B**), because at high T_{EMR} the increased loss of sugar in the NF permeate can be fully compensated for by the increased product concentration that can be obtained per time interval from the extract stream.

Overall, the detailed analysis demonstrates nicely that at low T_{EMR} the integrated process assumes operating points that allow for cost-optimized SMB operation. The EMR is operated rather unfavourably with a low purity feed (consider that concentration difference between feed and equilibrium is driving force of the reaction) and conversion close to equilibrium while allowing the SMB to be operated with a maximized product concentration in the feed and a large m_3-m_2 difference which results in high SMB productivity and low raffinate purity. At high temperature the situation is inversed. In order to provide cost optimized conditions for the enzyme reaction the SMB is operated under complete separation conditions (low m_3-m_2 difference) which supports the driving force of the reactions and the conversion in the reactor is relatively far removed from the equilibrium.

4.5 Conclusions

In this work we presented a comprehensive design and cost-based optimization strategy for a novel integrated SMB&R process scheme combining biocatalysis taking place in an EMR with SMB chromatography and NF. A key feature of the presented process model constitutes the incorporation of the temperature dependence of the enzyme reaction using a comprehensive model description [169] for the parameterization of the biocatalyst, which allowed us to investigate the enzyme reactor temperature as a design parameter during process optimization. To this end, a detailed model-based procedure for the evaluation of the thermodynamic and kinetic enzyme parameters under process conditions was established enabling us to devise an enzyme-efficient method to operate the reactor under constant conversion. Constant conversion is a prerequisite for robust operation of the integrated process and a major challenge due to the inherent instability of the biocatalysts under elevated temperatures.

In principle, our simulations suggest the most cost-effective operation at low EMR temperatures. However, in practice the benefit of the low reactor temperature operation is countered by two major limitations: firstly, the increased probability of microbial contamination at low temperatures, which is a particular issue when working with carbohydrates [55], suggesting operating temperatures above 50°C. Secondly, low reactor temperatures demand for high t_{EMR}'s (**Figure 4.6B**) in order to cope with decreased catalytic activity. In practice, this might translate into infeasible reactor sizes necessary for meeting the envisioned *TP* requirements necessitating operation at higher temperatures.

In order to further reduce the increased costs at high temperatures immobilization might be a suitable option, as the enzyme has been already extensively optimized by the means of enzyme engineering. Besides a potential improvement of the functional half live of the enzyme, immobilized enzyme would further enable operation in a packed bed reactor which could alleviate the sizing/scaling problem compared to the EMR operation by allowing for an easy adjustment of bed length and hence residence times. However, the immobilized biocatalyst needs to be accounted for also in process model making reactor design more complex and immobilization costs need to be considered in the optimization.

We therefore propose that the established toolbox of models represents a generic way to establish and optimize the integration of thermodynamically limited enzyme reaction and spatially separated SMB separation in an SMB&R concept.

4.6 Supplementary material

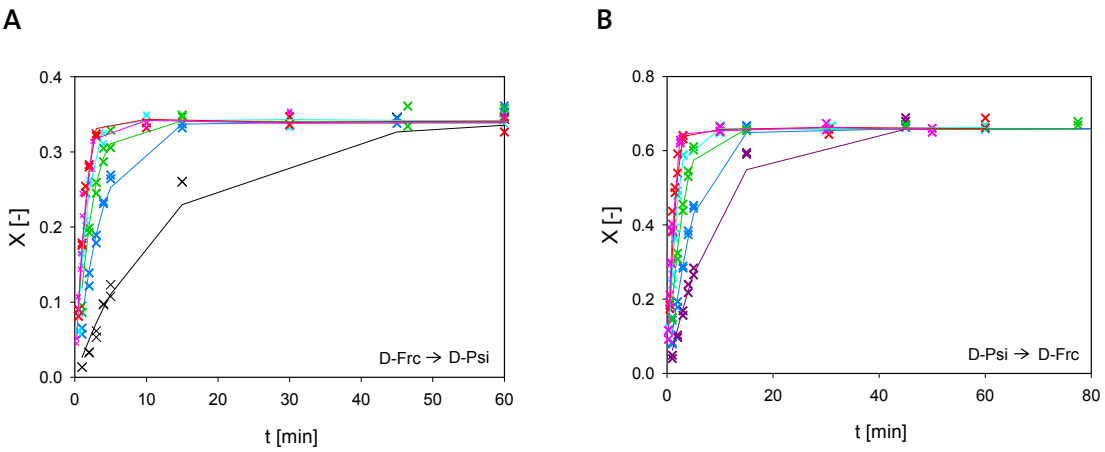

Supplementary Figure 4.1. Experimental (crosses) and fitted (lines) data for progress curves of (**A**) forward (D-Fructose → D-Psicose) and (**B**) reverse (D-Psicose → D-Fructose) reaction of PcDTE Var8 at 50°C and pH 7.0 using substrate concentrations of 2.5 g L^{-1} (red), 5.2 g L^{-1} (pink), 10.4 g L^{-1} (cyan), 21 g L^{-1} (green), 42 g L^{-1} (blue), 84 g L^{-1} (purple) and 167 g L^{-1} (black)

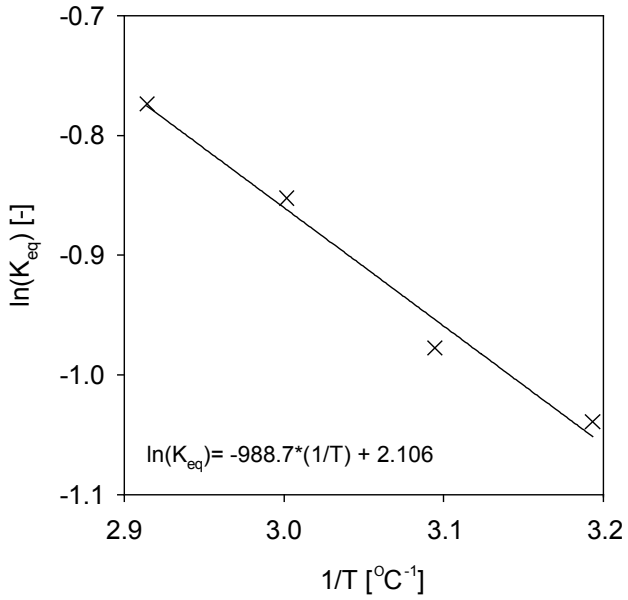

Supplementary Figure 4.2: Van`t Hoff plot of ln (K_{Eq}) versus 1/T determined from conversion experiments of D-fructose to D-psicose at 40°C, 50°C, 60°C and 70°C temperatures (crosses) and results of linear fitting (solid line)

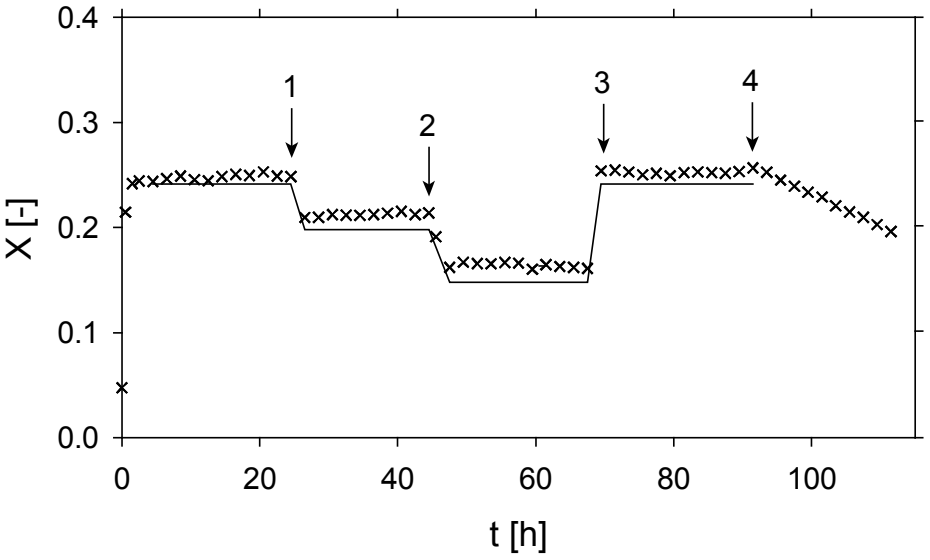

Supplementary Figure 4.3: Stable long-term operation of the EMR at 70°C applying a model-based enzyme injection strategy for keeping a constant, active enzyme concentration: experimental conversion *X* measured at the reactor outlet (crosses), simulated conversion (black line), the arrows indicate time-points of action: 1= feed flow-rate was changed from 0.175 to 0.35 mL min^{-1}, 2= feed flow-rate changed from 0.35 to 0.7 mL min^{-1}, 3= feed flow-rate changed back to 0.175 mL min^{-1}, 4= stop enzyme injections

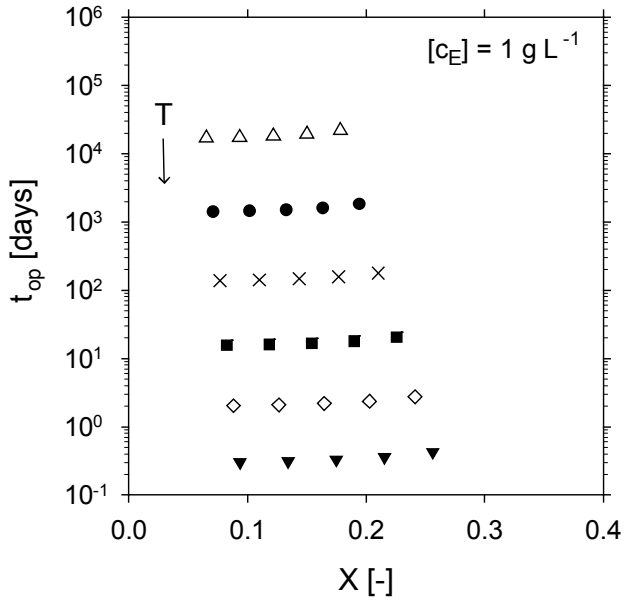

Supplementary Figure 4.4: Maximum possible operating periods $t_{op,E}$ as function of conversion *X* and reactor starting T_{EMR}: 20°C (empty triangles), 30°C (black circles), 40°C (crosses), 50°C (black squares), 60°C (white diamonds), 70°C (black triangles)

5 A separation-integrated enzyme cascade reaction to overcome thermodynamic limitations

5.1 Introduction

One-pot cascade reactions are considered an attractive alternative to the conventional step-by-step scheme that is often applied in organic chemical synthesis. They frequently exploit enzymes as myriads of these selective biocatalysts evolved to operate under broadly similar reaction conditions. This enables compact reaction schemes that avoid laborious protection/deprotection steps and intermediate isolation [15]. Among many other benefits [172], running concomitantly multiple reactions in one vessel allows combining critical steps which suffer from an unfavorable position of the reaction equilibrium with energetically highly favorable steps to achieve high yield, and indeed this has been exploited in a number of elegant synthetic cascade strategies [173, 174]. However, these strategies depend both on the availability of such irreversible reaction steps and the respective stereo-selective biocatalyst, which often limits their general applicability.

In sugar chemistry, the existence of multiple similar hydroxyl groups require demanding protection group chemistry and the use of selective enzymes appears particularly attractive [4]. In fact, cascade reactions with a maximum of only three consecutive enzymatic steps allow the synthesis of already 13 of the 20 rare standard hexoses from either cheap D-glucose, D-fructose, D-galactose (all accessible from natural sources) or L-sorbose (from Reichstein's vitamin C process [175]) [26]. While this could be highly attractive for increasing the flexibility and compactness of rare sugar synthesis, these cascade reactions consist out of isomerases and epimerases with the corresponding unfavorable positions of the reaction equilibrium [86], which imposes a severe yield limitation and thus prevents such cascade reactions from being implemented.

A promising possibility to alleviate this problem in a potentially generic way is to compensate for the absence of the energetically favorable reactions at the end of the cascade by on-line integration of reaction cascade and product removal in a continuous process (**Figure 5.1A**). However, the complex character of the cascade reaction imposes a number of challenging boundary conditions: [i] the applied separation technique would need to be sufficiently selective to separate the product from substrate and intermediate(s); [ii] the technique needs to be highly efficient to produce the target compound in industrially relevant amounts and productivities; and [iii] the continuous operation of reaction and separation requires both to operate under broadly the same conditions. While these are formidable prerequisites, continuous countercurrent chromatography, technically realized as simulated moving bed chromatography (SMB, [102]) often fulfills these criteria [176]. In fact, single enzymatic or chemical reactions were integrated with SMB chromatography [116, 177]. Here, we present the practical integration of a reaction cascade with SMB chromatography to enable the highly efficient production of the rare sugar D-psicose from sucrose involving three biocatalytic steps, the last two of

which employ thermodynamically unfavorable isomerase- and epimerase-catalyzed reactions.

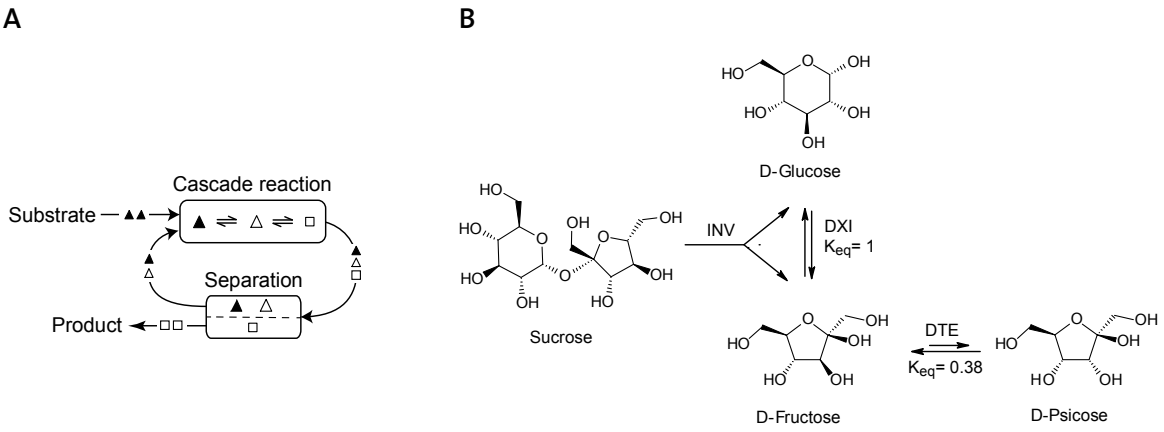

Figure 5.1. (**A**) Integrated operation of enzyme cascade reaction and product removal. (**B**) Enzyme reaction cascade for the manufacturing of the rare sugar D-psicose (4) from sucrose with the yield limited by the position of the isomerization and the epimerization. Enzymes that participate in the reaction: invertase (INV), D-xylose isomerase (DXI), D-tagtose epimerase (DTE). Equilibrium constants of the iso- and epimerase reactions at 50°C are indicated.

D-psicose, like many of the 20 rare sugars in the standard set of hexoses [4], has a high potential as low-calorie sweetener or active pharmaceutical ingredient [4]. Manufacturing of D-psicose was recently demonstrated from abundant D-fructose using the enzyme D-tagatose epimerase (DTE) [116]. We took advantage of the availability of sugar-converting enzymes from either natural sources (invertase, INV) or our own enzyme engineering efforts (xylose isomerase (DXI), see below, and DTE [81]) to set up a continuous three step cascade consisting of the hydrolysis of sucrose to D-glucose and D-fructose, the isomerization of D-glucose to D-fructose, and the epimerization of D-fructose to the final product D-psicose (**Figure 5.1B**). Ligand exchange chromatography [178] using Ca^{2+}-substituted stationary phases was employed for the separation of the sugar mixture using water was as the liquid phase.

5.2 Experiments and results

To realize this integrated set up, we addressed first the cascade reaction. We selected enzymes from thermophilic organisms, as they usually exhibit high thermal and operational stability and thus can be employed at elevated temperatures, which is required in sugar processing to reduce microbial contamination and the viscosity of typically highly concentrated feed streams [55]. High temperatures also increase catalytic activity and can

shift reaction equilibria towards a more favorable position. We used the extreme thermophilic bacterium *Thermotoga neapolitana* as the source of two of the enzymes, invertase (TnINV)[179] and D-xylose isomerase (TnDXI)[46], and completed the set with a previously thermostabilized DTE from *Pseudomonas cichorii* (PcDTE Var8, [81]).

We next looked into the specific activities of the three catalysts and found the isomerization step to be substantially slower (k_{cat}= 1.56 s^{-1} for TnDXI Mut1F1, a threefold mutant of the wildtype enzyme [180] (see **Supplementary Table 5.3**), than the other two steps in the cascade (k_{cat} = 118 s^{-1} for TnINV and k_{cat} = 36 s^{-1} for PcDTE Var8, all at 50°C) and therefore increased its specific activity for D-glucose by 4-fold applying iterative saturation mutagenesis [181] (resulting in the variant TnDXI Gen2, see **5.3.3.5**).

Subsequently, we optimized the joint operation of all three enzymes. Activity profiles at different pH were recorded for all three enzymes (see **Supplementary Figure 5.6**) and a working pH of 7.0 was assigned for cascade operation, representing a trade-off of the optimum operating pH's of the individual biocatalysts. To determine the optimal temperature for the cascade, we examined the influence of temperature on activation, unfolding and deactivation of each biocatalyst in an isothermal enzyme-membrane reactor (EMR) setup as described before (**Chapter 4**). Briefly, an EMR was continuously supplied with fresh starting material, and conversion at different temperatures was determined by HPLC from periodically collected samples of the outlet stream. The resulting curves were fitted to biocatalyst inactivation models using a previously described procedure [169] (see **Supplementary Figure 5.8**, resulting in inactivation rate constants of each biocatalyst species at 50°C (TnINV: 3 x 10^{-7} s^{-1}, TnDXI Gen2: 1.4 x 10^{-4} s^{-1}, PcDTE Var8: 2.9 x 10^{-6} s^{-1}). With this information, we calculated the amount of enzyme that needed to be injected periodically into the EMR in order to compensate for inactivated enzyme and thus to keep the conversion of substrate to intermediates and product constant (**Chapter 4**). This procedure allowed the continuous and enzyme-efficient operation of the cascade under quasi-constant conditions over a period of at least 2 days with a feed concentration of 171 g L^{-1} (500 mM) sucrose (**Figure 5.2**).

An excellent agreement between the experimental and simulated concentrations could be observed (**Figure 5.2**). As the hydrolysis of sucrose is irreversible under these conditions, we reasoned that the ensuing separation could be reduced from a quaternary to a ternary problem by providing sufficient TnINV in the EMR to run the first reaction essentially to completion.

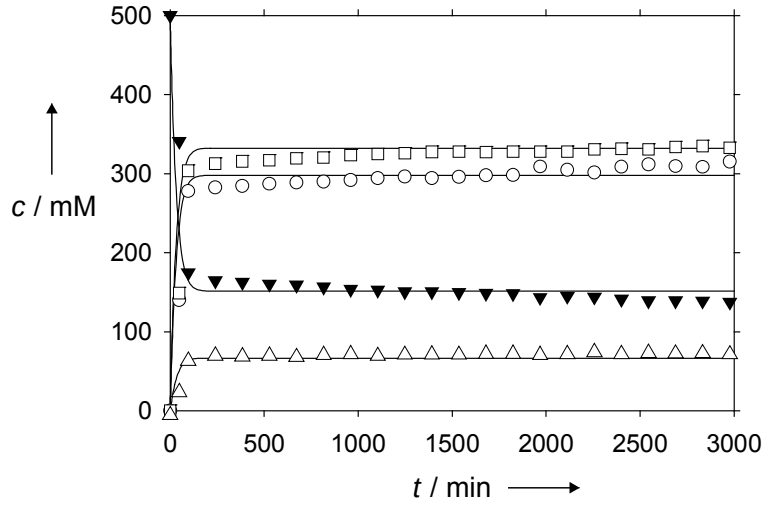

Figure 5.2. Constant production of 4 over 3,000 min from 1 by a three enzyme cascade in an EMR at 50°C, with concentrations of sucrose (filled triangles), D-glucose (empty squares), D-fructose (empty circles), and D-psicose (empty triangles) indicated. The solid lines indicate simulated concentrations of the respective compounds.

Next, we investigated the multi-component separation of D-glucose, D-fructose and D-psicose by SMB using a lab-scale plant, employing eight DOWEX 50 WX4-400 (Ca^{2+}) chromatographic columns. In classical 4 zone SMB, a standard technique for the continuous separation of sugars [56], each SMB zone is characterized by a designated flow-rate ratio *m*, representing the ratio of net liquid-phase flow to simulated stationary phase flow, and a periodic shifting time of the outlet ports t_{sw}, reflecting the simulated, countercurrent movement of the stationary phase. The sugar feed stream is provided to the SMB unit between the two central zones II and III. The compound that is retained most strongly is transported to the extract port, located upstream between zone I and II, whereas the compound that is retained more weakly is carried in direction of the fluid flow movement to the raffinate port located between zones III and IV. Zones I and IV are used to regenerate solid and mobile phases. The desorbent stream leaving the SMB through zone 4 was discarded as waste stream (open loop SMB).

Although SMB chromatography is typically designated for the separation of binary mixtures, it can be easily adapted for the processing of multi-component mixtures if the product elutes either as the first or the last compound: D-psicose eluted as last compound, after D-fructose and D-glucose. SMB experiments were carried out at 50°C using a 1 M (180 g L^{-1}) feed solution containing the three hexoses at those concentrations that were predicted to leave the EMR during integrated operation (464 mM D-glucose, 409 mM D-fructose, 127 mM D-psicose). We first identified an operating point suitable for the separation of D-fructose and D-psicose (point #1 in **Table 5.1**). Fractions were collected from

extract, raffinate and waste stream and analyzed via HPLC revealing high purity of D-psicose in the extract and high recovery of D-fructose (RC_{Frc}) in the raffinate stream for this operating point, but only moderate recovery of D-glucose (RC_{Glc} =87 %). The balance was found in the waste stream indicating that the mobile phase was not fully regenerated. As predicted by the triangle theory for SMB-design [182], RC_{Glc} could be easily increased up to 99.5 % by stepwise decreasing the mass flow ratio in the zone 4 (points #2 to #4 in **Table 5.1**).

Table 5.1. SMBpre-experiments for an increased sugar recovery in the recycling stream

	SMB operating parameters					SMB performance		
#	t_{sw}	m_I	m_{II}	m_{III}	m_{IV}	PU_{Ex}	RC_{Frc}	RC_{Glc}
	[min]	[-]	[-]	[-]	[-]	[%]	[%]	[%]
1	5.1	1.406	0.704	1.132	0.500	99.9	99.9	87
2	5.1	1.406	0.704	1.132	0.475	99.9	99.9	94
3	5.1	1.406	0.704	1.132	0.450	99.9	99.9	97
4	5.1	1.406	0.704	1.132	0.300	99.9	99.9	99.5

Having separately identified the optimal conditions for the operation of the cascade reactions and the SMB, we next addressed integration of reaction and separation (**Figure 5.3**, for a more detailed scheme see also **Supplementary Figure 5.12** in **5.3**).

In fully integrated mode, fresh sucrose is mixed with the D-glucose/D-fructose-enriched recycling stream and then enters the EMR, where it is partially converted to D-psicose to a target conversion of ≈ 11%. The EMR-outlet stream enters the SMB unit for separation into product stream (pure D-psicose, leaving between zone I and II) and a mixed recycling stream containing the intermediate sugars (leaving between zone III and IV). To compensate the dilution of the recycling stream during SMB operation, it is concentrated via a nanofiltration device (NF). The implementation of the optimum SMB operating point exhibiting full RC_{Frc} and RC_{Glc} (#4, **Table 5.1**) led to a strongly diluted raffinate stream, which required unfeasibly high NF concentration factors for our lab-scale system.

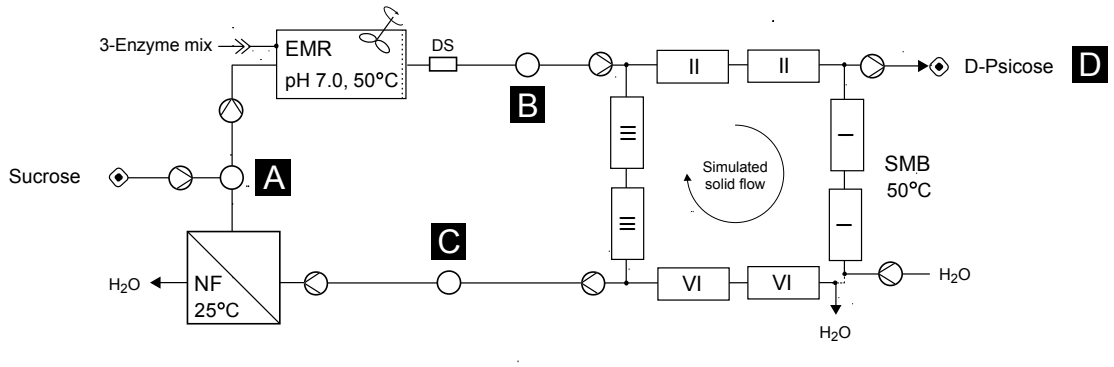

Figure 5.3. Direct-coupling of multi-enzyme-cascade reaction, SMB separation and NF recycling for the continuous production of rare sugar D-psicose. The letters indicate interfaces at which sampling took place

Thus, we decided to adopt operating point #3 of **Table 5.1**, which led to a concentration factor of 1.8 to obtain again a total sugar concentration (D-glucose and D-fructose) of 180 g L^{-1} in the recycling stream. The EMR was operated at 50°C and received initially 1.5 mg ml^{-1} TnINV, 8.9 mg ml^{-1} TnDXI Gen2 and 0.95 mg ml^{-1} PcDTE Var8.

During the operation, 1.50 µg TnINV, 0.37 mg TnDXI Gen2 and 4.12 µg PcDTE Var8 were injected every 30 min to compensate for losses due to heat inactivation. In order to shorten the settling time, a feed solution containing sucrose, D-glucose and D-fructose at the projected steady state target concentrations was used during the start-up (**5.3.10**). Finally, for monitoring the process during the integrated operation, 3 stirred sampling reservoirs (depicted as A, B, C in **Figure 5.3**) were installed in the interface of the unit operation.

Stable operation of the integrated process was accomplished for more than 4,000 min (**Figure 5.4**), 3,800 min of it in a fully integrated manner. The process immediately delivered 12.5 g L^{-1} D-psicose in highest purities (PU_{Ex} ≥ 99.9 %). Taking into account the incomplete rejection of the NF membrane for D-glucose and D-fructose, the theoretical process yield was 92 % on sucrose, and we found an experimental yield of 89 % by comparing the molar mass flow of sucrose entering the process with the one of D-psicose leaving the system through the extract port (**5.3.10**). This deviation resulted from the small amount of D-glucose leaving the system in the SMB waste stream. This could be easily circumvented on lager scale by further reducing the setpoint for m_{IV} and employing a NF plant that can cope with the higher dilution of the raffinate flow. The experimental yield compares well with a process yield of approximately 14 %, which could be maximally obtained running the same cascade reaction in batch mode.

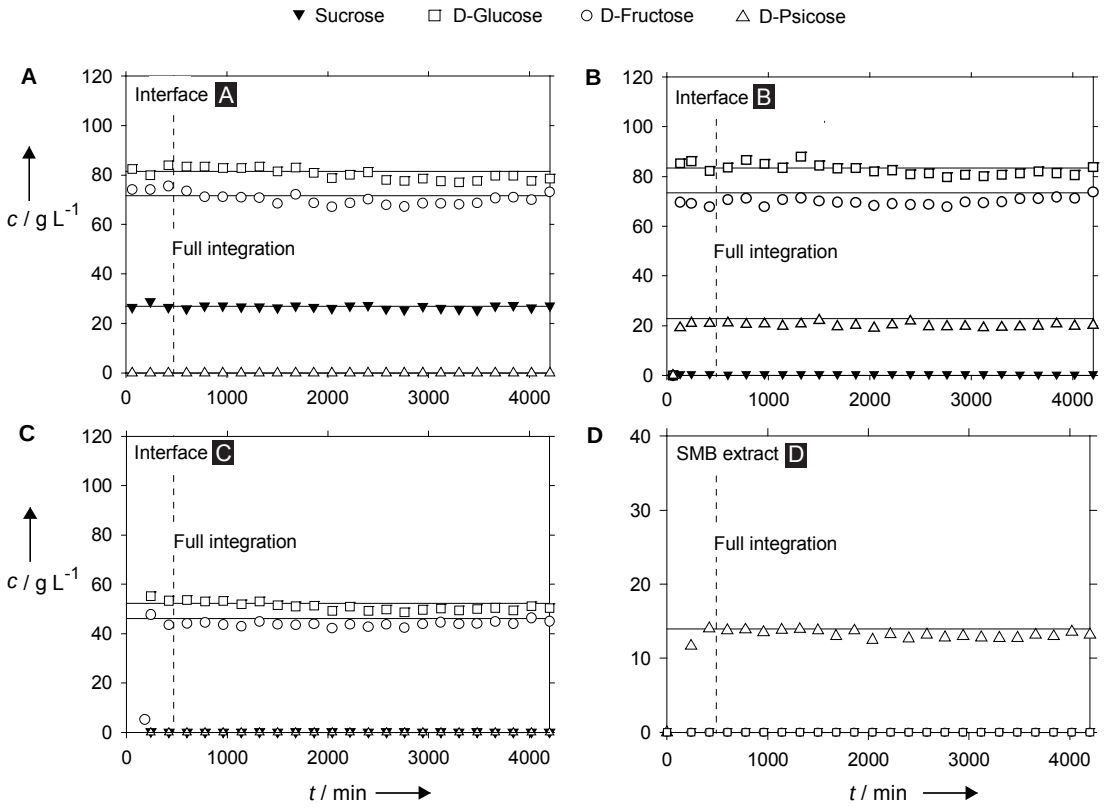

Figure 5.4. Concentration profiles of the starting material sucrose, intermediates D-glucose and D-fructose and the rare sugar product D-psicose during operation of the integrated process. Samples were taken at different sampling interfaces (compare Fig. 3): (**A**) interface A (located between NF and EMR), (**B**) interface B (located between EMR and SMB), (**C**) interface C (located between SMB and NF) and (**D**) at the extract port D. The time point of full integration is indicated by a dashed line in each plot.

A total of 146 mg enzyme was provided over the investigated run time of 4,200 min, translating into a total turnover of 0.3 kg of D-psicose per g of total enzyme and a remarkably high EMR space time yield of 1.6 kg L^{-1} day^{-1} of D-psicose. We produced preparative amounts of pure D-psicose (14 g day^{-1}) in the course of this work that could be isolated from the aqueous phase in high yields (≥ 85%) according to a previously described protocol (**Chapter 3**).

In summary, we demonstrate an efficient and, given the achieved yield and productivity, eminently practical strategy for D-psicose synthesis employing epimerases and isomerases. Given the diversity of aqueous media-compatible stationary phases and the wide range of hexose-interconverting iso- and epimerases[4], we argue that this integrated synthetic strategy enables generic access to a variety of rare hexoses.

5.3 Supplementary material

5.3.1 General

All chemicals except for D-fructose (Carbosynth, Compton, UK) and D-psicose (crystallized from SMB extract of separate runs [116]) were purchased from Sigma Aldrich (Buchs, Switzerland) in ACS grade. Oligonucleotide synthesis and DNA sequencing was done by Microsynth (Balgach, Switzerland). In general, *E. coli* Top10 cells (Invitrogen, Grand Island, USA) were used for molecular cloning and *E. coli* BL21(DE3) (NEB, Ipswich, USA) cells were used for protein expression.

Deionized water was used for the preparation of all solutions and as desorbent for SMB chromatography runs.

5.3.2 Invertase

5.3.2.1 Vector construction

The invertase gene (INV, also known as β-glucosidase [179]) from *Thermotoga neapolitana* (DSM No. 4359) was isolated directly from resuspended *T. neapolitana* cells (DSM No. 4359, DSMZ, Braunschweig, Germany) by PCR with primers TnINV_HindIII_f and TnINV_XhoI_r (**Supplementary Table 5.2**). PCR was done as follows in a total volume of 50 µL: 0.25 µL Phusion polymerase (0.5 U) (NEB), 10 µL 5x Phusion buffer, 5 µL of 10 µM of each primer, 2 µL 100% DMSO, 1 µL resuspended cells, 1 µL 50x dNTP (10 mM each), filled up to 50 µL with ddH_2O. Cycling conditions were 98°C for 1 min; 25 cycles of 98°C for 10 s, 55°C for 15 s and 72°C for 30 s; final extension at 72°C for 5 min. The PCR product was purified and cut with *Hin*dIII/*Xho*I before cloning into expression vector pAB228 (see **Supplementary Table 5.1** for details) according to standard protocols [183], resulting in plasmid pAB143.

5.3.3 Xylose isomerase

5.3.3.1 Vector construction

The gene of the xylose isomerase DXI was isolated directly from resuspended *T. neapolitana* cells (DSM No. 4359) with primers TnDXI_HindIII_f and TnDXI_XhoI_r (**Supplementary Table 5.2**). PCR and cloning of DXI was done exactly as for the invertase gene described above. Mutations that were already known to enhance activity of TnDXI [180] were introduced via the QuickChange method (Stratagene, La Jolla, USA) but using Phusion polymerase instead of PfuTurbo as suggested by the manual. The final vector pAB114 containing the gene for TnDXI Mut1F1 as described earlier [180] was used as starting point for directed evolution.

The gene *gutB* from *Bacillus subtilis* (DSM No. 21393), encoding the protein sorbitol dehydrogenase (BsSD) required for the screening assay for the optimization of DXI (see **5.3.3.4**), was isolated by PCR directly from resuspended cells as described above for DXI using primers gutB_NheI_f and gutB_EcoRI_r. It was inserted via restriction sites *Nhe*I and *Eco*RI into expression plasmid pAB139, resulting in plasmid pAB182.

Supplementary Table 5.1. Plasmids used in this work

Nr	Name	Description	Reference
1	pAB92	SEVA [184] vector backbone, *bla* resistance gene, P_{tet}-P_{T7} fusion promoter, MCS, *ori* pBR322	Bosshart et al. [185]
2	pAB114	Plasmid pAB92 with TnDXI Mut1F1 and C-terminal 6xHis tag	Sriprapundh et al. [180], this work
3	pAB186	Plasmid pAB114 containing mutation T186C,S187I, N270I	**5.3.3.5**
4	pAB139	pAB92 with codon-optimized *KpRD*-gene from *K. pneumoniae* containing an N-terminal 6His-tag, *kamR*-resistance gene, *ori* pBBR1	Bosshart et al. [185]
5	pAB228	SEVA vector backbone, *kan* resistance gene, P_{tet}-P_{T7} fusion promoter, MCS, *ori* pBR322	Bosshart et al. [185]
6	pAB143	SEVA vector backbone, *kan* resistance gene, P_{tet}-P_{T7} fusion promoter, *ori* pBR322, TnINV from *T. neapolitana* with C-terminal 6His tag	**5.3.2.1**
7	pAB182	Plasmid pAB139 with gene *gutB* from *Bacillus subtilis,* N-terminal 6xHis tag	**5.3.3.1**

Supplementary Table 5.2. Primers used for the construction and site-directed mutagenesis of TnDXI

Nr	Name	Sequence
1	TnDXI_HindIII_f	5'-ATCATAAGCTTATGGCTGAATTCTTTCCAGAAATC-3'
2	TnDXI_XhoI_r	5'-ATCATCTCGAGCCTCAGTTCCAGAATGGTCTTC-3'
3	TnDXI_V186TF187S_f	5'-GAGAAGGGTACACCTCCTGGGGTGGAAG-3'
4	TnDXI_V186TF187S_r	5'-CTTCCACCCCAGGAGGTGTACCCTTCTC-3'
5	TnDXI_L283P_f	5'-CTTCCAGCACGAACCGAGAATGGCAAG-3'
6	TnDXI_L283P_r	5'-CTTGCCATTCTCGGTTCGTGCTGGAAG-3'
7	TnDXI_LibW49_f	5'-TGCCTTCNNKCACACCTTCGTGAACGAG-3'
8	TnDXI_LibW49_r	5'-AGGTGTGMNNGAAGGCAACGGAGAACTTC-3'
9	TnDXI_LibC99_f	5'-CATCGAGTACTTCNNKTTCCACGACAGAG-3'
10	TnDXI_LibC99_r	5'-CTCTGTCGTGGAAMNNGAAGTACTCGATG-3'
11	TnDXI_LibF100_f	5'-CTTCTGCNNKCACGACAGAGACATCGC-3'
12	TnDXI_LibF100_r	5'-TGTCGTGMNNGCAGAAGTACTCGATGTTG-3'
13	TnDXI_LibR103_f	5'-GCTTCCACGACNNKGACATCGCTCC-3'
14	TnDXI_LibR103_r	5'-GGAGCGATGTCMNNGTCGTGGAAGC-3'
15	TnDXI_LibW139_f	5'-GCTCCTCNNKGGTACTGCAAACCTCTTTTC-3'
16	TnDXI_LibW139_r	5'-CAGTACCMNNGAGGAGCTTCACGTTGC-3'
17	TnDXI_LibG140T141_f	5'-GAAGCTCCTCTGGNDTNDTGCAAACCTCTTTTCC-3'
18	TnDXI_LibG140T141_r	5'- GGAAAAGAGGTTTGCAHNAHNCCAGAGGAGCTTC-3'
19	TnDXI_LibV186S187_f	5'-GAGGAGAAGGGTACNDTNDTTGGGGTGGAAGAG-3'
20	TnDXI_LibV186S187_r	5'-CTCTTCCACCCCAAHNAHNGTACCCTTCTCCTC-3'
21	TnDXI_LibA269_f	5'-CAACATCGAGNNKATTCACGCCACAC-3'
22	TnDXI_LibA269_r	5'-GTGTGGCGTGAATMNNCTCGATGTTG-3'
27	TnDXI_LibN270_f	5'-CAACATCGAGGCANNKCACGCCACACTCG-3'
28	TnDXI_LibN270_r	5'-CGAGTGTGGCGTGMNNTGCCTCGATGTTG-3'
23	TnDXI_LibA272_f	5'-GAGGCAATTCACNNKACACTCGCCGGTC-3'
24	TnDXI_LibA272_r	5'-GACCGGCGAGTGTMNNGTGAATTGCCTC-3'
25	TnDXI_LibN337_f	5'-CAAAAGGTGGGCTCNNKTTCGATGCGAAGG-3'
26	TnDXI_LibN337_r	5'-CCTTCGCATCGAAMNNGAGCCCACCTTTTG-3'
27	gutB_NheI_f	5'-ATCATGCTAGCACTCACACAGTACCTCAAAAC-3'
28	gutB_EcoRI_r	5'-ATCATGAATTCTCAGCGATTTGGATACACC-3'
29	TnINV_HindIII_f	5'-ATCATAAGCTTATGTTCAAACCCCACTACCAC-3'
30	TnINV_XhoI_r	5'-ATCATCTCGAGAGAAATCCATACGTTTTTCAAC-3'

5.3.3.2 Expression and purification of B. subtilis sorbitol dehydrogenase (BsSD)

Plasmid pAB182 was used to transform chemically competent *E. coli* BL21(DE3) cells. A single colony was picked and precultured in 5 mL LB supplemented with 50 µg mL^{-1} kanamycin (LB-kan). An aliquot of 200 µL of this preculture was used to inoculate 50 mL of M9 medium containing 0.4 % D-glucose and 50 µg mL^{-1} kanamycin. An aliquot of 15 mL of this preculture was used to inoculate a 3 L bioreactor (3 g L^{-1} KH_2PO_4, 3.7 g L^{-1} Na_2HPO_4, 1.2 g L^{-1} citrate, 0.64 g L^{-1} $MgSO_4*7H_2O$, 2.88 g L^{-1} $(NH_4)SO_4$, 2.37 g L^{-1} $(NH_4)Cl_2$, 0.81 mL L^{-1} of 1M stock solution of $CaCl_2*2H_2O$, 0.32 mL L^{-1} of trace element solution (TES), 2 µg L^{-1} of thiamine, 16 g L^{-1} D-glucose). Cells were grown at 37°C until an OD_{600} of 16 was reached, then the feed was started at 45 mL h^{-1} (same medium as for batch, except 300 g L^{-1} D-glucose) and temperature was reduced to 30°C. Protein production was induced with IPTG (final concentration of 0.2 mM) and expression was done for 6 h. Cells were harvested by centrifugation (4,000 rcf, 30 min) and cell pellet was stored at -80°C until further use.

A portion of 30 g of the cell pellet was resuspended in 30 mL of lysis buffer (50 mM Tris pH 8.0, 100 mM NaCl, 30 mM imidazole and 0.1 mg mL^{-1} lysozyme) and incubated for 20 min at room temperature (RT). The suspension was frozen at -20°C for 20 min and thawed again at RT. $MgCl_2$ was added to a final concentration of 1 mM and a spatula tip of DNaseI was added to reduce the viscosity of the lysate. This crude cell lysate was centrifuged for 20 min at 40,000 rcf to remove cell debris. The cleared cell lysate was then loaded on 3 x 2 mL of Ni-Sepharose and washed extensively with lysis buffer. Protein was eluted with 5 x 2 mL of elution buffer (50 mM Tris pH 8.0, 100 mM NaCl, 200 mM imidazole); main fractions were pooled and dialyzed twice against 2 L of 10 mM Tris buffer pH 8.0. Protein concentration was determined spectrophotometrically at 280 nm using the extinction coefficient (ε) and the molecular weight (Mw) calculated for BsSD using the online tool ProtParam [168](ε = 22265 M^{-1} cm^{-1} and Mw = 39371 Da). The purity of the eluted protein fractions was > 95% as judged from SDS-PAGE. The purified protein was aliquoted and stored at -80°C.

5.3.3.3 Establishment of a high-throughput screening assay for DXI activity

In order to screen for TnDXI Mut1F1 variants that exhibit an improved catalytic rate for the conversion of D-glucose to D-fructose we established an NADH-coupled assay that can reliably detect D-fructose in the presence of D-glucose. It is based on the previously purified BsSD that specifically reduces D-fructose to sorbitol by concomitant oxidation of NADH [186]. From the rate of NADH oxidation by BsSD the amount of D-fructose produced from D-glucose by TnDXI variants could be calculated via a calibration curve of different defined amounts of D-fructose in presence of D-glucose (**Supplementary Figure 5.1**). The slope of

NADH oxidation by BsSD could be shown to exhibit a linear relationship up to 20% D-fructose (total sugar concentration of 250 mM).

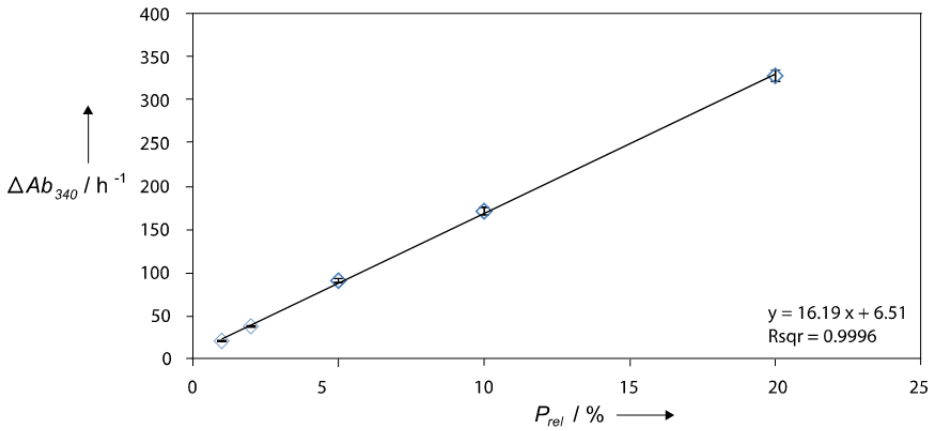

Supplementary Figure 5.1. Calibration curve of decrease in absorbance at 340 nm wavelength for different amounts of D-fructose in presence of D-glucose (total sugar concentration: 250 mM). Error bars indicate standard deviation of three independent experiments. A linear fit to the five data points indicates high specificity of BsSD for D-fructose (nearly no oxidation of NADH in absence of D-fructose).

5.3.3.4 High-throughput screening protocol

Site-saturation mutagenesis of TnDXI Mut1F1 was done as described previously [81] using primers with degenerated codons listed in **Supplementary Table 5.2**. From single-site NNK libraries 93 clones were picked into a 96-deep well plate (500 µL of LB medium supplemented with 100 ug mL^{-1} ampicillin (LB-amp)) together with 3 parent colonies as control. Precultures were grown overnight at 37°C and 220 rpm and 20 µL of it was used to inoculate 1 mL of ZYM-5052 autoinduction medium [187] supplemented with 100 µg mL^{-1} of ampicillin. The remaining preculture was directly frozen at -20°C for later use. The expression culture was inoculated at 30°C for 16 h at 180 rpm and cells were harvested by centrifugation (3,320 rcf, 10 min) before they were stored at -20°C until further use. Cells were lysed by addition of 100 µL of 50 mM Tris pH 7.0, 0.1 mg mL^{-1} lysozyme for 20 min at RT before they were frozen for 20 min at -20°C and thawed again at RT. Another 100 µL of 50 mM Tris pH 7.0, 2 mM $MnCl_2$, spatula tip of DNaseI was added to decrease viscosity and saturate the enzyme with Mn^{2+}. A portion of 100 µL of crude cell lysate was heat-treated for 10 min at 70°C and the denatured host proteins were removed by centrifugation (3,320 rcf, 10 min).

An aliquot of 20 µL of cleared heat-treated lysate was added to 100 µL of 600 mM D-glucose in 50 mM Tris pH 7.0 and incubated for 16 h at 42°C (in round two reduced to 1 h). An aliquot of 120 µL of detection solution (50 mM Tris pH 9.0, 14 µg mL^{-1} of purified BsSD, 1 mM NADH) was added and the decline in absorbance at 340 nm was followed at 30°C in a

Perkin Elmer Wallac 1420 Victor plate-reader (Perkin Elmer, Waltham, USA). Concentration of D-fructose in each well could then be derived from the slope of the absorbance decline using a calibration curve (**Supplementary Figure 5.1**).

Variants that showed at least 1.2- fold higher conversion of D-glucose to D-fructose were regrown in triplicates from the preculture stored at -20°C and re-measured in triplicates. They were considered as hits if their activity could be reproducibly shown to be above 1.2-fold over the parent variant.

5.3.3.5 Screening of TnDXI Mut1F1 variants

It has been proposed that it is preferable to use a thermostable homolog of a biocatalysts instead of a mesostable one because the stable fold of a thermophilic enzyme (expressed as difference in free energy of folding ΔG_u) can accommodate more mutations that are beneficial in terms of activity but destabilize the protein fold [188]. Therefore we decided to use a highly thermostable xylose isomerase homolog from the hyperthermophile *T. neapolitana* (TnDXI) as template for the directed evolution of an efficient biocatalyst for the conversion of D-glucose to D-fructose [189]. This template had already been subjected to mutagenesis to improve isomerization of D-glucose to D-fructose at lower temperatures and lower pH [180]. This resulted in variant TnDXI Mut1F1 that still exhibited a similar degree of thermostability compared to wild type. Based on the structures of TnDXI (PDB ID: 1A0E) and the highly similar structure of *Streptomyces rubiginosus* with bound D-glucose in the active site (PDB ID: 3KBN from [190]) we selected residues that form the active site as interesting targets for site-saturation mutagenesis. Inspection of the two substrates D-xylose and D-glucose revealed that both substrates had the same configuration at C2, C3 and C4 with the exception that D-xylose, as a C5-sugar, was lacking the C6 of D-glucose. Therefore we reasoned that residues that are in close proximity to O6 of D-glucose (or O5 of D-xylose, respectively) represent prime targets for site-saturation mutagenesis as more precise positioning of the non-natural substrate D-glucose might lead to an improved catalytic activity for this substrate. A second patch of potentially interesting residues was chosen based on the effect of a mutation at position G219 (corresponding to position N270 in TnDXI) on the inhibition of xylose isomerase by Ca^{2+} ([191], see also **Supplementary Figure 5.3.**). All together we selected 13 sites for targeting by site-saturation mutagenesis, of which 2 pairs were randomized together using NDT degenerated codons (G140-T141 and T186-S187) and the remaining 9 residues were randomized separately using NNK degenerated codons (**Supplementary Figure 5.2**). A set of 5 residues in vicinity to the O6 of D-glucose as well as 1 residue in the patch A269-A272 were excluded due to high conservation judged by a sequence alignment of DXI homologs, which made us suspect that they were involved in the catalytic reaction machinery and mutagenesis was likely to lead to inactive variants.

		1st round		2nd round		3rd round	
Residues	Deg. Codon	Screening / Hits	Nomenclature	Screening / Hits	Nomenclature	Screening / Hits	Nomenclature
49 TRP	NNK	no hit				no hit	
99 CYS	NNK					no hit	
100 PHE	NNK	no hit				no hit	
101 HIS	-	-					
103 ARG	NNK					no hit	
139 TRP	NNK	no hit				no hit	
140 GLY	NDTNDT	G140G, T141C				no hit	
141 THR							
186 THR	NDTNDT	1-B08: T186C, S187I; 1-B06: T186C, S187C; 5-E01:T186C, S187G	**1-B08: TnXylA Gen1**				
187 SER							
188 TRP	-						
232 GLU	-						
269 ALA	NNK					no hit	
270 ASN	NNK	A01: N270I		B01: N270I B08: N270I	**B01: TnXylA Gen2**		
271 HIS	-						
272 ALA	NNK					no hit	
296 ASP	-						
337 ASN	NNK					no hit	
339 ASP	-	-					

Supplementary Figure 5.2. Screening scheme for site-saturation mutagenesis of TnDXI Mut1F1 residues in proximity of the active site cavity. Residues in cyan were randomized by the indicated degenerated codon. Residues indicated in red were excluded, as they are part of the catalytic machinery, highly conserved and/or involved in coordination of the two metal ions in the active center. Hits found during screening are highlighted in green with mutations indicated. Degeneracy: N = A/T/G/C; K = G/T; D = A/G/T

Screening of 93 variants for NNK degenerated codons and 465 variant for two sites with each NDT degenerated codons ensured coverage of around 95%, i.e. the probability that each amino acid encoded by the degenerated codon was visited at least once [192]. Randomization of position 270 delivered a beneficial mutation (N270I) that improved isomerase activity by 1.45-fold compared to parent TnDXI Mut1F1 (determined from heat-treated lysate). Positions G140-T141 that were randomized with NDT degenerated codons yielded only a single mutation T141C whereas G140 remained unchanged, leading to a 1.4-fold improvement in catalytic activity determined from heat-treated lysate. For positions T186-S187 we obtained mutations T186C-S187I that improved isomerase activity 1.6-fold (**Supplementary Figure 5.2**). This double mutation was termed TnDXI Gen1 and used as parent for the second round of mutagenesis. Randomization of position N270 yielded again mutation N270I as in the first round and improved the activity 2.5-fold compared to TnDXI Gen1. This variant with mutations T186C, S187I, N270I was termed TnDXI Gen2.

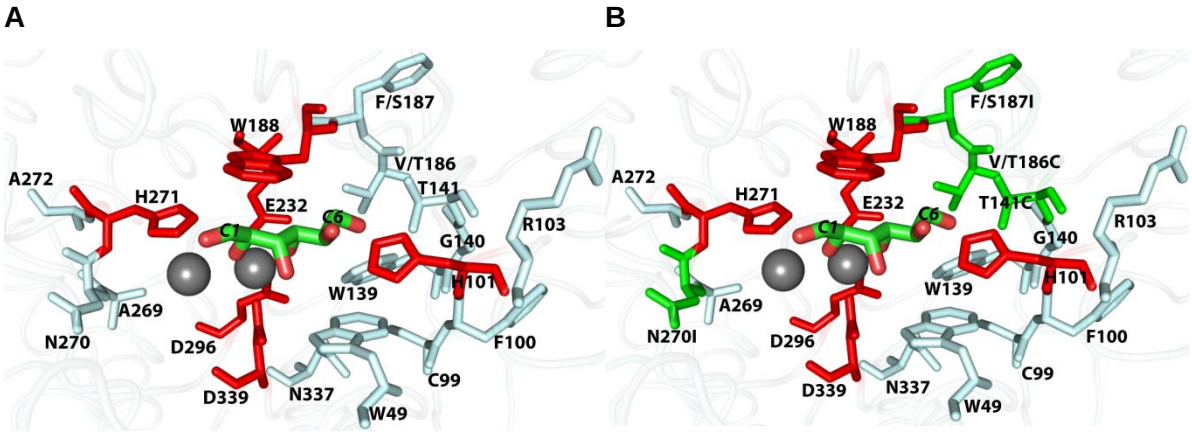

Supplementary Figure 5.3. Active site residues that were considered for screening. The figure was prepared based on a superposition of the X-ray structure of TnDXI (PDB ID 1AoE) and the X-ray structure of SrDXI (PDB ID 3KBN). (**A**) D-fructose (green sticks) and the two metal ions in the active site (grey spheres) are indicated, surrounded by residues that were targeted by site-saturation mutagenesis (cyan sticks) or excluded from screening (red sticks). For site F/S187 and V/T186 the first letter indicates the amino acid that occurred in TnDXI WT, the second letter indicates the mutations that were found by Sriprapundh et al. [180](**B**) Residues colored in green are sites that exhibited beneficial mutations during the initial screening.

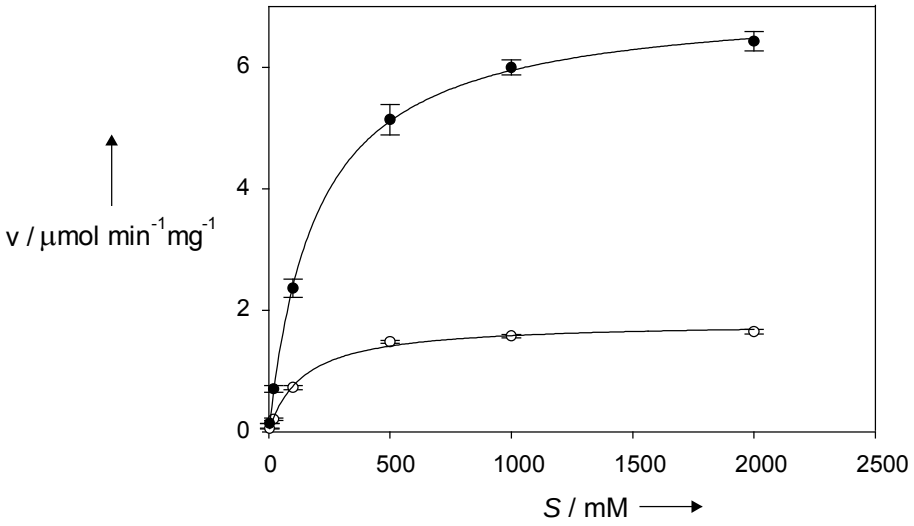

Supplementary Figure 5.4. Michaelis-Menten plot of variants TnDXI Mut1F1 (empty circles) and TnDXI Gen2 (filled circles) determined at 50°C using D-glucose as substrate (S). Error bars indicate standard errors of catalytic rates for 3 independent measurements.

Randomization of the two amino acid positions G140-T141 that had yielded a beneficial mutation in the initial screening did not result in an improvement when randomized and screened on TnDXI Gen2 as a template, and neither did any of the other 8 remaining single sites (**Supplementary Figure 5.2.**). Therefore, variant TnDXI Gen2 was considered the final variant exhibiting overall a 3.9-fold improved catalytic activity (**Supplementary Figure 5.4**).
In summary we could enhance the catalytic activity of TnDXI by nearly another 4-fold compared to the already improved variant TnDXI Mut1F1 by screening 13 sites in vicinity of the O6 of D-glucose and the loop A269-A272 which was of great use for the isomerization of D-glucose to D-fructose at elevated temperatures.

5.3.4 Expression and IMAC purification of biocatalysts

Plasmids carrying the genes for TnInv, TnDXI Gen2, or PcDTE Var8 were used to transform competent *E. coli* BL21(DE3) cells. Each of the three enzymes (TnInv, TnDXI Gen 2 and PcDTE Var8) was overexpressed during cultivation in a 3 L bioreactor and purified via IMAC chromatography as described above for BsSD with the exception that a high-pressure M-110P homogenizer (Microfluidics, Evesham, UK) was used for cell lysis and an additional heat-treatment step preceded the IMAC chromatography step. In brief, 50 g cell pellets were resuspended in 50 mL of 50 mM Tris pH 7.0 and disrupted at 1,000 bar in 4- 6 cycles. The cell lysate was heat-treated for 10 min at 70°C in a water bath and centrifuged for 20 min at 20,000 rcf to remove precipitated *E.coli* protein and cell debris. The cleared cell lysate was then loaded on 3 x 2 mL Ni-Sepharose and washed extensively with wash buffer (50 mM Tris pH 7.0, 30 mM imidazole, 100 mM NaCl). Protein was eluted with 5 x 2 mL elution buffer (50 mM Tris pH 7.0, 200 mM imidazole, 100 mM NaCl), main fractions were pooled and dialyzed twice against 2 L of 10 mM sodium phosphate buffer, pH 7.0. TnDXI Gen2 and PcDTE Var8 were also dialyzed against 0.1 mM $MnCl_2$. Protein concentrations were determined spectrophotometrically at 280 nm using ε and Mw's calculated using ProtParam: for TnInv, ε = 95,800 M^{-1} cm^{-1} and Mw = 50,970 Da, for TnDXI Gen2, ε = 56,060 M^{-1} cm^{-1} and Mw = 51,911 Da and for PcDTE Var8, ε = 46,410 M^{-1} cm^{-1} and Mw = 33,790 Da. Again, the purity of the eluted protein fractions were analyzed by SDS-PAGE and found to show > 95% and the purified enzyme was aliquoted and stored at -80°C.

5.3.5 Determination of enzyme activity as a function of pH

The enzyme activity at different pH values was determined at 30°C (for TnDXI Gen2) and 50°C (for TnInv and PcDTE Var8) using a BioShake iQ shaker (Q.Instruments, Jena, Germany). Purified enzyme was added to a solution containing 100 mM substrate in 90 mM buffer (pH 3.5 – 6.0 sodium acetate buffer; pH 6.0 – 7.0 sodium phosphate buffer; pH 7.0 – 9.0 Tris-HCl buffer) and progress curves were determined by regularly removing

20 µL of reaction mixture and stopping the reaction by mixing this aliquot with 145 µL of 0.1 M HCl. The solution was neutralized by adding 135 µL of 0.1 M NaOH. Conversion was determined by HPLC using a LC ICS-3000 system (Dionex, Olten, Switzerland) equipped with a CarboPac PA1 column (250 mm x 4 mm I.D.) preceded by a CarboPac PA1 guard column (50 mm x 4 mm I.D., both Dionex). Samples were eluted isocratically with 60 mM NaOH (for the analysis of samples containing sucrose, D-glucose and D-fructose) or with 25 mM NaOH (for the analysis of samples containing D-psicose and/or D-glucose and D-fructose) both at a flow rate of 2.0 mL min^{-1} and detected by triple pulsed amperometry using an EC detector with a gold electrode (Dionex). The initial reaction rates were used to calculate enzyme activities and normalized by the highest activity measured for each enzyme (**Supplementary Figure 5.5.**).

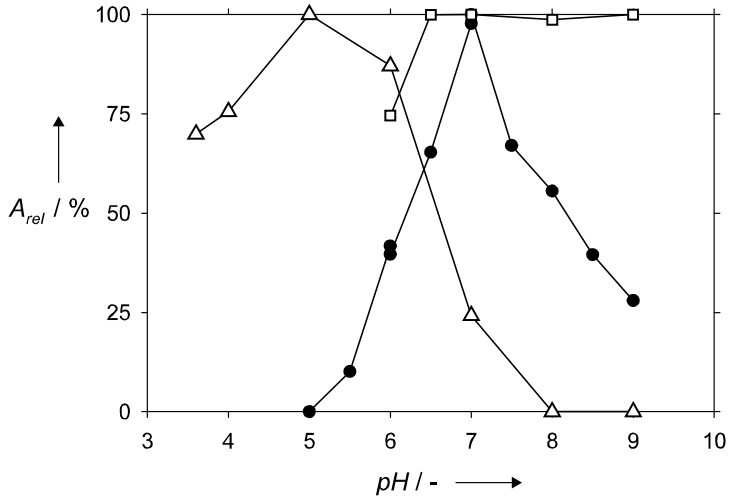

Supplementary Figure 5.5. Effect of pH on relative activity (A_{rel}) of TnInv (empty triangles, up), TnDXI Gen2 (filled circles) and PcDTE Var8 (empty squares).

5.3.6 Enzyme kinetic measurements

Enzyme kinetics for TnInv and TnDXI Gen2 were determined at 50°C on a BioShake iQ shaker (Q.Instruments) with a 1.5 mL Eppendorf tube adaptor recording progress curves in 10 mM sodium phosphate (pH 7.0) and at substrate concentrations specified in **Supplementary Table 5.3.** The substrate solutions were preheated before the reaction was started by adding purified enzyme.

An aliquot of 20 µL of purified TnINV (0.32 mg mL^{-1}) was added for each experiment to the respective sucrose containing solution and the reaction progress was followed by adding 20 µL of the reaction mixture to 280 µL of stopping solution (1 mM $ZnCl^2$ solution, precooled at 4°C). The samples were measured by HPLC as described above using the LC ICS-3000 system (Dionex)

For glucose isomerase measurements, 40 µL of purified TnDXI Gen2 (5 mg mL^{-1}) was added to the respective D-glucose- or D-fructose- containing solution (pre-heated to 50°C) and the progress of the reaction was followed by sampling 20 µL of the reaction mixture at periodic time intervals into 145 µL 0.1 M HCl to stop the reaction, before 135 µL of 0.1 M NaOH was added. Samples were measured on a Dionex HPLC as described before. The linear part of the progress curves delivered the initial rates that were then fitted to a Michaelis-Menten kinetic model using SigmaPlot 12.2 (Systat Software Inc., San Jose, USA). Michaelis-Menten plots and kinetic parameters at 50°C extracted from the fitting procedure are depicted in **Supplementary Figure 5.6** and **Supplementary Table 5.3**, respectively.

Supplementary Table 5.3. Experimental condition and enzyme kinetic parameters determined at 50°C and pH 7.0 from progress curve measurements for TnInv and TnDXI Gen2. Numbers in parentheses are standard errors of fitting average values of three independent progress curves for each substrate concentration; Suc = sucrose, DGlc = D-glucose, DFrc = D-fructose, DPsi = D-psicose

Enzyme	Reaction	Substrate concentration [mM]	k_{cat} [s^{-1}]	K_m [mM]
TnInv	Suc → DGlc +DFrc	1/4/10/40/100/100/250/600	117.9(± 2.21)	16 (± 1.6)
TnDXI Gen2	DGlc → DFrc	4/20/100/500/1000/2000	6.1 (± 0.05)	195.1 (± 6.4)
	DFrc → DFrc		9.8	347.6
PcDTE Var8*)	DFrc → DPsi	14.6/29.2/58.3/116.7/233/933	35.9 (± 0.45)	39 (± 0.42)
	DPsi → DFrc	14.6/29.2/58.3/116.7/233/467	41.6 (± 0.27)	23 (± 0.28)

*) Please note that enzyme kinetic parameters for PcDTE Var8 are mentioned here only for the sake of completeness (they had been determined under identical experimental conditions and reported before (**Chapter 4**))

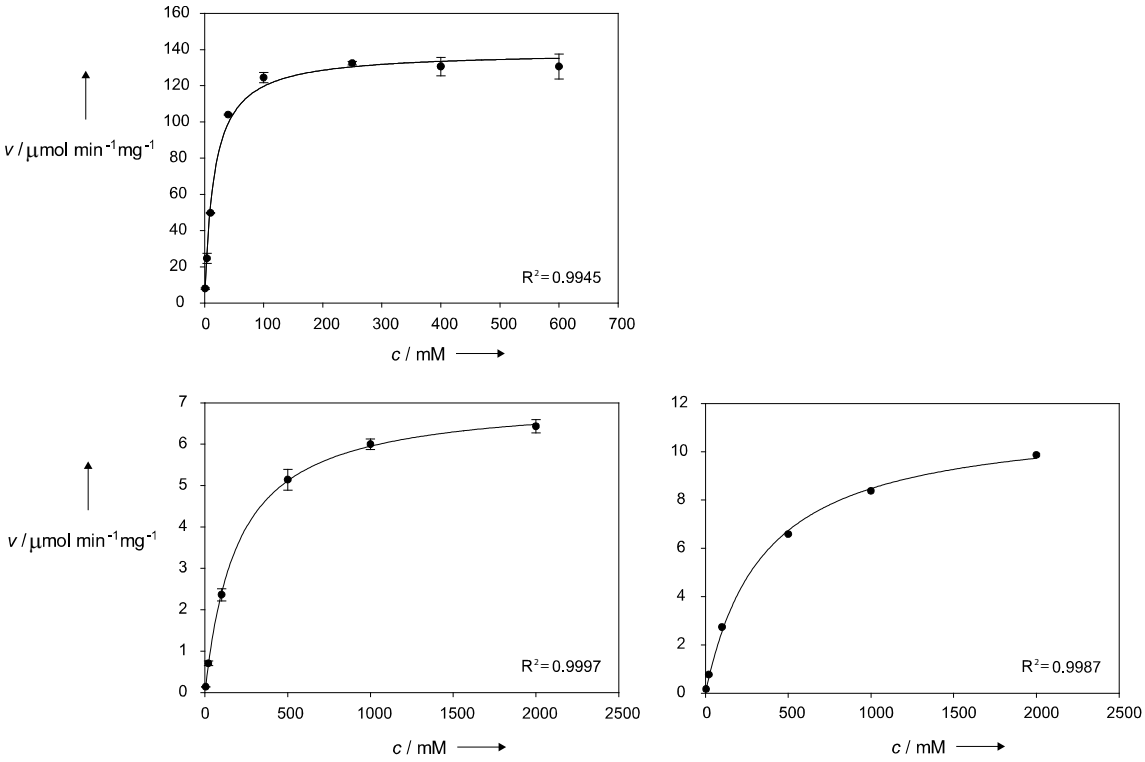

Supplementary Figure 5.6. Michaelis-Menten plots of sucrose hydrolysis using TnInv (top row) and the isomerization of D-Glucose to D-fructose (bottom row, left) and D-fructose to D-glucose (bottom row, right) using TnDXI Gen2. All kinetics were determined at 50°C.

5.3.7 Enzyme membrane reactor (EMR)

Biocatalysis was performed in a heat-jacketed enzyme membrane reactor (EMR) with an inner volume of 8.6 mL (Julich Fine Chemicals, Julich, Germany). The EMR was equipped with an Ultracel regenerated cellulose membrane with a cut-off of 10 kDa (Millipore Cooperation, Bedford, USA) and stirred at 800 rpm using a magnetic stirrer. The temperature was controlled using an external thermostat (Huber, Offenburg, Germany).

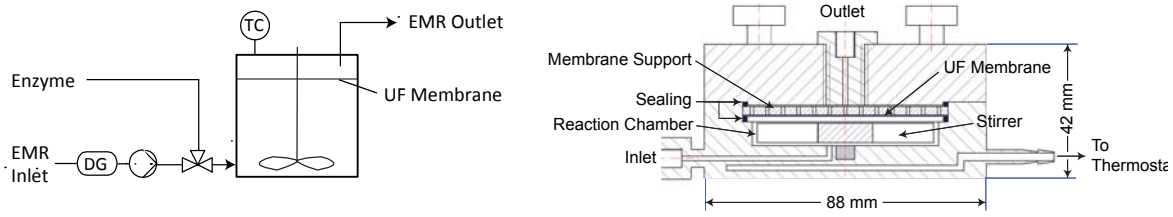

Supplementary Figure 5.7. Scheme of the entire EMR set-up and detailed representation in cross-section (*courtesy of Sonja Wahler*). Abbreviations: DG, degasser; TC, temperature control; UF, ultra-filtration

5.3.7.1 Thermal enzyme inactivation experiments

Experiments for the determination of inactivation parameters were started by prefilling the EMR with buffered substrate solution (10 mM sodium phosphate pH 7.0 and substrate as specified in **Supplementary Table 5.4**) using an Agilent 1200 series HPLC pump (Agilent Technologies, Palo Alto, USA). The EMR was heated-up to the respective temperature and then supplemented with enzyme using the autosampler of the Agilent HPLC. Details are provided in **Supplementary Table 5.4**.

Supplementary Table 5.4. Experimental conditions of the thermal inactivation runs performed for the model-based estimation of operational enzyme stability at different temperatures

Enzyme	Nr.	Substrate concentration	Enzyme concentration	Residence time	Reactor temperature	Experimental runtime
TnInv	A1	0.5 M sucrose	0.42 µM	17.2 min	50°C	3,020min
	A2				60°C	3,020min
	A3				70°C	2,054min
TnDXI Gen2*)	B1	1 M D-glucose	10.3 µM	43.0 min	50°C	5,140min
	B2				60°C	2,900min
PcDTE Var8	C1	1 M D-fructose	5.96 µM	49.1 min	50°C	5,550min
	C2		3.91 µM	49.1 min	60°C	5,070min
	C3		7.82 µM	24.6 min	65°C	3,870min
	C4		3.91 µM	49.1 min	70°C	2,310min

* 0.1mM $MnCl_2$ were additionally supplemented to the buffered substrate solution

At the reactor outlet the converted sugar solution was sampled using a Frac-920 Fraction Collector (GE Healthcare, Uppsala, Sweden) and analyzed on an Agilent 1200 series HPLC system equipped with an Agilent refractive index detector (RI) using a 100 mm x ID 7.8 mm AMINEX Fast Carbohydrate (Pb^{2+}) column at 85°C with a Carbo-P guard column (both Biorad, Reinach, Switzerland). Water was used as the mobile phase at a flow rate of 0.25 mL min^{-1} (for analyzing mixtures of sucrose and/or D-glucose and D-fructose) or 2.0 mL min^{-1} (for analyzing mixtures of D-fructose and D-psicose).

A non-linear regression method according to Levenberg-Marquardt has been implemented in MATLAB (Mathworks, Natick, USA) for fitting the experimental inactivation experiments to established enzyme decay models [169, 193] in order to estimate thermal activation and inactivation of the biocatalysts. For details on the method we refer to **Chapter 4**. An overlay of the experimental and fitted data and the extracted parameterization is presented in **Supplementary Figure 5.8**. In general, we observed a very good agreement between experiment and simulation.

A

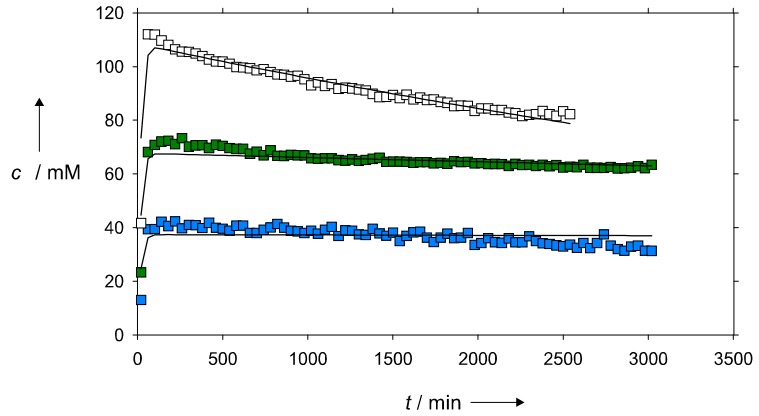

Parameters for TnINV	
ΔG_{act} [kJ mol^{-1}]	66.7 (±0.15)
ΔH_{EU} [kJ mol^{-1}]	59.5 (±6.06)
T_M [K]	344 (±1. 15)
ΔG_{inact} [kJ mol^{-1}]	119.7 (±0.30)

B

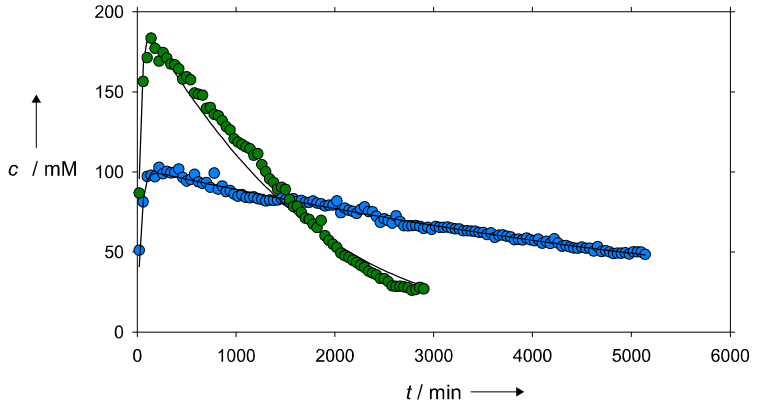

Parameters for TnDXI Gen2	
ΔG_{act} [kJ mol^{-1}]	74.7 (±0.02)
ΔH_{EU} [kJ mol^{-1}]	34.5 (±1.37)
T_M [K]	465 (±15.60)
ΔG_{inact} [kJ mol^{-1}]	103.2 (±0.57)

C

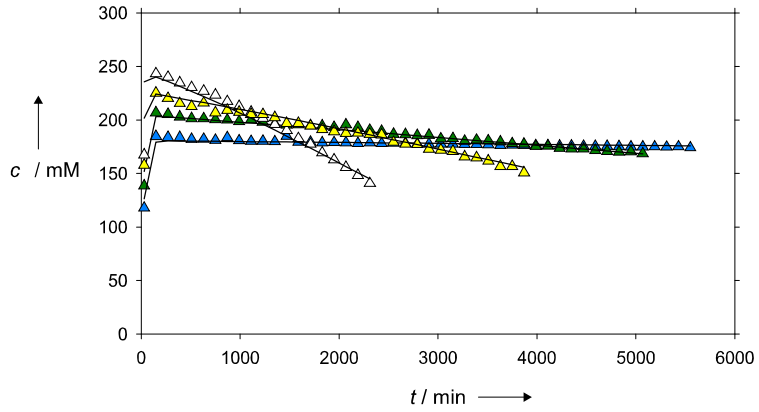

Parameters for PcDTE Var8*)	
ΔG_{act} [kJ mol^{-1}]	69.6 (±0.02)
ΔH_{EU} [kJ mol^{-1}]	67.6 (±1.15)
T_M [K]	355 (±0.98)
ΔG_{inact} [kJ mol^{-1}]	113.6 (±0.17)

*) from previous work (**Chapter 4**)

Supplementary Figure 5.8. Experimental concentration (symbols) and fitting results (line) of D-glucose (squares), D-fructose (circles) and D-psicose (triangles) measured at the EMR outlet during isothermal inactivation experiments for (**A**) TnInv (**B**) TnDXI Gen2 and (**C**) PcDTE Var8 at 70°C (white), 65°C (yellow), 60°C (green) and 50°C (blue) and the corresponding thermodynamic stability parameters

5.3.7.2 Standalone EMR experiment

A stand-alone EMR experiment with periodic enzyme injections was conducted at 50°C to demonstrate the feasibility of multi-enzyme EMR operation with constant conversion. A defined amount of each biocatalyst was added in the beginning of the experiment using a manual Rheodyne manual injection valve (Ercatech, Bern, Switzerland) equipped with a 20 mL loop and located in-flow between the pump and HPLC autosampler resulting in an initial concentration of 0.111 g L^{-1} TnInv, 1.500 g L^{-1} TnDXI Gen2 and 0.120 g L^{-1} PcDTE Var8 in the reactor. A buffered sucrose solution (0.5 M sucrose, 10 mM sodium phosphate buffer, 0.1 mM $MnCl_2$, pH 7.0) was supplied at a flow-rate of 0.25 ml min^{-1}. Based on the inactivation parameters for each biocatalyst that had been calculated (**Supplementary Figure 5.8**), we calculated the amount of enzyme that had to be periodically replenished, as described before (**Chapter 4**). Amounts of 1.1 x 10^{-7} g TnInv, 6.4 x 10^{-5} g TnDXI Gen2 and 5.0 x 10^{-7} g PcDTE Var8 were supplied every 30 min during the entire experiment using the Agilent HPLC autosampler set-up to inject new enzyme ("enzyme refresh").

As described in **5.3.7.1**, samples were fractionated at the EMR outlet and analyzed using the AMINEX Fast Carbohydrate (Pb^{2+}) column (Biorad). The cascade reaction was simulated in MATLAB by introducing a continuous reactor model that incorporated an irreversible Michaelis-Menten (MM) kinetic model for the conversion of sucrose to D-glucose and D-fructose by TnInv, a reversible MM kinetic model for the isomerization between D-glucose and D-fructose by TnDXI Gen2, and another reversible MM kinetic model for the epimerization of D-fructose and D-psicose by PcDTE Var8. Enzyme kinetic values that listed in **Supplementary Table 5.3** were used as parameters for the simulation.

5.3.8 Simulated moving bed (SMB) chromatography

A laboratory-scale implementation of an SMB plant based on the Amersham AEKTA basic-10 system (GE Healthcare, Uppsala, Sweden) was operated in a 2-2-2-2 configuration using DOWEX 50WX4-400(Ca^{2+}) cation exchange material (Sigma-Aldrich) packed into eight stainless steel columns (150 mm x 8 mm, ε= 0.24, Morvay Analytics, Basel, Switzerland) as solid phase and water as a mobile phase. In brief, the SMB set-up consisted of two P-900 pump modules: one assigned to deliver the inlet streams (eluent and feed), the other to provide the outlet streams (extract and raffinate). Six-port manifolds were placed at the inlet of each column that connected the columns to each other and to multi-position valves that directed the SMB inlet (feed and eluent) and outlet (extract and raffinate) flows. Check valves (CV-3000, Upchurch Scientific, Oak Harbor, USA) were installed between columns to ensure correct flow direction. Back pressure relief valves (1000 psi, Upchurch Scientific) were implemented downstream of the feed and eluent pump in order to

accommodate for local pressure build-up during valve switching. An additional multi-position valve that was connected to a three-port manifold installed at the outlet of each column was dedicated to direct the waste outlet stream from zone IV in order to realize the open-loop arrangement used in this work. The SMB columns were kept at a constant temperature by two column ovens (adjustable up to 100°C, Henggeler, Germany) while the SMB plant including all valves, pumps and eluent reservoirs was located in an incubator chamber heated to 35°C (Binder, Tuttlingen, Germany). The SMB unit was controlled with a modified version of the UNICORN software (GE Healthcare) [98, 99].

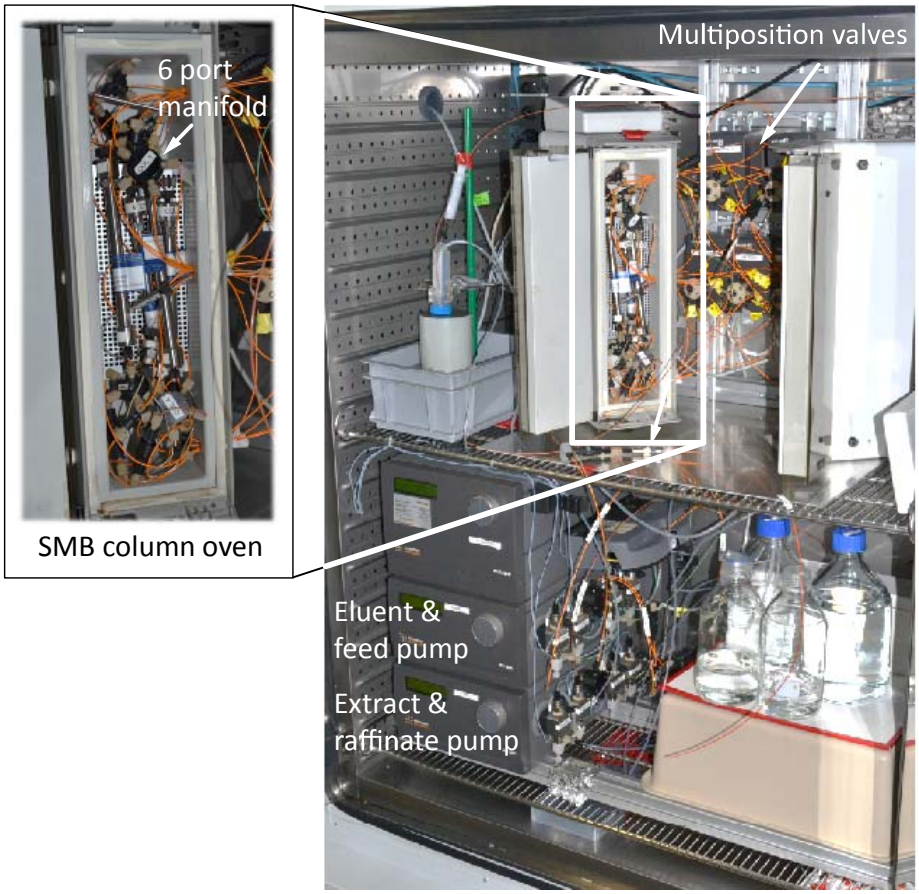

Supplementary Figure 5.9. Lab-scale AEKTA SMB-plant

5.3.8.1 Standalone SMB experiments

Stand-alone SMB experiments were carried out at 50°C using a feed solution containing 464 mM D-glucose, 409 mM D-fructose, and 127 mM D-psicose. Please note that this feed composition was chosen to match the concentrations of the components projected for the later integrated operation of the SMB from model predictions. The characteristic SMB operating parameters [182], namely the dimensionless flow-rate ratios (m_1, m_2, m_3, m_4) and

the switch time (t_{sw}) as well as the corresponding external liquid flow rates (Q) were summarized in **Supplementary Table 5.5.**:

Supplementary Table 5.5. Operating parameters for the SMB pre-experiments at 50°C:

	SMB operating parameters					External flow-rates [mL min^{-1}]				
	t_{sw}	m_1	m_2	m_3	m_4	Q_{Elu}	Q_{Ex}	Q_F	Q_{Raff}	Q_W
#	min									
1	5.1	1.406	0.704	1.132	0.500	1.960	0.792	0.483	0.712	0.939
2	5.1	1.406	0.704	1.132	0.475	1.960	0.792	0.483	0.741	0.911
3	5.1	1.406	0.704	1.132	0.450	1.960	0.792	0.483	0.769	0.882
4	5.1	1.406	0.704	1.132	0.300	1.960	0.792	0.483	0.938	0.713

Samples of the feed stream and all outlet streams (extract, raffinate and waste) were collected and analyzed on an AMINEX Fast Carbohydrate column (Biorad) as previously described (temperature= 85°C, eluent flow-rate= 0.25 mL min^{-1} H_2O).
The extract purity PU_{Ex} is defined as

$$PU_{Ex} = 100\frac{c_{Psi,Ex}}{c_{tot\ ,Ex}}[\%] \qquad \textbf{Supplementary Eq. 5.1}$$

respectively, with $c_{Psi,Ex}$ representing the D-psicose concentration in the SMB extract (*Ex*) and c_{tot} the total amount of sugar measured in the respective stream.
The amount of D-fructose (RC_{Frc}) and D-glucose (RC_{Glc}) recovered in the raffinate stream are given by

$$RC_{Frc} = 100\frac{c_{Frc,Raff}\ Q_{Raff}}{\left(Q_{Ex}c_{Frc,Ex} + c_{Frc,Raff}\ Q_{Raff} + c_{Frc,W}\ Q_W\right)}\ [\%] \qquad \textbf{Supplementary Eq. 5.2}$$

$$RC_{Frc} = 100\frac{c_{Frc,Raff}\ Q_{Raff}}{\left(Q_{Ex}c_{Frc,Ex} + c_{Frc,Raff}\ Q_{Raff} + c_{Frc,W}\ Q_W\right)}\ [\%] \qquad \textbf{Supplementary Eq. 5.3}$$

5.3.9 Nanofiltration (NF)

A custom designed cross-flow NF device (MMS, Urdorf, Switzerland) with an integrated gear pump (cross flow-rate = 1.2 L min^{-1}, Scherzinger, Furtwangen, Germany) was used for the concentration of the recycling stream using a 28 cm^2 polyamide NF membrane with a nominal cut-off of 90 Da ([101], FILMTEC NF-90, Dow Chemicals, Houston, USA). The retentate flow was set using a LIQUID FLOW flow-controller (Bronkhorst, Reinach, Switzerland) and controlled by the software LabView (National Instruments, Austin, USA). In preliminary experiments the rejection (*REJ*) of the NF-90 membrane for D-glucose and D-fructose was experimentally determined as 98.2 % and 98.0 % for a feed concentration of

500mM D-glucose and D-fructose, respectively, investigating fluxes between 1.0 x 10^{-5} m s^{-1} and 2.0 x 10^{-5} m s^{-1}.

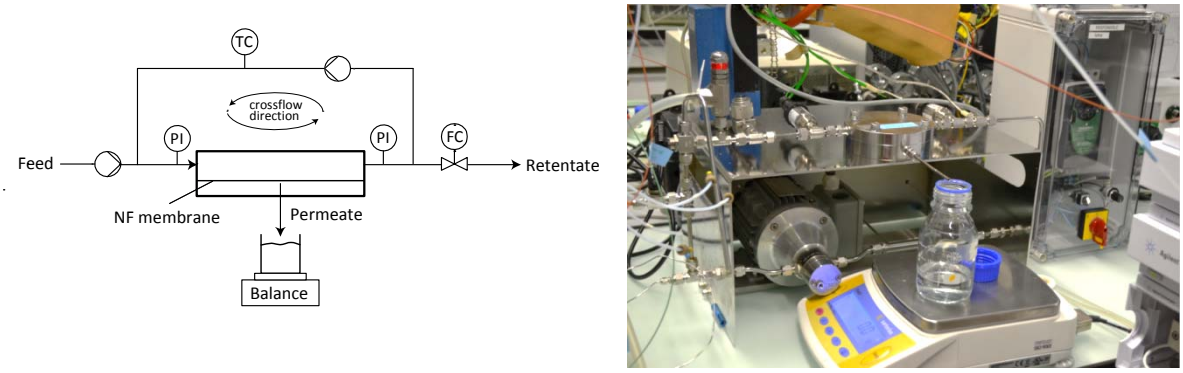

Supplementary Figure 5.10. Scheme of the custom designed cross-flow NF plant. Abbreviations: PI, pressure indicator; FC, flow controller; TC, external temperature control

5.3.10 Integrated process (IP)

The major unit operations (described in chapters 5.3.7 (EMR), 0 (SMB) and 5.3.9 (NF)) were connected using either 0.020" ID PEEK tubing with 1/16" fittings or 0.062" ID ETFE tubing with 1/8" fittings (Ercatech)). A simple desalting installation (DS, **Supplementary Figure 5.11A**) was integrated in the process design between EMR and SMB, which allowed the complete removal of the buffer ions which would otherwise impair the long-term stability of the Ca^{2+}-substituted SMB column. For the application in an continuous process, the DS was composed of a manual, two-position Rheodyne 7030 six port valve with a double three-way switching pattern and two VICI PEEK columns (150 mm x ID 7.5 mm, Schenkon, Switzerland) packed with mixed bed resin Dowex Marathon MR-3 (Sigma Aldrich). For the sake of simplicity the desalting columns were pre-equilibrated with SMB feed solution and alternatingly switched into the flow to achieve continuous desalting of the SMB feed stream. A desalting time of 6 h per column was estimated based on previous capacity measurements for Dowex Marathon MR-3 for the projected buffer concentration.

For sample taking form the various relevant positions in the integrated installation, three sampling devices (**Supplementary Figure 5.11B**) were positioned between the unit operations and denominated as sampling device B (between EMR and SMB), sampling device C (between SMB and NF) and sampling device A (between NF and EMR). HPLC pumps were located up- and downstream of each sampling device (**Supplementary Figure 5.12A**). The inlet streams were degassed (DG) and two additional online L-7614 membrane degasser (Merck, Darmstadt, Germany) were installed in front of the EMR and SMB feed port.

A

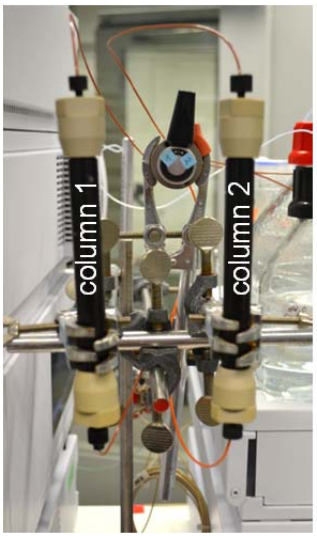

B

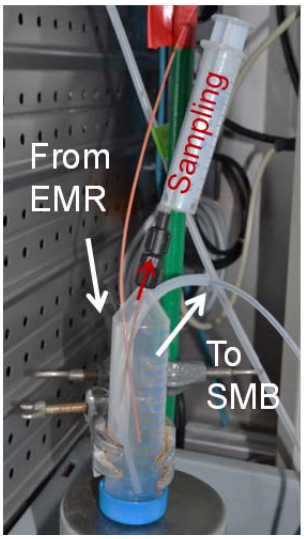

Supplementary Figure 5.11. (**A**) In process desalting installation and (**B**) sample taking device

A detailed scheme of the integrated process and a summary of all applied flows and simulated concentrations during the process are given in **Supplementary Figure 5.12**.
In order to reach the steady state regime more quickly, we chose a short-cut start up procedure in which the NF installation was pre-filled with sugar solutions that already resembled those of the predicted steady state regime [116]. Specifically, the integrated run was started by heating the EMR to 50°C and filling it with buffered sugar solution containing sucrose, D-glucose and D-fructose at the projected steady state target concentrations. The EMR (already coupled to the desalting column, **Supplementary Figure 5.11A**) was operated for approximately 150 min (≈ 13 residence times) at a flow-rate of 0.767 ml min^{-1} before the EMR outlet stream was directed to sampling device B, that served as a stirred 15 mL feed reservoir for the SMB plant, which in turn was started up as soon as the filling level of the reservoir was reached. Once the expected steady state concentrations at the SMB outlet ports were obtained, the raffinate stream was connected to sampling device C, which again served as 15 mL feed reservoir, in this case for the NF device. As part of the short cut start up scheme, the NF had been prefilled with sugar solution containing D-glucose and D-fructose prior to coupling, equivalent to the steady state retentate (target) concentration. Finally, before connecting the NF retentate stream to the sample taking reservoir A, we had to exchange the start-up feed (containing the starting sugar and the two intermediates) with the final process feed (containing only 0.5 M (171 g L-1) sucrose as the starting sugar).

A

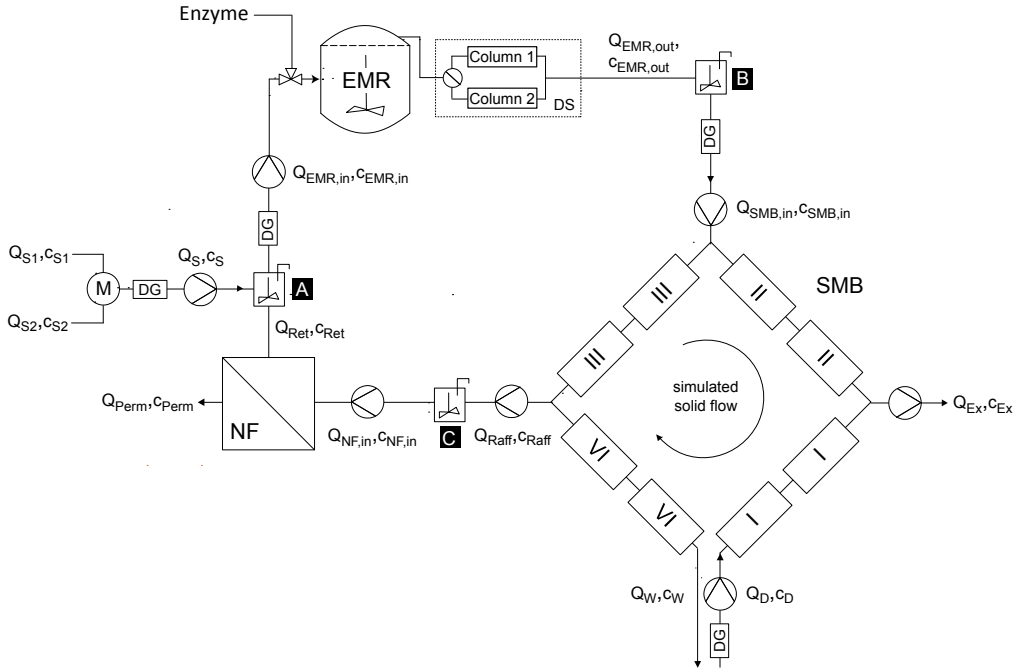

B

Flow-rate [mL min^{-1}]		Concentration [mM]						
			Suc	D-Glc	D-Frc	D-Psi	PO_4 Buffer (pH 7.0)	Mn^{2+}
Q_S	0.074	c_S	500	0	0	0	33.7	0.68
Q_{S1}	0.045	c_{S1}	500	0	0	0	54.9	0
Q_{S2}	0.029	c_{S2}	500	0	0	0	0	1.76
$Q_{EMR,in}$	0.488	$c_{EMR,in}$	75	452	398	0	5	0.1
$Q_{EMR,out}$	0.488	$c_{EMR,out}$	0	464	409	127	0	0
$Q_{SMB,in}$	0.483	$c_{SMB,in}$	0	464	409	127	0	0
Q_{Raff}	0.769	c_{Raff}	0	291	257	0	0	0
Q_{Ex}	0.792	c_{Ex}	0	0	0	77	0	0
Q_D	1.960	c_D	0	0	0	0	0	0
Q_W	0.882	c_W	0	0	0	0	0	0
$Q_{NF,in}$	0.767	$c_{NF,in}$	0	291	257	0	0	0
Q_{Ret}	0.416	c_{Ret}	0	532	468	0	0	0
Q_{Perm}	0.351	c_{Perm}	0	9.4	8.3	0	0	0

Supplementary Figure 5.12. (**A**) Detailed process scheme specifying the applied flow-rates and (**B**) the simulated steady state concentrations during integrated process operation. Abbreviations: EMR = enzyme membrane reactor, SMB = simulated moving bed plant, NF = nanofiltration, DS = desalting installation, DG = degasser, M = gradient mixer of the feed pump, A,B,C = sample taking devices

Please note that slightly higher input than outlet flows ($Q_{Samp,A}$ =0.12 mL h^{-1}, $Q_{Samp,B}$ = 0.12 mL h^{-1} and $Q_{Samp,C}$ =0.3 mL h^{-1}) were considered in the design of the individual unit operations in order to allow for the frequent removal of solution through sample taking during the run.

The relevant equation, through-put (*TP*), EMR space time yield (STY_{EMR}) and integrated process yield (*Y*) used for calculating process performance parameters are summarized below:

$$TP = Q_{Ex}\, c_{Psi,Ex} \qquad \textbf{Supplementary Eq. 5.4}$$

$$STY_{EMR} = \frac{TP}{V_{EMR}} \qquad \textbf{Supplementary Eq. 5.5}$$

$$Y = 100\frac{TP}{(Q_S - \sum Q_{Samp})\, 2c_{suc,S}} \qquad \textbf{Supplementary Eq. 5.6}$$

6 Conclusions and outlook

This thesis presents the first implementation and model-based optimization of a novel integrated process concept for the high-yield production of rare sugars. In this work, we chose the rare hexose D-psicose as a model compound that could be produced from D-fructose or sucrose via a single thermodynamically limited epimerase reaction or a multi-enzyme reaction cascade, respectively.

Thus, this work is one important step towards an economically feasible implementation of the "Izumoring" concept, introduced by Granstrom et al. in 2004 [3] that suggested the use of available iso- and epimerase enzymes for the generic production of most rare sugars starting from only few bulk sugars. Whereas in the initial "Izumoring" concept the unfavorable equilibrium position of epimerase and isomerase reactions was not taken into consideration, integration of the suggested reaction network(s) with SMB chromatography and NF allowed to produce the rare sugars, both in high *Y* and high *PU*.

In the presented integrated process concept, we found that, despite the increased complexity that inevitably emerges from the very nature of an integrated process design compared to a simple enzyme reactor, the experimental runs were found to be highly robust. We attribute this, at least in parts, to the linear adsorption behavior of the sugars on the employed stationary phase (over the investigated concentration range) and the associated capability to cope with minor concentration fluctuations in the SMB feed stream. As a similar adsorption behavior is published for other hexose epi- and isomers, we anticipate that this robustness also translates for other sugar mixtures and thus, that this integrated process constitutes a generic approach for the synthesis of rare sugar with similar behavior in terms of robustness.

In addition to the observed robustness the process also proved to be highly productive, this becomes evident from the preparative amounts (i.e. more than 500 g) of D-psicose that we could produce during this work utilizing only lab-scale equipment. The result is particularly noteworthy insofar as the potential of the process was not fully exploited as shown by the *in silico* optimization study (**Chapter 4**). A decisive role for the high *TP* observed could be definitely attributed to the high *PR*'s of the EMR during integrated operation. Effectively, the PR_{EMR} in our experimental integrated process run (**Chapter 4**) were found to be comparable or even higher than the productivities of many simple enzymatic biotransformations using an EMR [194]. Further, the integration process presented for the production of the rare sugars D-psicose could serve as an outline for the model-based design and optimization of integrated manufacturing processes for other rare sugars (e.g. the production of L-tagatose from L-sorbose using the enzyme DTE or the production of L-galactose using a two-enzyme-cascade employing DTE and L-rhamnose isomerase). The

modular, systematic approach established for the characterization of the involved unit operation (EMR, SMB, NF) is an essential step to speed-up process development times and evaluate the potential of the system based on *in silico* investigations. We further highlight that the presented modular approach could in principle be helpful to adapt the process to new requirements (e.g. to exchange the EMR by a plug-flow reactor, to embed advanced SMB concepts).

One general drawback of the integration of biocatalysis and chromatography is the necessity to operate all involved unit operations using the same, preferentially aqueous mobile phase/solvent. Albeit ligand exchange chromatography using water as a mobile phase fulfilled this prerequisite at the first sight, it proved incompatible with the addition of only trace amounts of charged ion species, including cofactors such as Mn^{2+} that were required to saturate the catalytic active site of TnDXI or buffer species that were instrumental to adjust the pH for the enzyme reaction. In the investigated process concept, the spatial segregation of enzyme reaction and separation facilitated the installation of a desalting column between EMR and SMB that allowed us to run these two devices under slightly different conditions (buffered/non-buffered). For the sake of simplicity two mixed bed desalting columns were used in the current implementation that were alternately switched into the flow until they reached their desalting capacity whereas the other column could be exchanged in the meantime. Ultimately, the problem might be solved in a more elegant and sustainable manner by the implementation of an in-place regeneration procedure of the desalting columns.

Although the thermostability of the biocatalyst PcDTE was significantly increased in a doctoral thesis performed concomitantly with this work (resulting in the thermostable enzyme variant PcDTE Var 8), our *in silico* optimization study clearly pointed out that even this thermostabilized enzyme still constituted the major cost contributor at elevated EMR temperatures. In principle this suggests to operate the EMR at lower temperatures, which however increases the risk of microbial contamination and demands higher EMR residence times and therefore, significant investments for excessively large EMR equipment. This issue could be resolved by genetically engineering the improved biocatalysts to exhibit higher specific activity on D-fructose, but at the same time retaining the same thermostability as Var8. The development of such an enzyme variant has recently been achieved in our laboratory [185] and therefore offers the opportunity to reduce the cost contribution of the biocatalyst optimization at intermediate and high temperatures even further.

7 References

[1] He, X. M., Agnihotri, G., Liu, H. W., Novel enzymatic mechanisms in carbohydrate metabolism. *Chem. Rev.* **2000**, *100*, 4615.

[2] Robyt, J. F., Beginnings, in: *Essentials of Carbohydrate Chemistry (Ed.: C.R. Cantor)*, Springer Verlag, New York, **1998**, pp. 1.

[3] Granström, T. B., Takata, G., Tokuda, M., Izumori, K., Izumoring. *J. Biosci. Bioeng.* **2004**, *97*, 89.

[4] Beerens, K., Desmet, T., Soetaert, W., Enzymes for the biocatalytic production of rare sugars. *J. Ind. Microbiol. Biot.* **2012**, *39*, 823.

[5] Oh, D. K., Tagatose: properties, applications, and biotechnological processes. *Appl. Microbiol. Biotechnol.* **2007**, *76*, 1.

[6] Levin, G. V., Zehner, L. R., Saunders, J. P., Beadle, J. R., Sugar substitutes - Their energy values, bulk characteristics, and potential health benefits. *Am. J. Clin. Nutr.* **1995**, *62*, 1161.

[7] Buemann, B., Toubro, S., Raben, A., Blundell, J., Astrup, A., The acute effect of D-tagatose on food intake in human subjects. *Brit. J. Nutr.* **2000**, *84*, 227.

[8] Lu, Y., Levin, G. V., Donner, T. W., Tagatose, a new antidiabetic and obesity control drug. *Diabetes Obes. Metab.* **2008**, *10*, 109.

[9] Espinosa, I., Fogelfeld, L., Tagatose: from a sweetener to a new diabetic medication? *Expert. Opin. Inv. Drug.* **2010**, *19*, 285.

[10] Matsuo, T., Suzuki, H., Hashiguchi, M., Izumori, K., D-psicose is a rare sugar that provides no energy to growing rats. *J. Nutr. Sci. Vitamino.l* **2002**, *48*, 77.

[11] Sun, Y., Hayakawa, S., Ogawa, M., Fukada, K., Izumori, K., Influence of a rare sugar, D-psicose, on the physicochemical and functional properties of an aerated food system containing egg albumen. *J. Agric. Food Chem.* **2008**, *56*, 4789.

[12] Sato, M., Yokoi, N., Kurose, H., Yamasaki, T., D-Ribose competitively reverses inhibition by D-psicose of larval growth in *Caenorhabditis elegans*. *Biol. Pharm. Bull.* **2009**, *32*, 950.

[13] Lim, Y. R., Oh, D. K., Microbial metabolism and biotechnological production of d-allose. *Appl. Microbiol. Biotechnol.* **2011**, *91*, 229.

[14] Woodyer, R. D., Christ, T. N., Deweese, K. A., Single-step bioconversion for the preparation Of L-gulose and L-galactose. *Carbohyd. Res.* **2010**, *345*, 363.

[15] Fessner, W.-D., Aldolases: Enzymes for making and breaking C–C Bonds, in: *Asymmetric organic synthesis with enzymes (Ed.: V. Gotor, I. Alfonso, E. García-Urdiales)*, Wiley-VCH, Weinheim, **2008**, p. 275.

[16] McDonald, E. J., A new synthesis of D-psicose. *Carbohyd. Res.* 1967, *5*, 209.

[17] Young, I. S., Baran, P. S., Protecting-group-free synthesis as an opportunity for invention. *Nat. Chem.* **2009**, *1*, 193.

[18] Anastas, P. T. Warner, J., *Green Chemistry: Theory and Practice*, Oxford University Press, Oxford, **1998**.

[19] Martinez, R. F., Liu, Z. L., Glawar, A. F. G., Yoshihara, A., Short and sweet: D-Glucose to L-glucose and L-glucuronic acid. *Angew. Chem. Int. Edit.* **2014**, *53*, 1160.

[20] Beadle, J. R., Saunders, J. P., Wajda, T. J., Google Patents **1992**.

[21] Gunther, W. R., Wang, Y., Ji, Y., Michaelis, V. K., Sn-Beta zeolites with borate salts catalyse the epimerization of carbohydrates via an intramolecular carbon shift. *Nat. commun.* **2012**, *3*, 1109.

[22] Bornscheuer, U. T., Huisman, G. W., Kazlauskas, R. J., Lutz, S., *et al.*, Engineering the third wave of biocatalysis. *Nature* **2012**, *485*, 185-194.

[23] Granstrom, T. B., Izumori, K., Leisola, M., A rare sugar xylitol. Part II: biotechnological production and future applications of xylitol. *Appl. Microbiol. Biotechnol.* **2007**, *74*, 273.

[24] Granstrom, T. B., Izumori, K., Leisola, M., A rare sugar xylitol. Part I: the biochemistry and biosynthesis of xylitol. *Appl. Microbiol Biotechnol* **2007**, *74*, 277.

[25] Saha, B. C., Racine, F. M., Biotechnological production of mannitol and its applications. *Appl. Microbiol Biotechnol.* **2011**, *89*, 879.

[26] Izumori, K., Izumoring: a strategy for bioproduction of all hexoses. *J. Biotechnol.* **2006**, *124*, 717.

[27] Stoop, J. M. H., Chilton, W.S., Pharr, D.M., Substrate stereo-specificity of the NAD-dependent mannitol dehydrogenase from celery. *Phytochemistry* **1996**, *43*, 5.

[28] Woodyer, R. D., Wymer, N. J., Racine, F. M., Khan, S. N., Saha, B. C., Efficient production of L-ribose with a recombinant *Escherichia coli* biocatalyst. *Appl. Environ. Microbiol.* **2008**, *74*, 2967.

[29] Kallnik, V., Schultz, C., Schweiger, P., Deppenmeier, U., Properties of recombinant Strep-tagged and untagged hyperthermophilic D-arabitol dehydrogenase from *Thermotoga maritima*. *Appl. Microbiol. Biotechnol.* **2011**, *90*, 1285.

[30] Takata, M. K., Yamaguchi, F., Nakanose, Y., Watanabe, Y., Neuroprotective effect of D-psicose on 6-hydroxydopamine-induced apoptosis in rat pheochromocytoma (PC12) cells. *J. Biosci. Bioeng.* **2005**, *100*, 511.

[31] Li, Z. J., Cai, L., Qi, Q. S., Wang, P. G., Enzymatic synthesis of D-sorbose and D-psicose with aldolase RhaD: Effect of acceptor configuration on enzyme stereoselectivity. *Bioorg. Med. Chem. Lett.* **2011**, *21*, 7081.

[32] Yang, J., Zhu, Y., Li, J., Men, Y, Sun, Y., Ma, Y., Biosynthesis of rare ketoses through constructing a recombination pathway in an engineered *Corynebacterium glutamicum*. *Biotechnol. Bioeng.* **2014**, doi: 10.1002/bit.25345.

[33] Clapes, P., Fessner, W. D., Sprenger, G. A., Samland, A. K., Recent progress in stereoselective synthesis with aldolases. *Curr. Opin. Chem. Biol.* **2010**, *14*, 154.

[34] Li, Z. J., Cai, L., Qi, Q. S., Styslinger, T. J., Synthesis of rare sugars with L-fuculose-1-phosphate aldolase (FucA) from *Thermus thermophilus* HB8. *Bioorg. Med. Chem. Lett.* **2011**, *21*, 5084.

[35] Macauley, S., McNeil, B., Harvey, L.M., The genus *Gluconobacter* and its applications in biotechnology. *Crit. Rev. Biotechnol.* **2001**, *21*, 25.

[36] Kim, H. J., Hyun, E. K., Kim, Y. S., Lee, Y. J., Oh, D. K., Characterization of an *Agrobacterium tumefaciens* D-psicose 3-epimerase that converts D-fructose to D-psicose. *Appl. Environ. Microbiol.* **2006**, *72*, 981.

[37] Ishida, Y., Kamiya, T., Itoh, H., Kimura, Y., Izumori, K., Cloning and characterization of the D-tagatose 3-epimerase gene from *Pseudomonas cichorii* ST-24. *J. Ferment. Bioeng.* **1997**, *83*, 529.

[38] Park, C.-S., Yeom, S.-J., Lim, Y.-R., Kim, Y.-S., Oh, D.-K., Characterization of a recombinant thermostable L-rhamnose isomerase from *Thermotoga maritima* ATCC 43589 and its application in the production of L-lyxose and L-mannose. *Biotechnol. Lett.* **2010**, *32*, 1947.

[39] Prabhu, P., Thanh, T. N. D., Jeya, M., Kang, L. W., Lee, J. K., Cloning and characterization of a rhamnose isomerase from *Bacillus halodurans*. *Appl. Microbiol. Biotechnol* **2010**, *89*, 635.

[40] Leang, K., Takada, G., Fukai, Y., Morimoto, K., *et al.*, Novel reactions of L-rhamnose isomerase from *Pseudomonas stutzeri* and its relation with D-xylose isomerase via substrate specificity. *Biochim. Biophys. Acta* **2004**, *1674*, 68.

[41] Cheng, L., Mu, W., Jiang, B., Thermostable L-arabinose isomerase from *Bacillus stearothermophilus* IAM 11001 for D-tagatose production: gene cloning, purification and characterisation. *J. Sci. Food Agr.* **2009**, *90*, 1327.

[42] Kim, B.C., Lee, Y.H., Lee, H.S., Lee, D.W., Cloning, expression and characterization of l-arabinose isomerase from *Thermotoga neapolitana*: bioconversion of D-galactose to D-tagatose using the enzyme. *FEMS Microbiol. Lett.* **2002**, *212*, 121.

[43] Yoon, S. H., Kim, P., Oh, D. K., Properties of L-arabinose isomerase from *Escherichia coli* as biocatalyst for tagatose production. *World. J. Microb. Biot.* **2003**, *19*, 47.

[44] Mizanur, R. M., Takata, G., Izumori, K., Cloning and characterization of a novel gene encoding L-ribose isomerase from *Acinetobacter sp* strain DL-28 in *Escherichia coli*. *BBA-Gene Struct. Expr.* **2001**, *1521*, 141.

[45] Nguyen, V. D., Le, T. H., Kim, J. I., Lee, J. W., Koo, Y. M., Separation of D-psicose and D-fructose using simulated moving bed chromatography. *J. Sep. Sci.* **2009**, *32*, 1987.

[46] Vieille, C., Hess, J. M., Kelly, R. M., Zeikus, J. G., Xyla cloning and sequencing and biochemical characterization of xylose isomerase from *Thermotoga neapolitana*. *Appl. Environ. Microb.* **1995**, *61*, 1867.

[47] Bandlish, R. K., Michael Hess, J., Epting, K. L., Vieille, C., Kelly, R. M., Glucose-to-fructose conversion at high temperatures with xylose (glucose) isomerases from *Streptomyces murinus* and two hyperthermophilic *Thermotoga species*. *Biotechnol. Bioeng.* **2002**, *80*, 185.

[48] Kim, H. J., Kang, S. Y., Park, J. J., Kim, P., Novel activity of UDP-galactose-4-epimerase for free monosaccharide and activity improvement by active site-saturation mutagenesis. *Appl. Biochem. Biotechnol.* **2011**, *163*, 444.

[49] Takeda, K., Yoshida, H., Izumori, K., Kamitori, S., X-ray structures of *Bacillus pallidus* D-arabinose isomerase and its complex with L-fucitol. *BBA Proteins Proteom.* **2010**, *1804*, 1359.

[50] Itoh, H., Sato, T., Izumori, K., Preparation of D-psicose from D-fructose by immobilized D-tagatose 3-epimerase. *J. Ferment. Bioeng.* **1995**, *80*, 101.

[51] Itoh, H., Sato, T., Takeuchi, T., Khan, A. R., Izumori, K., Preparation of D-sorbose from D-tagatose by immobilized D-tagatose 3-epimerase. *J. Ferment. Bioeng.* **1995**, *79*, 184.

[52] Itoh, H., Izumori, K., Enzymatic production of L-tagatose and L-fructose from L-sorbose and L-psicose, respectively. *J. Ferment. Bioeng.* **1996**, *81*, 351.

[53] Itoh, H., Okaya, H., Khan, A. R., Tajima, S., Purification and characterization of D-tagatose 3-epimerase from *Pseudomonas Sp*, St-24. *Biosci. Biotech. Bioch.* **1994**, *58*, 2168.

[54] Ishida, Y., Kamiya, T., Izumori, K., Production of D-tagatose 3-epimerase of *Pseudomonas cichorii* ST-24 using recombinant *Escherichia coli*. *J. Ferment. Bioeng.* **1997**, *84*, 348.

[55] Bhosale, S. H., Rao, M. B., Deshpande, V. V., Molecular and industrial aspects of glucose isomerase. *Microbiol. Rev.* **1996**, *60*, 280.

[56] Rearick, D. E., Kearney, M., Costesso, D. D., Simulated moving-bed technology in the sweetener industry. *Chemtech.* **1997**, *27*, 36.

[57] Takeshita, K., Suga, A., Takada, G., Izumori, K., Mass production of D-psicose from D-fructose by a continuous bioreactor system using immobilized D-tagatose 3-epimerase. *J. Biosci. Bioeng.* **2000**, *90*, 453.
[58] Morimoto, K., Park, C.-S., Ozaki, M., Takeshita, K., Large scale production of D-allose from D-psicose using continuous bioreactor and separation system. *Enzyme Microb. Technol.* **2006**, *38*, 855.
[59] Bechtold, M., Makart, S., Heinemann, M., Panke, S., Integrated operation of continuous chromatography and biotransformations for the generic high yield production of fine chemicals. *J. Biotechnol.* **2006**, *124*, 146.
[60] Kim, N. H., Kim, H. J., Kang, D. I., Jeong, K. W., Conversion shift of D-fructose to D-psicose for enzyme-catalyzed epimerization by addition of borate. *Appl. Environ. Microbiol.* **2008**, *74*, 3008.
[61] EFSA, Scientific opinion on the re-evaluation of boric acid (E 284) and sodium tetraborate (borax) (E 285) as food additives. *EFSA Journal* **2013**, *11*, 3407.
[62] Strohlein, G., Assuncao, Y., Proplesch, R., Mazzotti, M., Morbidelli, M., Reactive chromatography. *Chem. Ing. Tech.* **2005**, *77*, 1819.
[63] Samant, K. D., Ng, K. M., Systematic development of extractive reaction processes. *Chem. Eng. Technol.* **1999**, *22*, 877.
[64] Kelkar, V. V., Ng, K. M., Design of reactive crystallization systems incorporating kinetics and mass-transfer effects. *AIChE J.* **1999**, *45*, 69.
[65] Mazzotti, M., Kruglov, A., Neri, B., Gelosa, D., Morbidelli, M., A continuous chromatographic reactor: SMBR. *Chem. Eng. Sci.* **1996**, *51*, 1827.
[66] Agreda, V. H., Partin, L. R., Heise, W. H., High-purity methyl acetate via reactive distillation. *Chem. Eng. Prog.* **1990**, *86*, 40.
[67] Degarmo, J. L., Parulekar, V. N., Pinjala, V., Consider reactive distillation. *Chem. Eng. Prog.* **1992**, *88*, 43.
[68] Barker, P. E., Ganetsos, G., Production of high-purity fructose from barley syrups using semicontinuous chromatography. *J. Chem. Technol. Biotechnol.* **1985**, *35*, 217.
[69] Azevedo, D. C. S., Rodrigues, A. E., Fructose-glucose separation in a SMB pilot unit: modeling, simulation, design, and operation. *AIChE J.* **2001**, *47*, 2042.
[70] Azevedo, D. C. S., Rodrigues, A. E., Separation of fructose and glucose from cashew apple juice by SMB chromatography. *Sep. Sci. Technol.* **2005**, *40*, 1761.
[71] Juza, M., Development of an high-performance liquid chromatographic simulated moving bed separation from an industrial perspective. *J. Chromatogr. A* **1999**, *865*, 35.
[72] Paredes, G., Mazzotti, M., Optimization of simulated moving bed and column chromatography for a plasmid DNA purification step and for a chiral separation. *J. Chromatogr. A* **2007**, *1142*, 56.
[73] Rajendran, A., Paredes, G., Mazzotti, M., Simulated moving bed chromatography for the separation of enantiomers. *J. Chromatogr. A* **2009**, *1216*, 709.
[74] Lode, F., Houmard, M., Migliorini, C., Mazzotti, M., Morbidelli, M., Continuous reactive chromatography. *Chem. Eng. Sci.* **2001**, *56*, 269.
[75] Hashimoto, K., Adachi, S., Noujima, H., Ueda, Y., A new process combining adsorption and enzyme reaction for producing higher-fructose syrup. *Biotechnol. Bioeng.* **1983**, *25*, 2371.
[76] Meissner, J. P., Carta, G., Continuous regioselective enzymatic esterification in a simulated moving bed reactor. *Ind. Eng. Chem. Res.* **2002**, *41*, 4722.

[77] Meurer, M., Altenhoner, U., Strube, J., Untiedt, A., Schmidt-Traub, H., Dynamic simulation of a simulated-moving-bed chromatographic reactor for the inversion of sucrose. *Starch* **1996**, *48*, 452.

[78] Shieh, M. T., Barker, P. E., Combined bioreaction and separation in a simulated counter-current chromatographic bioreactor-separator for the hydrolysis of lactose. *J. Chem. Technol. Biot.* **1996**, *66*, 265.

[79] Bechtold, M., Makart, S., Reiss, R., Alder, P., Panke, S., Model-based characterization of an amino acid racemase from *Pseudomonas putida* DSM 3263 for application in medium-constrained continuous processes. *Biotechnol. Bioeng.* **2007**, *98*, 812.

[80] Makart, S., Bechtold, M., Panke, S., Separation of amino acids by simulated moving bed under solvent constrained conditions for the integration of continuous chromatography and biotransformation. *Chem. Eng. Sci.* **2008**, *63*, 5347.

[81] Bosshart, A., Panke, S., Bechtold, M., Systematic optimization of interface interactions increases the thermostability of a multimeric enzyme. *Angew. Chem. Int. Edit.* **2013**, *52*, 9673.

[82] Bechtold, M., Panke, S., *In situ* product recovery integrated with biotransformations. *CHIMIA* **2009**, *63*, 345.

[83] Stark, D., von Stockar, U., *In situ* product removal (ISPR) in whole cell biotechnology during the last twenty years. *Adv. Biochem. Eng.* **2003**, *80*, 149.

[84] Woodley, J. M., Bisschops, M., Straathof, A. J. J., Ottens, M., Future directions for in-situ product removal (ISPR). *J. Chem. Technol. Biot.* **2008**, *83*, 121.

[85] Stankiewicz, A., Moulijn, J. A., Process intensification. *Ind. Eng. Chem. Res.* **2002**, *41*, 1920.

[86] Goldberg, R. N., Tewari, Y. B., Bhat, T. N., Thermodynamics of enzyme-catalyzed reactions - a database for quantitative biochemistry. *Bioinform.* **2004**, *20*, 2874.

[87] Guiochon, G., Katti, A. M., Shirazi, S. G., *Fundamentals of Preparative and Nonlinear Chromatography*, Academic Press, Boston, **1994**.

[88] Strauss, U. T., Faber, K., Deracemization of (+/-)-mandelic acid using a lipase-mandelate racemase two-enzyme system. *Tetrahedron* **1999**, *10*, 4079.

[89] Schulte, M., Strube, J., Preparative enantioseparation by simulated moving bed chromatography. *J. Chromatogr. A* **2001**, *906*, 399.

[90] Rao, N. N., Lutz, S., Wurges, K., Minor, D., Continuous Biocatalytic Processes. *Org. Process Res. Dev.* **2009**, *13*, 607.

[91] Villadsen, J., Innovative technology to meet the demands of the white biotechnology revolution of chemical production. *Chem. Eng. Sci.* **2007**, *62*, 6957.

[92] Michel, M., Epping, A., Jupke, A., Modeling and determination of model parameters, in: *Preparative Chromatography (Ed.: H. Schmidt-Traub)*, Wiley-VCH, Weinheim **2005**, p. 215.

[93] Iida, T., Hayashi, N., Yamada, T., Yoshikawa, Y., Failure of D-psicose absorbed in the small intestine to metabolize into energy and its low large intestinal fermentability in humans. *Metabolism* **2010**, *59*, 206.

[94] Police, S. B., Harris, J. C., Lodder, R. A., Cassis, L. A., Effect of diets containing sucrose vs. D-tagatose in hypercholesterolemic mice. *Obesity* **2009**, *17*, 269.

[95] Beach, J. W., Kim, H. O., Jeong, L. S., Nampalli, S., A highly stereoselective synthesis of anti-Hiv 2',3'-dideoxynucleosides and 2',3'-didehydro-2',3'-dideoxynucleosides. *J. Org. Chem.* **1992**, *57*, 3887.

[96] Ma, T. W., Pai, S. B., Zhu, Y. L., Lin, J. S., Structure-activity relationships of 1-(2-deoxy-2-fluoro-beta-L-arabinofuranosyl)pyrimidine nucleosides as anti-hepatitis B virus agents. *J. Med. Chem.* **1996**, *39*, 2835.

[97] Oh, D.-K., Kim, N.-H., Kim, H.-J., Park, C.-S., D-Psicose production from D-fructose using an isolated strain, *Sinorhizobium sp. World J. Microb. Biot.* **2007**, *23*, 559.

[98] Abel, S., Babler, M. U., Arpagaus, C., Mazzotti, M., Stadler, J., Two-fraction and three-fraction continuous simulated moving bed separation of nucleosides. *J. Chromatogr. A* **2004**, *1043*, 201.

[99] Paredes, G., Makart, S., Stadler, J., Mazzotti, M., Simulated moving bed operation for size exclusion plasmid purification. *Chem. Eng. Technol.* **2005**, *28*, 1335.

[100] Mazzotti, M., Storti, G., Morbidelli, M., Optimal operation of simulated moving bed units for nonlinear chromatographic separations. *J. Chromatogr. A* **1997**, *769*, 3.

[101] Zhu, A., Long, F., Wang, X., Zhu, W., Ma, J., The negative rejection of H^+ in NF of carbonate solution and its influences on membrane performance. *Chemosphere* **2007**, *67*, 1558.

[102] Juza, M., Mazzotti, M., Morbidelli, M., Simulated moving-bed chromatography and its application to chirotechnology. *Trends Biotechnol.* **2000**, *18*, 108.

[103] Straathof, A. J. J., Panke, S., Schmid, A., The production of fine chemicals by biotransformations. *Curr. Opin. Biotech.* **2002**, *13*, 548.

[104] Weijers, S. R., Van't Riet, K., Enzyme stability in downstream processing .1. Enzyme inactivation, stability and stabilization. *Biotechnol. Adv.* **1992**, *10*, 237.

[105] Helfferich, F. G., *Ion exchange*, Dover Publications, Mineola, **1995**.

[106] Hong, S. K., Elimelech, M., Chemical and physical aspects of natural organic matter (NOM) fouling of nanofiltration membranes. *J. Membrane Sci.* **1997**, *132*, 159.

[107] Sheldon, R. A., Enzyme Immobilization: the quest for optimum performance. *Adv. Synth. Catal.* **2007**, *349*, 1289.

[108] Eijsink, V. G. H., Bjork, A., Gaseidnes, S., Sirevag, R., Rational engineering of enzyme stability. *J. Biotechnol.* **2004**, *113*, 105.

[109] Eijsink, V. G. H., Gaseidnes, S., Borchert, T. V., van den Burg, B., Directed evolution of enzyme stability. *Biomol. Eng.* **2005**, *22*, 21.

[110] Liese, A., Seelbach, K. , Buchholz, A., Haberland, J., Processes, in: *Industrial biotransformations* (Ed.: A. Liese, K. Seelbach, C. Wandrey), Wiley-VCH, Weinheim **2000**, p. 147.

[111] Hossain, M. A., Izuishi, K., Tokuda, M., Izumori, K., Maeta, H., D-Allose has a strong suppressive effect against ischemia/reperfusion injury: a comparative study with allopurinol and superoxide dismutase. *J. Hepato. Biliary Pan.* **2004**, *11*, 181.

[112] van Rantwijk, F., Oosterom, M. W. V., Sheldon, R. A., Glycosidase-catalysed synthesis of alkyl glycosides. *J. Mol. Catal. B* **1999**, *6*, 511.

[113] Hayashi, N., Iida, T., Yamada, T., Okuma, K., Study on the postprandial blood glucose suppression effect of D-psicose in borderline diabetes and the safety of long-term ingestion by normal human subjects. *Biosci. Biotech. Bioch.* **2010**, *74*, 510.

[114] Hossain, M. A., Kitagaki, S., Nakano, D., Nishiyama, A., Tokuda, M., Rare sugar D-psicose improves insulin sensitivity and glucose tolerance in type 2 diabetes Otsuka Long-Evans Tokushima Fatty (OLETF) rats. *Biochem. Bioph. Res. Co.* **2011**, *405*, 7.

[115] Suna, S., Yamaguchi, F., Kimura, S., Tokuda, M., Jitsunari, F., Preventive effect of D-psicose, one of rare ketohexoses, on di-(2-ethylhexyl) phthalate (DEHP)-induced testicular injury in rat. *Toxicol. Lett.* **2007**, *173*, 107.

[116] Wagner, N., Fuereder, M., Bosshart, A., Panke, S., Bechtold, M., Practical aspects of integrated operation of biotransformation and SMB separation for fine chemical synthesis. *Org. Process Res. Dev.* **2012**, *16*, 323.
[117] Griffin, G. J., Purification and concentration of xylose and glucose from neutralized bagasse hydrolysates using 3,5-dimethylphenylboronic acid and modified Aliquat 336 as coextractants. *Sep. Sci. Technol.* **2005**, *40*, 2337.
[118] Griffin, G. J., Shu, L., Solvent extraction and purification of sugars from hemicellulose hydrolysates using boronic acid carriers. *J. Chem. Technol. Biotechnol.* **2004**, *79*, 505.
[119] Lim, B. C., Kim, H. J., Oh, D. K., High production of D-tagatose by the addition of boric acid. *Biotechnol. Prog.* **2007**, *23*, 824.
[120] Duggan, P. J., Fructose-permeable liquid membranes containing boronic acid carriers. *Aust. J. Chem.* **2004**, *57*, 291.
[121] Bhuiyan, S. H., Itami, Y., Takada, G., Izumori, K., Preparation of L-talose and D-gulose from L-tagatose and D-sorbose, respectively, using immobilized L-rhamnose isomerase. *J. Biosci. Bioeng.* **1999**, *88*, 567.
[122] Caruel, H., Rigal, L., Gaset, A., Carbohydrate separation by ligand-exchange liquid-chromatography - Correlation between the formation of sugar cation complexes and the elution order. *J. Chromatogr.* **1991**, *558*, 89.
[123] Jones, J. K. N., Wall, R. A., The separation of sugars on ion-exchange resins: 2. Separation of monosaccharides. *Can. J. Chem.* **1960**, *38*, 2290.
[124] Lim, B.-C., Kim, H.-J., Oh, D.-K., A stable immobilized d-psicose 3-epimerase for the production of d-psicose in the presence of borate. *Process Biochem.* **2009**, *44*, 822.
[125] Beste, Y. A., Lisso, M., Wozny, G., Arlt, W., Optimization of simulated moving bed plants with low efficient stationary phases: separation of fructose and glucose. *J. Chromatogr. A* **2000**, *868*, 169.
[126] Nicoud, R. M., Majors, R. E., Simulated moving bed chromatography for preparative separations. *LC GC N. Am.* **2000**, *18*, 680.
[127] Jeon, Y. J., Park, M. B., Kim, I. H., L-Ribose from L-arabinose by epimerization and its purification by 3-zone simulated moving bed chromatography. *Bioprocess Biosys. Eng.* **2010**, *33*, 87.
[128] Jupke, A., Epping, A., Schmidt-Traub, H., Optimal design of batch and simulation moving bed chromatographic separation processes. *J. Chromatogr. A* **2002**, *944*, 93.
[129] Guiochon, G., Felinger, A., Shirazi, D., Katti, A., *Fundamentals of preparative and nonlinear chromatography,* Academic Press, Amsterdam, **2006**.
[130] Michel, M., Epping, E., Jupke, A., Modeling and determination of model parameters, in: *Preparative chromatography (Ed.: H. Schmidt-Traub)*, Wiley-VCH, Weinheim **2005**, page(s) 271-272.
[131] Leao, C. P., Rodrigues, A. E., Transient and steady-state models for simulated moving bed processes: numerical solutions. *Comput. Chem. Eng.* **2004**, *28*, 1725.
[132] Pais, L. S., Loureiro, J. M., Rodrigues, A. E., Modeling strategies for enantiomers separation by SMB chromatography. *AIChE J.l* **1998**, *44*, 561.
[133] Katsuo, S., Mazzotti, M., Intermittent simulated moving bed chromatography: 1. Design criteria and cyclic steady-state. *J. Chromatogr. A* **2010**, *1217*, 1354.
[134] Acetti, D., Langel, C., Brenna, E., Fuganti, C., Mazzotti, M., Intermittent simulated moving bed chromatographic separation of (RS,RS)-2-(2,4-difluorophenyl)butane-1,2,3-triol. *J. Chromatogr. A* **2010**, *1217*, 2840.

[135] Fuereder, M., Panke, S., Bechtold, M., Simulated moving bed enantioseparation of amino acids employing memory effect-constrained chromatography columns. *J. Chromatogr. A* **2012**, *1236*, 123.
[136] Altenhoner, U., Meurer, M., Strube, J., Schmidt-Traub, H., Parameter estimation for the simulation of liquid chromatography. *J. Chromatogr. A* **1997**, *769*, 59.
[137] Seidel-Morgenstern, A., Experimental determination of single solute and competitive adsorption isotherms. *J. Chromatogr. A* **2004**, *1037*, 255.
[138] Forssén, P., Arnell, R., Fornstedt, T., An improved algorithm for solving inverse problems in liquid chromatography. *Comput. Chem. Eng.* **2006**, *30*, 1381.
[139] Felinger, A., Zhou, D., Guiochon, G., Determination of the single component and competitive adsorption isotherms of the 1-indanol enantiomers by the inverse method. *J. Chromatogr. A* **2003**, *1005*, 35.
[140] Kim, H., Kaczmarski, K., Guiochon, G., Mass transfer kinetics on the heterogeneous binding sites of molecularly imprinted polymers. *Chem. Eng. Sci.* **2005**, *60*, 5425.
[141] Kim, H., Kaczmarski, K., Guiochon, G., Isotherm parameters and intraparticle mass transfer kinetics on molecularly imprinted polymers in acetonitrile/buffer mobile phases. *Chem. Eng. Sci.* **2006**, *61*, 5249.
[142] Dose, E. V., Jacobson, S., Guiochon, G., Determination of isotherms from chromatographic peak shapes. *Anal. Chem.* **1991**, *63*, 833.
[143] Gramblička, M., Polakovič, M., Adsorption equilibria of glucose, fructose, sucrose, and fructooligosaccharides on cation exchange resins. *J. Chem. Eng. Data* **2007**, *52*, 345.
[144] Viard, V., Lameloise, M. L., Modeling glucose fructose separation by adsorption chromatography on ion-exchange resins. *J. Food Eng.* **1992**, *17*, 29.
[145] Luz, D. A., Rodrigues, A. K., Silva, F. R., Torres, A. E., Adsorptive separation of fructose and glucose from an agroindustrial waste of cashew industry. *Bioresour. Technol.* **2008**, *99*, 2455.
[146] Vente, J. A., Bosch, H., de Haan, A. B., Bussmann, P. J. T., Evaluation of sugar sorption isotherm measurement by frontal analysis under industrial processing conditions. *J. Chromatogr. A* **2005**, *1066*, 71.
[147] Chung, S. F., Wen, C. Y., Longitudinal dispersion of liquid flowing through fixed and fluidized beds. *AIChE J.* **1968**, *14*, 857.
[148] Gunn, D. J., Axial and radial dispersion in fixed beds. *Chem. Eng. Sci.* **1987**, *42*, 363.
[149] Azevedo, D. C. S., Rodrigues, A. E., Bilinear driving force approximation in the modeling of a simulated moving bed using bidisperse adsorbents. *Ind. Eng. Chem. Res.* **1999**, *38*, 3519.
[150] Quinones, I., Cavazzini, A., Guiochon, G., Adsorption equilibria and overloaded band profiles of basic drugs in a reversed-phase system. *J. Chromatogr. A* **2000**, *877*, 1.
[151] Catchpoole, H. J., Shalliker, R. A., Dennis, G. R., Guiochon, G., Visualising the onset of viscous fingering in chromatography columns. *J. Chromatogr. A* **2006**, *1117*, 137.
[152] Korson, L., Drosthan.W, Millero, F. J., Viscosity of water at various temperatures. *J. Phys. Chem.* **1969**, *73*, 34.
[153] Pais, L. S., Loureiro, J. M., Rodrigues, A. E., Modeling, simulation and operation of a simulated moving bed for continuous chromatographic separation of 1,1'-bi-2-naphthol enantiomers. *J. Chromatogr. A* **1997**, *769*, 25.
[154] Sutton, P. W., Adams, J. P., Archer, I., Auriol, D., *et al.*, Biocatalysis in the fine chemical and pharmaceutical industries, in: *Practical methods for biocatalysis and*

biotransformations 2 (Ed.: J. Whittall, P.W. Sutton), John Wiley & Sons, New York, **2012**, pp. 1.
[155] Anastas, P., Eghbali, N., Green chemistry: principles and practice. *Chem. Soc. Rev.* **2010**, *39*, 301.
[156] Wandrey, C., Liese, A., Kihumbu, D., Industrial biocatalysis: Past, present, and future. *Org. Process Res. Dev.* **2000**, *4*, 286.
[157] Hilterhaus, L., Liese, A., Industrial application and processes using isomerases, in: *Enzyme Catalysis in Organic Synthesis (Ed.: K. Drauz, H. Groeger, O. May)*, Wiley-VCH, Weinheim, **2012**, p. 1685.
[158] Bechtold, M., Makart, S., Heinemann, M., Panke, S., *2nd BioPerspectives Congress*, *Elsevier Science*, Wiesbaden, **2005**, pp. 146.
[159] Bechtold, M., Füreder, M., Wagner, N., Panke, S., Potenzial von Prozessintegration mit Adsorbern zur Herstellung seltener Monosaccharide - eine modellbasierte Untersuchung. *Chem. Ing. Tech.* **2010**, *82*, 65.
[160] Woodley, J. M., Breuer, M., Mink, D., A future perspective on the role of industrial biotechnology for chemicals production. *Chem. Eng. Res. Des.* **2013**, *91*, 2029.
[161] Fessner, W. D., Badia, J., Eyrisch, O., Schneider, A., Sinerius, G., Enzymatic syntheses of rare ketose 1-phosphates. *Tetrahedron. Lett.* **1992**, *33*, 5231.
[162] Flickinger, M. C., Drew, S. W., *The encyclopedia of bioprocess technology: fermentation, biocatalysis, and bioseparation*, John Wiley & Sons, New York, **1999**.
[163] Tufvesson, P., Lima-Ramos, J., Nordblad, M., Woodley, J. M., Guidelines and cost analysis for catalyst production in biocatalytic processes. *Org. Process Res. Dev.* **2011**, *15*, 266.
[164] Heinzle, E., Biwer, A. P., Cooney, C. L., *Development of sustainable bioprocesses: modeling and assessment*, John Wiley & Sons, New York, **2006**.
[165] Tufvesson, P., Fu, W. J., Jensen, J. S., Woodley, J. M., Process considerations for the scale-up and implementation of biocatalysis. *Food Bioprod. Process* **2010**, *88*, 3.
[166] Gibbs, P. R., Uehara, C. S., Neunert, U., Bommarius, A. S., Accelerated biocatalyst stability testing for process optimization. *Biotechnol. Progr.* **2005**, *21*, 762.
[167] Lumry, R., Eyring, H., Conformation Changes of Proteins. *J. Phys. Chem.* **1954**, *58*, 110.
[168] Gasteiger, E., Gattiker, A., Hoogland, C., Ivanyi, I., *et al.*, ExPASy: the proteomics server for in-depth protein knowledge and analysis. *Nucleic Acids Res.* **2003**, *31*, 3784.
[169] Bechtold, M., Panke, S., Model-based characterization of operational stability of multimeric enzymes with complex deactivation behavior: An *in silico* investigation. *Chem. Eng. Sci.* **2012**, *80*, 435.
[170] Bommarius, A. S., Broering, J. M., Established and novel tools to investigate biocatalyst stability. *Biocatal. Biotransfor.* **2005**, *23*, 125.
[171] Illanes, A., Wilson, L., Enzyme reactor design under thermal inactivation. *Crit. Rev. Biotechnol.* **2003**, *23*, 61.
[172] Santacoloma, P. A., Sin, G., Gernaey, K. V., Woodley, J. M., Multienzyme-catalyzed processes: next-generation biocatalysis. *Org. Process Res. Dev.* **2011**, *15*, 203.
[173] Gall, M., Thomsen, M., Peters, C., Pavlidis, I. V., Enzymatic conversion of flavonoids using bacterial chalcone isomerase and enoate reductase. *Angew. Chem. Int. Edit.* **2014**, *53*, 1439.
[174] Rachwalski, M., Vermue, N., Rutjes, F. P. J. T., Recent advances in enzymatic and chemical deracemisation of racemic compounds. *Chem. Soc. Rev.* **2013**, *42*, 9268.
[175] Bremus, C., Herrmann, U., Bringer-Meyer, S., Sahm, H., The use of microorganisms in L-ascorbic acid production. *J. Biotechnol.* **2006**, *124*, 196.

[176] Lorenz, H., Seidel-Morgenstern, A., Processes to separate enantiomers. *Angew. Chem. Int. Edit.* **2014**, *53*, 1218.
[177] O'Brien, A. G., Horvath, Z., Levesque, F., Lee, J. W., Continuous synthesis and purification by direct coupling of a flow reactor with Simulated Moving Bed chromatography. *Angew. Chem. Int. Edit.* **2012**, *51*, 7028.
[178] Stefansson, M., Westerlund, D., Ligand-exchange chromatography of carbohydrates and glycoconjugates. *J. Chromatogr. A* **1996**, *720*, 127.
[179] Dipasquale, L., Gambacorta, A., Siciliano, R. A., Mazzeo, M. F., Lama, L., Purification and biochemical characterization of a native invertase from the hydrogen-producing *Thermotoga neapolitana* (DSM 4359). *Extremophiles* **2009**, *13*, 345.
[180] Sriprapundh, D., Vieille, C., Zeikus, J. G., Directed evolution of *Thermotoga neapolitana* xylose isomerase: high activity on glucose at low temperature and low pH. *Protein Eng.* **2003**, *16*, 683.
[181] Reetz, M. T., Carballeira, J. D., Iterative saturation mutagenesis (ISM) for rapid directed evolution of functional enzymes. *Nat. Protoc.* **2007**, *2*, 891.
[182] Migliorini, C., Mazzotti, M., Morbidelli, M., Continuous chromatographic separation through simulated moving beds under linear and nonlinear conditions. *J. Chromatogr. A* **1998**, *827*, 161.
[183] Sambrook, J., Russell, D.W., *Molecular cloning: a laboratory manual,* Laboratory Press, Cold Spring Harbour, **2001**.
[184] Silva-Rocha, R., Martinez-Garcia, E., Calles, B., Chavarria, M., *et al.*, The Standard European Vector Architecture (SEVA): a coherent platform for the analysis and deployment of complex prokaryotic phenotypes. *Nucleic Acids Res.* **2013**, *41*, 666.
[185] Bosshart, A., Enzyme engineering for intensified processes for the production of rare monosaccharides, *Doctoral thesis (ETH Zurich)*, **2014**, NO. 22128.
[186] Ng, K., Ye, R. Q., Wu, X. C., Wong, S. L., Sorbitol dehydrogenase from *Bacillus subtilis* - purification, characterization and gene cloning. *J. Biol. Chem.* **1992**, *267*, 24989.
[187] Studier, F. W., Protein production by auto-induction in high-density shaking cultures. *Protein Expres. Purif.* **2005**, *41*, 207.
[188] Besenmatter, W., Kast, P., Hilvert, D., Relative tolerance of mesostable and thermostable protein homologs to extensive mutation. *Proteins* **2007**, *66*, 500.
[189] Vieille, C., Hess, J. M., Kelly, R. M., Zeikus, J. G., Xyla cloning and sequencing and biochemical characterization of xylose isomerase from *Thermotoga neapolitana*. *Appl. Environ. Microbiol.* **1995**, *61*, 1867.
[190] Kovalevsky, A. Y., Hanson, L., Fisher, S. Z., Mustyakimov, M., *et al.*, Metal ion roles and the movement of hydrogen during reaction catalyzed by D-xylose isomerase: a Joint X-ray and neutron diffraction study. *Structure* **2010**, *18*, 688.
[191] Ben Hlima, H., Aghajari, N., Ben Ali, M., Haser, R., Bejar, S., Engineered glucose isomerase from *Streptomyces sp* SK is resistant to Ca^{2+} inhibition and Co^{2+} independent. *J. Ind. Microbiol. Biot.* **2012**, *39*, 537.
[192] Reetz, M. T., Kahakeaw, D., Lohmer, R., Addressing the numbers problem in directed evolution. *Chem. Bio. Chem.* **2008**, *9*, 1797.
[193] Rogers, T. A., Daniel, R. M., Bommarius, A. S., Deactivation of TEM-1 beta-lactamase investigated by isothermal batch and non-isothermal continuous enzyme membrane reactor methods. *Chem. Cat. Chem.* **2009**, *1*, 131.
[194] Yuryev, R., Strompen, S., Liese, A., Coupled chemo(enzymatic) reactions in continuous flow. *Beilstein J. Org. Chem.* **2011**, *7*, 1449.

8 Acknowledgments

I want to thank Prof. Sven Panke for supervising my work and giving me the opportunity to work in his lab. Thank you, Sven, it was a great time for me in the Panke Group and I am very grateful for your constant support and supervision and the freedom to develop and pursue own ideas in your lab. Thank to this, I have always experienced the Panke Lab as an inspiring and interdisciplinary working place! I also want to thank Matthias Bechtold for his academic input, great enzyme models and his constant support during and after his time as Group Leader of the Integrated Process Group. I also would like to express a special word of thanks to Prof. Marco Mazzotti for taking the time to read this thesis and be the co-referee of this work. Further, I like to thank Prof. Mazzotti and his research group for providing the Matlab program used for detailed SMB simulations in Chapter 2. Special thanks go further to Andreas Bosshart for great teamwork, inspiring discussions and the engineering of an "unrivalled" D-tagatose epimerase. Moreover, I want to particularly thank the students I had the pleasure to supervise and who contributed to this work with so much effort and enthusiasm. Thank you, Sonja, Jurek, Emil, Olivier and Sebastian!

A special thanks, also to Christian, Little Sven, Christoph, Sonja, Markus F., Martin, Rene, Andy, Matthias Bu., Alex, Giovanni, Martin, Marcel for a great starting time at the BPL.

Moreover, thank you, Luzi (the best office partner), Anne, Steven, Sabine, Tilmann, Irene, Michael, Johannes, Markus, Gaspar, Katja, Tania, Anke, Vijay, Corinna, Alex, Daniel and Philipp for a pleasent time we shared together.

Finally, I want to express my graditude to the people from the D-BSSE, the FIS, the DAS and the IT team, who really helped to solve all problems and facilitate the work in the lab. Thank you, for proving all this great services and support, I really enjoyed the time at the BPL!